The Study of Gamow–Teller strength in the ^{51}V(p,n)^{51}Cr reaction at intermediate energies

Victor M. Tshivhase

The Study of Gamow–Teller strength in the ^{51}V(p,n)^{51}Cr reaction at intermediate energies

V. M. Tshivhase

A thesis submitted to the Faculty of Science
of the University of Cape Town in fulfilment of the
requirements for the M.Sc. degree in Physics

Physics Department, University of Cape Town

Submitted in revised form September 1992

Abstract

The $^{51}V(p,n)^{51}Cr$ reaction was studied at four different proton beam energies namely 90, 120, 160, and 200 MeV. The experiment was performed in the angular range between 0 and 4°, using the beam swinger facility at National Accelerator Centre(NAC) at Faure, near Cape Town. The cross sections of the ground state, Isobaric Analog State, and the giant Gamow-Teller resonance were calculated at 0° for each beam energy. The ratio of the cross section of the giant Gamow-Teller resonance to the cross section of the Isobaric Analog State were studied at beam energies 90, 120, 160 and 200 MeV, and beam angles 0, 2 and 4°. The Gamow-Teller strength was estimated for energies 120, 160 and 200 MeV. The fractions of Fermi and Gamow-Teller strength in the Isobaric Analog State were also estimated.

Acknowledgements

I wish to express my sincere appreciation and gratitude to:

- Professor D. G. Aschman, my supervisor, for his help and guidance.
- Douw Steyn and Mark Murray who assisted with computing.
- Richard Newman and Rudolf Kabutz for sharing ideas.
- My parents for their support and encouragement.

Contents

List of Figures

List of Tables

Chapter 1

Introduction

1.1 Motivation for the present study

If (p,n) reactions are to be used as a probe of nuclear structure, then it is important to understand the relationship between beta-decay transition strengths and the (p,n) reaction on a nucleus with a resolvable transition to a state for which the beta-decay strength has been measured. These cases are rare for medium mass nuclei. One such case occurs in the nucleus ^{51}V. The beta-decay strength for the weak Gamow-Teller transition to the ground state of ^{51}Cr has been measured to have log $ft = 5.3893 \pm 0.0016$ [Aub 78]. The $J^P = \frac{7}{2}^-$ ground state of ^{51}Cr is well separated from the other excited states, and the transition from the $\frac{7}{2}^-$ ground state in ^{51}V can be measured in a (p,n) reaction on a monoisotopic Vanadium target using a neutron time of flight spectrometer. The cross-section is small, and thus good resolution is needed to see this state above background.

This thesis describes a study of the reaction ^{51}V(p,n) at proton beam energies of 90,120,160 and 200 MeV, and detection angles of 0°, 2° and 4° It was carried out at the National Accelerator Center, Faure, South Africa, using a neutron time-of-flight spectrometer.

Measurement of this ground state transition with its known beta-decay strength then enables extracting the Gamow-Teller strength to the excited states in a model-independent way.

The magnitude and distribution of Gamow-Teller strength for ^{51}V provide a test for a shell model calculation. A sum rule predicts the Gamow-Teller strength to be given by $B(GT_-) - B(GT_+) = 3(N - Z) = 15$ for the $^{51}_{23}V_{28}$ nucleus. The $B(GT_+)$ strength will be zero in a nucleus with complete Pauli blocking, but a shell model calculation predicts a $B(GT_+) = 5$.

The zero degree (p,n) spectra will contain some (L > 0) strength, and so not all the observed cross-section corresponds to the (L=0) Gamow-Teller or Fermi strength. A limited angular distribution can be used to test whether the observed cross-section is consistent with (L=0) strength. However a full multipole decomposition, based on angular distributions, is complicated and difficult, and highly model dependent, and is beyond the scope of the present work.

Chapter 2

Literature review

2.1 The $^{51}V(p,n)^{51}Cr$ reaction

The $^{51}V(p,n)^{51}Cr$ reaction was studied as early as 1962, by J.D.Anderson et al. [And 62]. The 14.8 MeV protons from the Livermore variable-energy cyclotron have been used at a laboratory angle of 23°. Neutron energies were determined using time-of-flight techniques. Only the Isobaric Analog State(IAS) transition could be seen at this low proton energy. The ground state and the giant Gamow-Teller transitions were not observed.

In 1984 Rapaport et al. [Rap 84] used the Indiana University beam-swinger facility to study $^{51}V(p,n)^{51}Cr$ reaction at proton energy 160 MeV only. Beam angles varied between 0° and 20°. The estimated differential cross sections of the ground state σ_{gs} and the IAS σ_{IA} were $0.08 + 0.02$ mb/sr and 3.1 mb/sr respectively. The $\Delta L=0$ response function[1] was used to derive the Gamow-Teller strength. Their shell-model calculation predicted the Gamow-Teller strength of 20.14 of which only 12.6 ± 2.5 was obtained experimetally.

Taddeucci et al. [Tad 87] examined the evidence for a proportionality relationship between 0° (p,n) cross sections and the corresponding Gamow-Teller and Fermi beta-decay transition strengths.

C.D.Goodman et al. [Goo 90] performed the (p,n) measurements for spectra containing GT strength known from β decay. Among these $^{51}V(p,n)^{51}Cr$ was one of the reaction studied at 120 MeV and 160 MeV proton energies. The ratios of the

---

[1] The $\Delta L=0$ response function was obtained from the 0° spectrum. see ref. [Rap 84].

cross section of the Gamow-Teller to the cross section of the Fermi in the IAS at 120 MeV and 160 MeV were 0.0243 ± 0.0011 and 0.0434 ± 0.0033 respectively.

2.2 Spin

It was first proposed by Sommerfeld and Debye in 1916 that an angular momentum should only be able to assume certain orientations with respect to a given direction [Som 16]. In 1922 Stern and Gerlach demonstrated the existence of an azimuthal quantization [Ger 22]. To explain hyperfine structure of spectral lines, Pauli in 1924 suggested that nuclei also possess spin [Pau 24].

As we know today spin is the intrinsic angular momentum of a particle. The three common fermions–the proton, neutron and electron possess spin $\frac{1}{2}$. To represent the spin, Pauli [Pau 27] used an operator $\vec{s}$ satisfying the commutation relations

$$[s_x, s_y] = i s_z,$$

$$+ \text{ cyclic permutations}$$

characteristic for angular momentum operators, and obeying the eigenvalue equations

$$\vec{s}^2 \chi_{s,m} = s(s+1)\chi_{s,m}$$

$$s_z \chi_{s,m} = m \chi_{s,m}$$

with $s = \frac{1}{2}$

$$\vec{s}^2 |\frac{1}{2}, m\rangle = \left(\frac{1}{2}\right)\left(\frac{3}{2}\right) |\frac{1}{2}, m\rangle$$

$$s_z |\frac{1}{2}, m\rangle = m |\frac{1}{2}, m\rangle, m = \pm\frac{1}{2}$$

An explicit representation of the spin operator $\vec{s}$ for spin $\frac{1}{2}$ is obtained conveniently by introducing the Pauli spin operator

$$\vec{\sigma} = 2\vec{s}$$

written in matrix form and in components in the standard representation as

$$\sigma_x = \frac{1}{2}\begin{pmatrix} 0 & 1 \\ 1 & 0 \end{pmatrix}, \sigma_y = \frac{1}{2}\begin{pmatrix} 0 & -i \\ i & 0 \end{pmatrix}, \sigma_z = \frac{1}{2}\begin{pmatrix} 1 & 0 \\ 0 & -1 \end{pmatrix}.$$

The Pauli matrices satisfy the relations

$$\sigma_x\sigma_y = -\sigma_y\sigma_x = \sigma_z, cyclic$$

$$\sigma_x^2 = \sigma_y^2 = \sigma_z^2 = I$$

and the identity

$$(\vec{\sigma}\cdot\vec{A})(\vec{\sigma}\cdot\vec{B}) = (\vec{A}\cdot\vec{B}) + i\vec{\sigma}\cdot\vec{A}\times\vec{B}$$

where $\vec{A}$ and $\vec{B}$ are any two vectors that commute with $\vec{\sigma}$, but not necessarily with each other.

2.3 Isospin

The protons and neutrons are considered as two charge states of the same particle, the nucleon. To distinguish between them W. Heisenberg in 1932 introduced the concept of isospin. The nucleon is assigned isospin $\tau = \frac{1}{2}$. The protons and neutrons are distinguished by $\tau_z = \pm\frac{1}{2}$, the expectation value of the third component of isospin operator $\vec{\tau}$.

For a system of A nucleons, the total isospin is defined as

$$\mathbf{T} = \sum_{i=1}^{A} \tau_i$$

The isospins $\vec{\tau}$ have the same mathematical properties as the spin vectors $\vec{\sigma}$, that is

$$\tau^2\chi = \tau(\tau+1)\chi, \tau_z\chi = \pm\frac{1}{2}\chi$$

where the z component refers to isospin space and not to ordinary space [Hod 71]. These functions and operators can be represented by the vectors and matrices for ordinary spin

$$\chi(p) = \begin{pmatrix} 1 \\ 0 \end{pmatrix}, \chi(n) = \begin{pmatrix} 0 \\ 1 \end{pmatrix},$$

$$\tau_x = \frac{1}{2}\begin{pmatrix} 0 & 1 \\ 1 & 0 \end{pmatrix}, \tau_y = \frac{1}{2}\begin{pmatrix} 0 & -i \\ i & 0 \end{pmatrix}, \tau_z = \frac{1}{2}\begin{pmatrix} 1 & 0 \\ 0 & -1 \end{pmatrix}.$$

The charge-transfer operators can be defined as

$$\tau^{\pm} = \tau_x \pm i\tau_y$$

so that

$$\tau^+\chi(p) = 0, \tau^+\chi(n) = \chi(p)$$

$$\tau^-\chi(n) = 0, \tau^-\chi(p) = \chi(n)$$

The z–axis component of the total isospin vector, T_z, is

$$T_z = \sum_{i=1}^{A} \tau_z^i = \frac{1}{2}(Z - N)$$

with eigenvalues for given T: T, T-1,...-(T-1), -T

These eigenvalues characterize the components of an isospin multiplet.

Because of charge independence the nuclear forces do not distinguish between neutrons and protons. These two nucleons (p and n) have nearly the same mass and the isospin vector T can point in any direction in isospin space as long as only the nuclear interaction H_N is present [Fra 75],

$$[H_N, \mathbf{T}] = 0$$

In the presence of the electromagnetic interaction the z–component of the isospin remains a good quantum number,hence

$$[H_N + H_\gamma, T_z] = 0$$

2.4 Nucleon–nucleon interaction potential

In the impulse approximation [Sat 83] at intermediate energies the effective nucleon–nucleon interaction reduces approximately to the free nucleon–nucleon scattering amplitude.

The nucleon–nucleon potential has an attractive long–range part due to the exchange of one pion, an intermediate–range attraction and a strong short–range repulsive core [Hua 91].

To avoid using the strong short–range repulsive core, an effective interaction that describes the relative wave function at large distances is employed. The details of effective interaction can be found in reference [Gle 83].

The effective interaction in terms of the Love and Franey [Lov 81] [Fra 75] t matrix has the form

$$t(\mathbf{r}, \mathbf{p}) = t_C(r) + t_{LS}\mathbf{L} \cdot \mathbf{S} + t_T(r)S_{12}(\hat{r})$$

$$\mathbf{L} = \mathbf{r} \times \mathbf{p}, \mathbf{r} = \mathbf{r}_1 - \mathbf{r}_2, \mathbf{p} = \frac{1}{2}(\mathbf{p}_1 - \mathbf{p}_2)$$

$$\mathbf{S} = \frac{1}{2}\vec{\sigma}, \vec{\sigma} = \vec{\sigma}_1 + \vec{\sigma}_2$$

where t_C, t_{LS}, t_T and $\vec{\sigma}$'s are central, spin–orbit, tensor components and Pauli spin operators respectively.

The t_C has four components due to the spin–isospin dependence, and t_{LS} and t_T have both isospin dependence and isospin independent parts,

$$t_C = t_o(r) + t_\sigma(r)\vec{\sigma}_1 \cdot \vec{\sigma}_2 + t_\tau(r)\vec{\tau}_1 \cdot \vec{\tau}_2 + t_{\sigma\tau}\vec{\sigma}_1 \cdot \vec{\sigma}_2\vec{\tau}_1 \cdot \vec{\tau}_2$$

$$t_{LS} = t^{\circ}_{LS}(r) + t^{1}_{LS}(r)\vec{\tau}_1 \cdot \vec{\tau}_2$$

$$t_T = t^{\circ}_T(r) + t^{1}_T\vec{\tau}_1 \cdot \vec{\tau}_2$$

The components of t are plotted as a function of energy at zero momentum transfer (q=0) in figure 2.1.

The (p,n) reaction depends on the isovector amplitudes $t_{\sigma\tau}$ and t_τ. The non–spin flip component t_τ decreases at intermediate energies. The spin flip component $t_{\sigma\tau}$ remains constant at intermediate energies. This explains the dominance of $t_{\sigma\tau}$ over t_σ at intermediate energies [Hua 91].

2.5 Beta decay

In β^--decay a neutron in a nucleus emits an electron and an antineutrino, becoming a proton in the process

$$n \longrightarrow p + e^- + \bar{\nu}_e$$

For nucleus made of Z protons, N neutrons and nucleon number A:

$$A(Z, N) \longrightarrow A(Z+1, N-1) + e^- + \bar{\nu}_e.$$

Similarly in β^+-decay

$$p \longrightarrow n + e^+ + \nu_e$$

$$A(Z, N) \longrightarrow A(Z-1, N+1) + e^+ + \nu_e$$

a proton is transformed into a neutron by emitting a positron and a neutrino.

The creation of leptons in β–decay can be explained from quantum field theory (QFT). According to Fermi the beta interaction Hamiltonian is

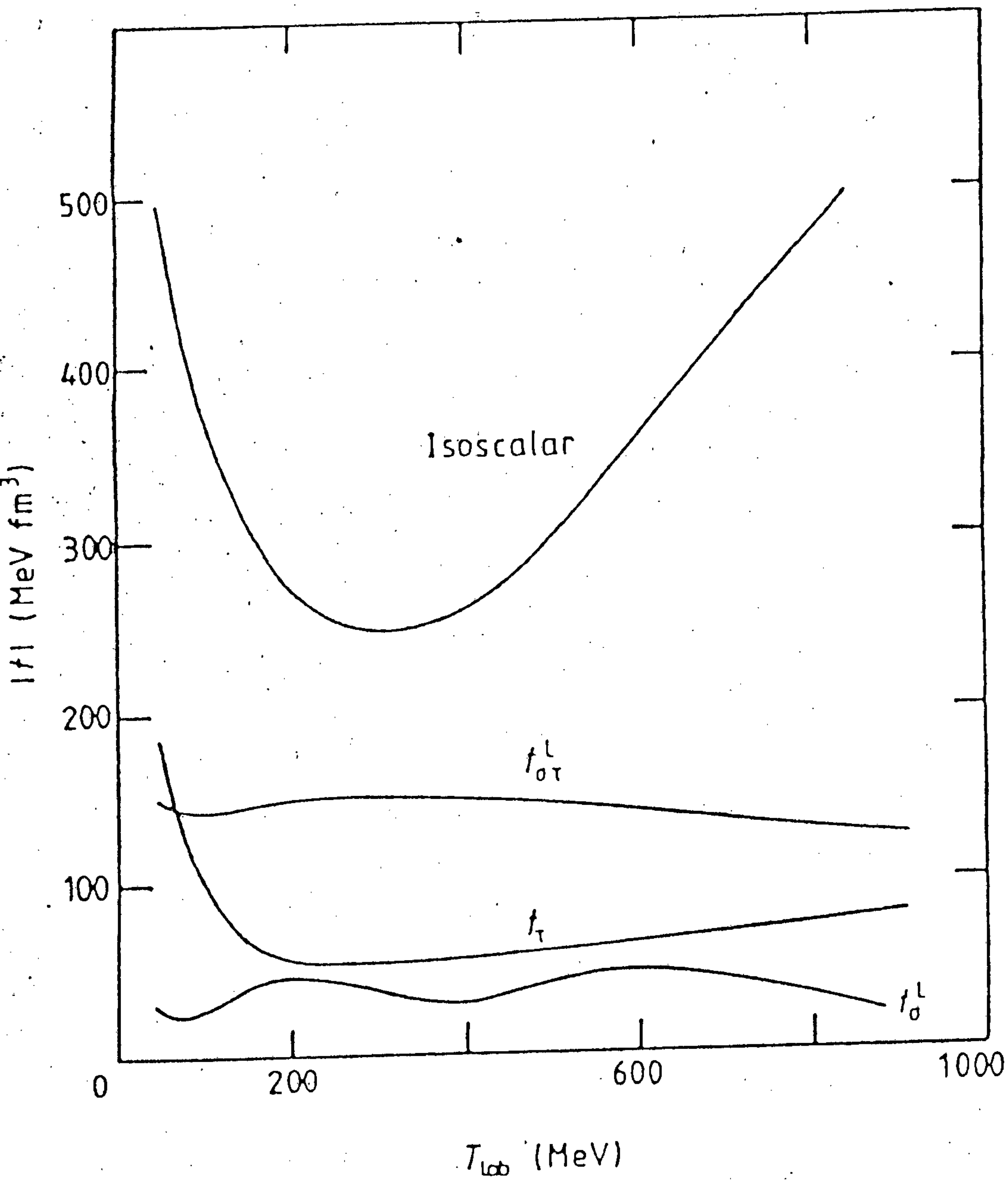

Figure 2.1: The t components plotted as a function of energy at zero momentum transfer (q=0), from reference [Ber 87]

$$H = C_v[(\bar{\psi}_p O_v \psi_n)(\bar{\psi}_e O_v \psi_\nu) + (\bar{\psi}_n O_v \psi_p)(\bar{\psi}_\nu O_v \psi_e)]$$

where:

- C_v - coupling constant (strength of interaction)
- ψ-field operators that destroy particles or create antiparticles.
- similarly $\bar{\psi}$-create particles or destroy antiparticles.

The first term is for β^--decay and the second is for β^+-decay.

The Fermi interaction which is vector coupled only allows transitions with no spin or parity change and is scalar in space and spin.

Gamow and Teller generalized the interaction by pointing out that five possible invariant interactions could be obtained by using the proper combinations of quantum operators.

The Gamow-Teller interactions allows spin changes but no parity changes, and is scalar in space but vector in spin.

For allowed decays the nuclear part of the $\beta^\pm$-decay transition operator has the form [Won 90]

$$O_\lambda(\beta) = G_V \sum_{k=1}^{A} \tau_k^\mp + G_A \sum_{k=1}^{A} \sigma_k \tau_k^\mp .$$

The transition strengths are obtained from beta decay lifetimes according to

$$(G_V)^2 B(F) + (G_A)^2 B(GT) = \frac{K}{ft} \tag{2.1}$$

where

$$\frac{K}{(G_V)^2} = 6166 \pm 2sec,$$

$$\left(\frac{G_A}{G_V}\right)^2 = (1.260 \pm 0.008)^2, \text{[Tad 87]}$$

B(F) and B(GT) are Fermi and Gamow–Teller matrix elements defined as

$$B(F)^{\pm} = \frac{1}{(2J_i+1)} |\langle f || \sum_k \tau_k^{\pm} || i \rangle|^2$$

$$B(GT)^{\pm} = \frac{1}{(2J_i+1)} |\langle f || \sum_k \sigma_k \tau_k^{\pm} || i \rangle|^2$$

2.6 Limitations of β–decay

In most cases a considerable fraction of the GT strength is energetically unobservable in β-decay of neutron-rich nuclei.

In β^+-decay the coulomb effect provides energy to drive the decay, but for a neutron rich parent state, β^+ -decay accesses only levels with isospin greater than that of the parent, and that portion of the GT strength function is mostly Pauli blocked. More of the strength function can be explored with β^+ -decay from a proton rich nucleus, but it is not possible to create heavy proton rich nuclei[Goo 83].

2.7 (p,n) reaction as Gamow–Teller probe

In β^- -decay a neutron is transformed into a proton. This occurs without transferring momentum into the nucleus, which implies that the nuclear excitations are due to change in intrinsic quantum numbers (s,t) of the nucleon [Goo 83].

To search for the GT strength we need a GT probe that can transform a neutron to a proton or vice versa without changing the orbital angular momentum of the nucleus. The probe should be applicable at high enough energies to reach states of interest. We should be able to establish a relationship between the (p,n) 0° cross sections and the GT strength.

The (p,n) reaction inserts a proton and removes a neutron. If performed at high energies and at zero degrees it induces similar transitions as in β^- -decay. The ^{51}V(p,n)^{51}Cr spectrum of the Isobaric Analog State discovery experiment is shown in figure 2.2.

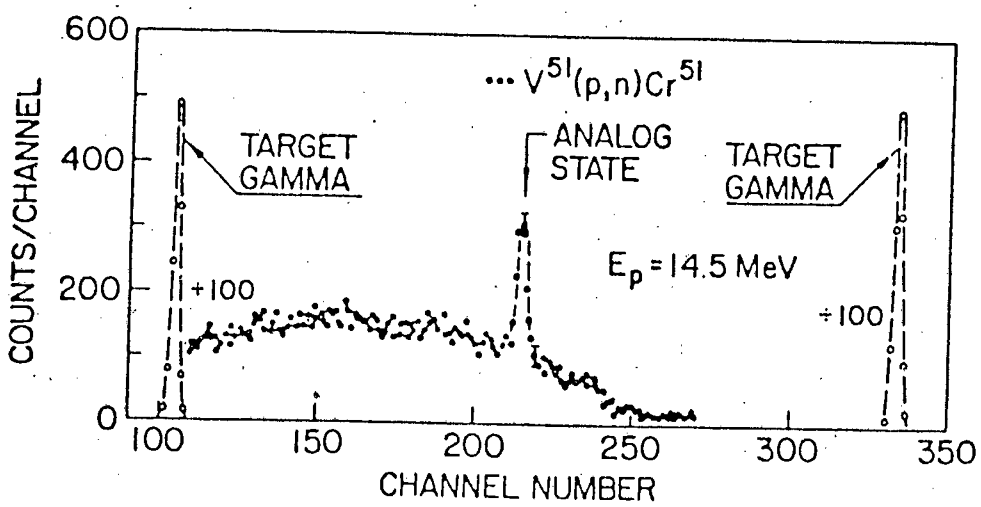

Figure 2.2: The Isobaric Analog State discovery spectrum by Anderson et al. (from reference [And 62]).

2.8 The cross section

In the distorted–wave approximation [Sat 64] the differential cross section is given by [Gol 80]

$$\frac{d\sigma}{d\Omega} = \left(\frac{\mu}{2\pi\hbar^2}\right)^2 \frac{k_f}{k_i}\frac{1}{(2J_i+1)(2s_p+1)} \sum |\chi_f^{(-)*}(r_p)\langle f|\sum_f v_{jp}(1-P_{jp})|i\rangle\chi_i^{(+)}(r_p)d^3r_p|^2,$$

where:

- μ is the reduced energy divided by c^2,
- k is the wave number,
- χ's are distorted waves,
- $\langle f|\sum_f v_{jp}(1-P_{jp})|i\rangle$ is the target matrix element,
- v_{ip} is the effective nucleon–nucleon interaction,
- P_{jp} is the permutation operator accounting for knockout exchange,

- and the sum is over initial and final spin projections of the projectile and target.

The impulse approximation [Ker 59] is also reasonable for beam energies higher than 100 MeV, so that v_{ip} is expected to be close to the free nucleon–nucleon t matrix.

The (p,n) reaction selects the isovector parts of v_{ip}, and for 0° scattering, only the low–momentum components contribute appreciably to the transition amplitude. The central parts of the isovector effective interaction dominate at low q and the non–central parts can be neglected [Lov 80][Pet 79] [Pe1 80] [Pe2 80]. With this simplification the DWBA 0° cross sections for (p,n) transitions with appreciable Fermi and/or Gamow–Teller strength can be described by [Lov 80] [Pet 79] [Pe1 80] [Pe2 80] [Goo 83]

$$\frac{d\sigma}{d\Omega}(0^\circ) = \left(\frac{\mu}{\pi\hbar^2}\right)^2 \frac{k_f}{k_i}[N_\tau^D|J_\tau|^2B(F) + N_{\sigma\tau}^D|J_{\sigma\tau}|^2B(GT)] \tag{2.2}$$

J_τ and $J_{\sigma\tau}$ are the magnitudes of the volume integrals of q = 0 components of the effective spin–independent $(\tau_1 \cdot \tau_2)$ and effective spin dependent $(\sigma_1 \cdot \sigma_2\tau_1 \cdot \tau_2)$ isovector central terms in $v_{jp}(1 - P_{jp})$, N_τ and $N_{\sigma\tau}$ are distortion factors calculated by Love et al., and q is the three momentum transfer.

2.9 Gamow–Teller strength from (p,n) reaction

Calculation of strength of different peaks in the (p,n) spectrum is done by calibrating the cross section to a known GT peak whose strength has been measured by β decay, using the relation [Goo 89]

$$B(GT)_{p,n} = \frac{(2J_i+1)_{p,n}}{(2J_i+1)_{beta}} B(GT)_{beta} \tag{2.3}$$

where B(GT) and J_i is the strength and spin of the parent state in β decay or (p,n) reaction. Once the strength of one peak is known, the strength of other peaks can be calculated using the proportionality relation [Hua 91],

$$B(GT)_2 = \frac{\sigma_2}{\sigma_1}\frac{k_1}{k_2}\frac{N^1_{\sigma T}}{N^2_{\sigma T}}B(GT)_1 \tag{2.4}$$

derived from eqn 2.2. The ratio of the distortion factors can be calculated and for energies less than 200MeV is close to unity [Tad 87].

The IAS in the even–A nuclei is a pure Fermi transition and in the odd–A nuclei is a mixture of GT and Fermi transition. Taddeucci et al. studied the energy dependence of the ratio of the GT to Fermi strength from (p,n) reactions up to 200 MeV

The ratio defined

$$R(E_p)^2 \equiv \frac{\sigma_{GT}(q=0)/B(GT)}{\sigma_F(q=0)/B(F)}$$

is related to beam energy by

$$R(E_p) = \frac{E_p}{E_\circ} \tag{2.5}$$

where $E_\circ$ is a constant equal to 45 MeV and 55 MeV for odd–A and even–A nuclei respectively.

Using the ratio R(E_p) we can extract the fraction of GT and Fermi strengths in the IAS. We have used the value of R(E_p) from ref. [Goo 90] based on data for even–A nuclei, this may be different from that for odd–A nuclei. The incoherent sum of GT and Fermi components may be written as

$$\sigma_{IAS} = \sigma_F + \sigma_{GT}$$

$$= [\hat{\sigma}_F B(F) + \hat{\sigma}_{GT} B(GT)]$$

The fraction of the cross section due to GT strength is given by

$$f_{GT} \equiv 1 - f_F = \frac{\sigma_{GT}}{\sigma_{IAS}} \tag{2.6}$$

$$= \left[1 + \frac{B(F)}{B(GT)R(E_p)^2}\right]^{-1}. \tag{2.7}$$

The Fermi transition strength is assumed to be

$$B(F) = N - Z \tag{2.8}$$

Chapter 3

Experimental arrangement

3.1 The Experiment

The experiment was performed using the beam swinger neutron time-of-flight facility [Nac 90] at the National Accelerator Centre (NAC) at Faure, near Cape Town. Figure 3.1 shows the layout of the cyclotron at NAC. The beam swinger facility is in line N. The proton beam was obtained from the cyclotron at energies of 66 MeV, 90 MeV, 120 MeV, 160 MeV and 200 MeV.

The target was a self-supporting ^{51}V metallic foil, 48.0 mg/cm^2 thick and 99.75% pure. Beam time structure was measured by looking at the elastically scattered protons detected in the fast scintillator system consisting of a ΔE and E detector.This system was located along the 30° line with respect to the undeflected incident proton beam. A 2.6 cm Cu degrader between the two detectors reduced the proton energies such that protons stopped in the E detector. The degrader was needed for high energy protons only, i.e at 160 to 200 MeV.

Neutrons escaping from the target passed through a narrow collimator in the shield wall of the beam swinger area, before reaching the neutron detectors. These six detectors were located transversely along the zero-degree beam line with respect to an undeflected proton beam at a distance of 174.6 m. The outgoing neutrons were observed at four different angles namely $\Theta_{Lab} = 0°, 2°, 4°$ and 10°. A natural lithium target was used under identical experimental conditions to obtain the product of neutron transmission, fractional live time of the data acquisition system and the neutron detection efficiency, TLϵ [New 91]. The time resolution for these detectors

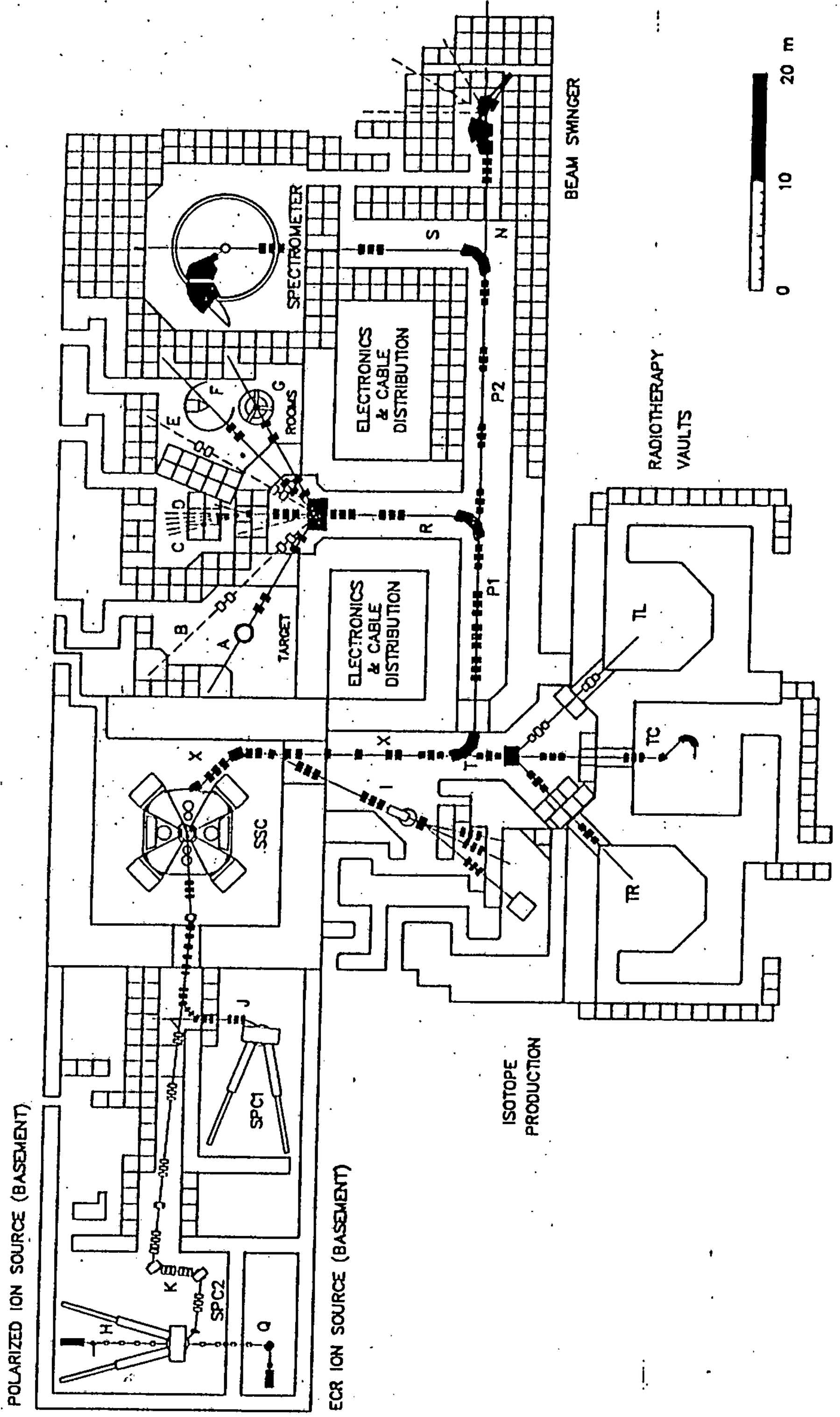

Figure 3.1: The layout of the NAC cyclotron. The beam swinger facility is located at the end of line N.

was also measured [Kab 90].

3.2 The Detectors

The two sets of detectors are the ΔE–E Proton telescope and the six neutron detectors.

3.2.1 The Neutron Counters

The design of a neutron counter is shown in figure 3.2. Each of the six counters consists of a 60cm x 10cm x 10cm NE 102A scintillator, two conical perspex light guides one on each end, and the two Hamamatsu R329 photomultiplier tubes mounted on the light guides. The high voltage for each photomultiplier tube was set at about -1650 V.The photomultiplier tubes with E931 base were sheathed in μ–metal cylinders to provide magnetic shielding. Optical grease NE 586 was applied between adjacent optical surfaces. The scintillator was covered with aluminium foil and black paper to improve the efficiency of light collection. The system was kept in an aluminium casing which was covered with black plastic to keep it light-tight. The springs in an aluminium casing were used to maintain optical contact.

3.2.2 The ΔE–E Proton Telescope

The telescope is composed of two types of detectors. This is illustrated in figure 3.3.

(a) The ΔE detector is made of small circular NE 102A plastic scintillator glued on a light guide and mounted on the Hamamatsu R329 photomultiplier tube. This is kept in a cylindrical aluminium tube.

(b) The E detector is made up of 10cm thick cylindrical NE 102A plastic scintillator, a light guide and the Hamamatsu R329 photomultiplier tube.

3.3 The Electronics

The schematic diagram of the main electronic circuit for time of flight is illustrated in figure 3.4. This is divided into four sections (figures 3.5 to 3.8) according to their

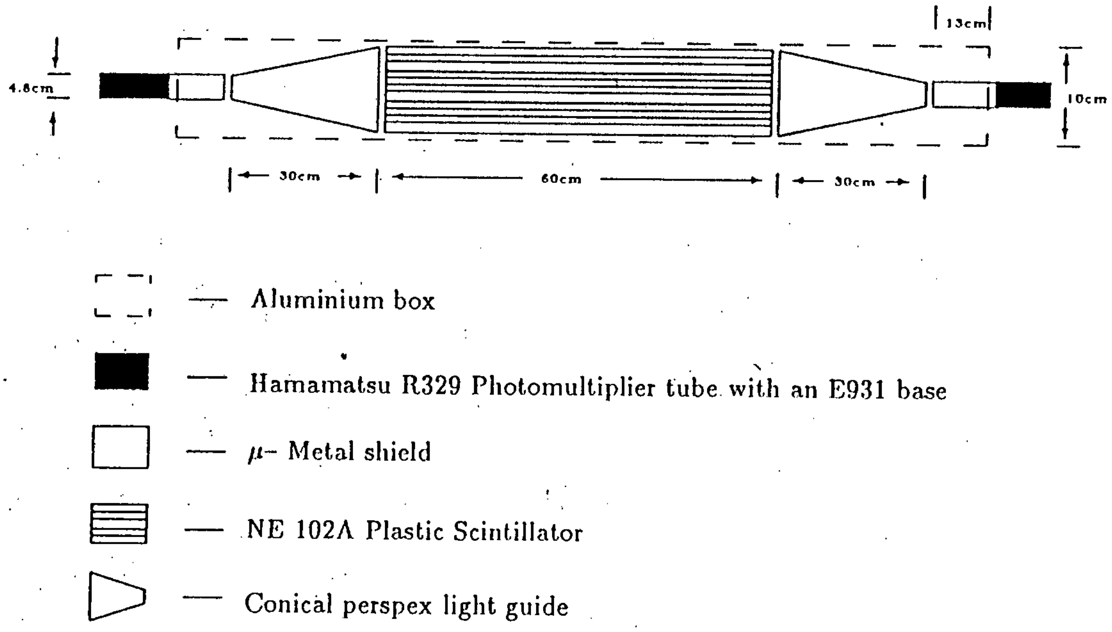

Figure 3.2: Design of a Neutron detector.

3.3 The Electronics

The schematic diagram of the main electronic circuit for time of flight is illustrated in figure 3.4. This is divided into four sections (figures 3.5 to 3.8) according to their functions. Figure 3.9 is the electronics for the beam resolution. These circuits shows only detector 1; sets 2 to 6 whose circuits are similar, are omitted for simplification.

3.3.1 The Time-of-Flight Spectra

The electronic circuit is shown in figure 3.5. The high negative voltage supply was the North Electronics Systems(N.E.S.) controlled by an IBM PC compatible computer. The anode signals from the Hamamatsu R329 photomultiplier tubes on each end of the detector are split by an EDA36 50Ω 6DB splitter into two signals, in order to determine the cosmic and neutron triggers. One anode signal is fed to an Ortec 934 Constant Fraction Discriminator(CFD) whose threshold was set below the 20 MeV deposited by a minimum ionizing μ going through 10cm of plastic

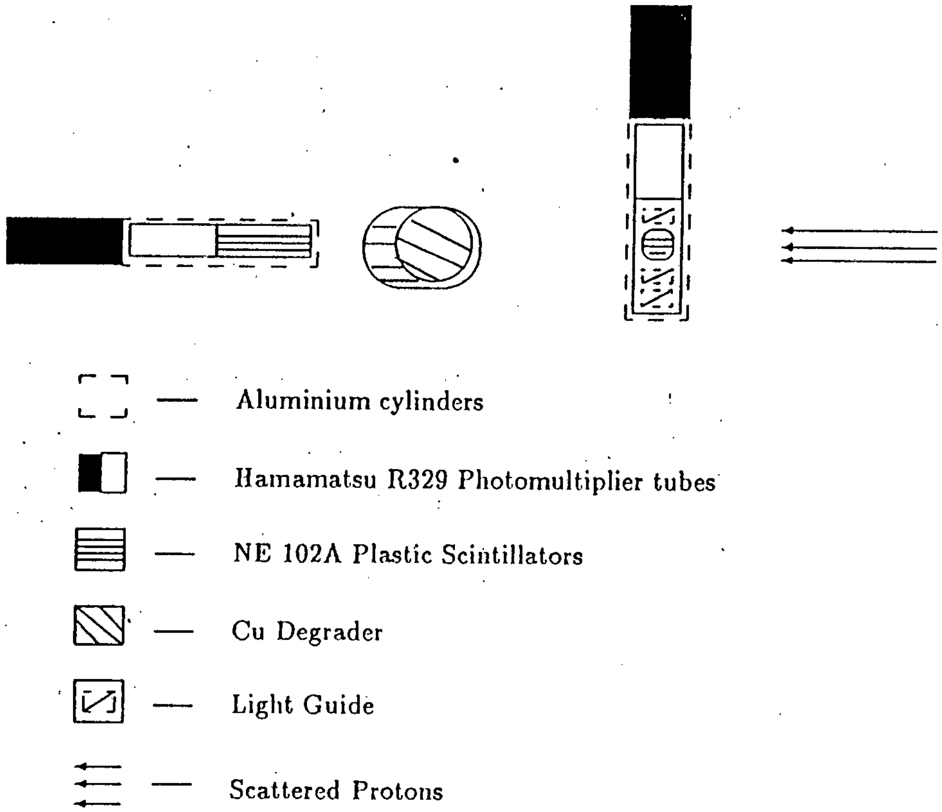

Figure 3.3: The arrangement of the ΔE–E proton telescope

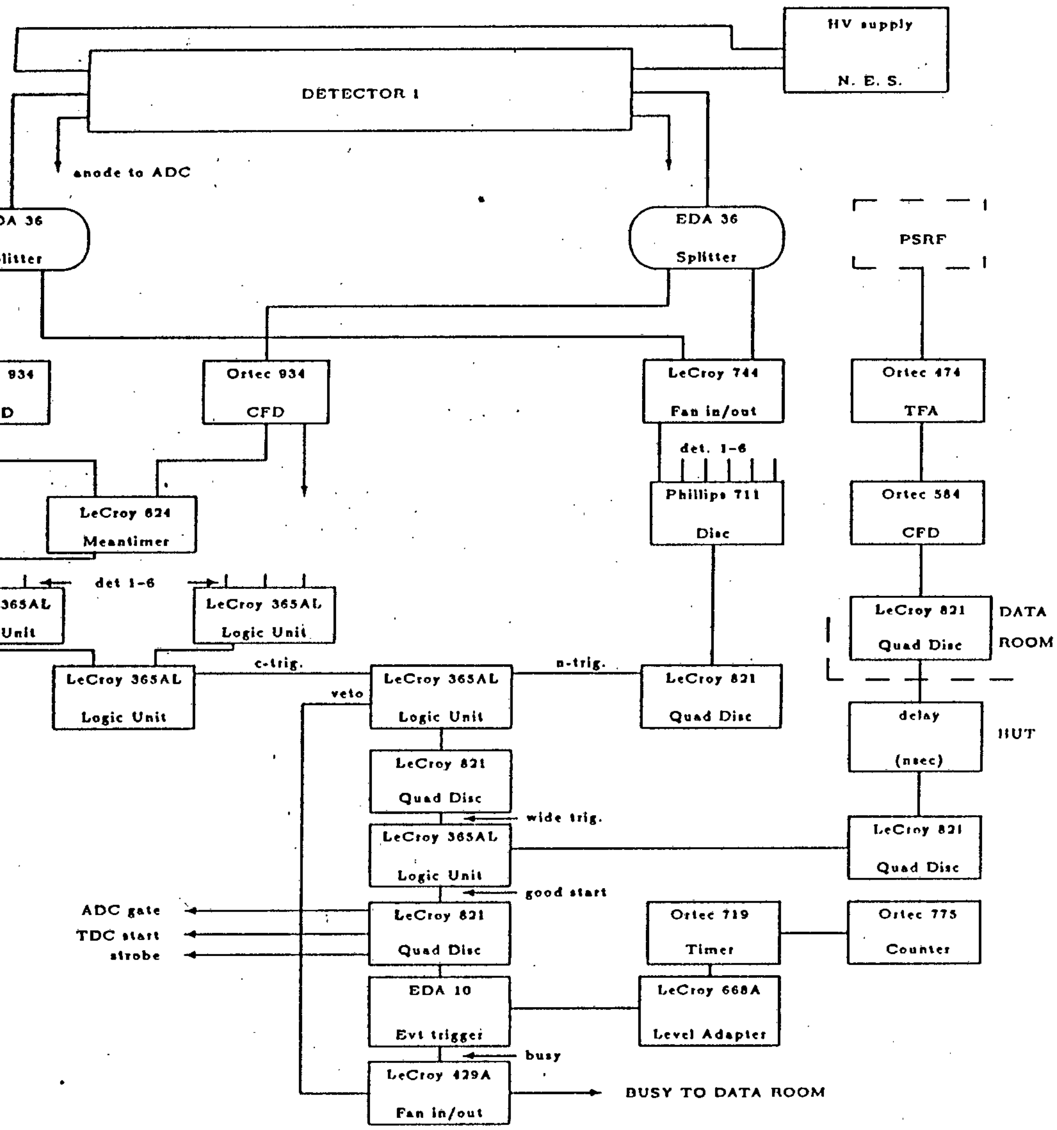

Figure 3.4: Main electronic circuit for the time of flight.

in LeCroy 365AL 4-fold Logic units to form a cosmic trigger. This trigger occurs if and only if all six counters fired within a 20 ns resolving time.

The second anode signals from the two splitters at both ends of the counter were passively summed in the LeCroy 744 Quad Linear gate Fan in/Fan out(Quad Fan in/Fan out). The outputs from six detectors are discriminated in the Phillips 711 six channel discriminator(6 Channel Disc). This was set at the neutron threshold,about 60 MeV for E_p = 200 MeV, to cut out the low energy signals and wrap-around. Its sum output is fanned out in the LeCroy 821 Quad Discriminator(Quad Disc) to provide a NIM neutron trigger. This is the output which occurs if any counter records pulse height above threshold.

The cosmic trigger and neutron trigger went into the LeCroy 365AL Logic unit, whose output is fed in the LeCroy 821 Quad Disc to form a wide trigger.

The pulse selected radio frequency(PSRF) sine wave is amplified in the Ortec 474 Timing Filter Amplifier (TFA) to a logic pulse and its output is discriminated in the Ortec 584 Constant Fraction Discriminator(CFD) whose output is fanned out in the LeCroy 821 Quad Disc. The LeCroy 821 Quad Disc was also needed for the adjustment of the pulse width.

The wide trigger is set wide enough to gate one pulse of the PSRF i.e a trigger signal of width ±265 ns. The wide trigger and the discriminated PSRF are set in coincidence in the LeCroy 365AL Logic unit. This is done in order to derive the start signal for the neutron time-of-flight measurement. The output is fanned out in the LeCroy 365AL Logic unit to provide the ADC gate, good TDC start, the strobe and the event trigger for the event trigger module(EVT).

On receiving the trigger, the EVT sets a busy flag, it waits a preset time before it initiates the new read-out cycle. The time is set in the Ortec 719 Timer(Timer) which is linked to the EVT via the LeCroy 688A Level Adapter–The LeCroy 688A Level Adapter converts the TTl input to NIM output. This Timer was set at 1 Hz and 10 Hz for Lithium and Vanadium runs respectively. The busy signal of the event trigger module is fanned out in the LeCroy 429A Logic Fan in/Fan out to provide the veto for either the cosmic or neutron trigger in the LeCroy 365AL Logic unit.

The twelve outputs from the twelve sets of Ortec 934 CFD are delayed and serve as the stops for the LeCroy 2228A Time-to-Digital Conveter(TDC). The TDC is started with the good TDC start.The VAX 11/730 computer reads the digital times of the stops relative to the start. These provide the time-of-flight spectra.

3.3.2 The Pattern Register

The electronic circuit in figure 3.6 gives information of the type of the event detected, that is whether it is a cosmic or a neutron event and also on which detector did the event occur. The anode from each end of the counter is split by the EDA36 50Ω 6DB splitter into two identical signals, to derive the cosmic bit, the neutron bit and event from each counter. One signal is discriminated in the Ortec 934 CFD whose output together with similar output from the other end of the counter are fed into the LeCroy 624 Octal MT. The meantime between the two ends of counter is discriminated in the Phillips 711 6 Channel Disc. This output is registered in the Bi Ra Nim in Register in channel 1 corresponding to counter number one. Similarly, outputs from counters 2 to 6 are registered in channels 2 to 6.

The cosmic trigger and neutron trigger described in Sec. 3.3.1 provides the cosmic bit and neutron bit. These are registered in channels 8 and 9. As soon as there is an event the strobe instructs pattern register module to read-and-clear. The strobe was also described earlier in Sec. 3.3.1. The register module is read by the VAX 11/730 computer. This provides the counting pattern for the counters.

3.3.3 The Amplitudes

The electronic circuit in figure 3.7 is used for pulse height analysis. The twelve anode signals from each end of the six counters are delayed by 320 ns to adjust their position relative to the ADC gate. Each is fed into the EDA29 50Ω attenuator where the height is adjusted before putting it through to the LeCroy 2249A Analog-to-Digital Converter(ADC). The ADC gate was described earlier in Sec. 3.3.1. These ADC inputs are read if they fall within the ADC gate. The ADC is read by the VAX 11/730 computer. These provide the amplitudes for pulses in each photomultiplier

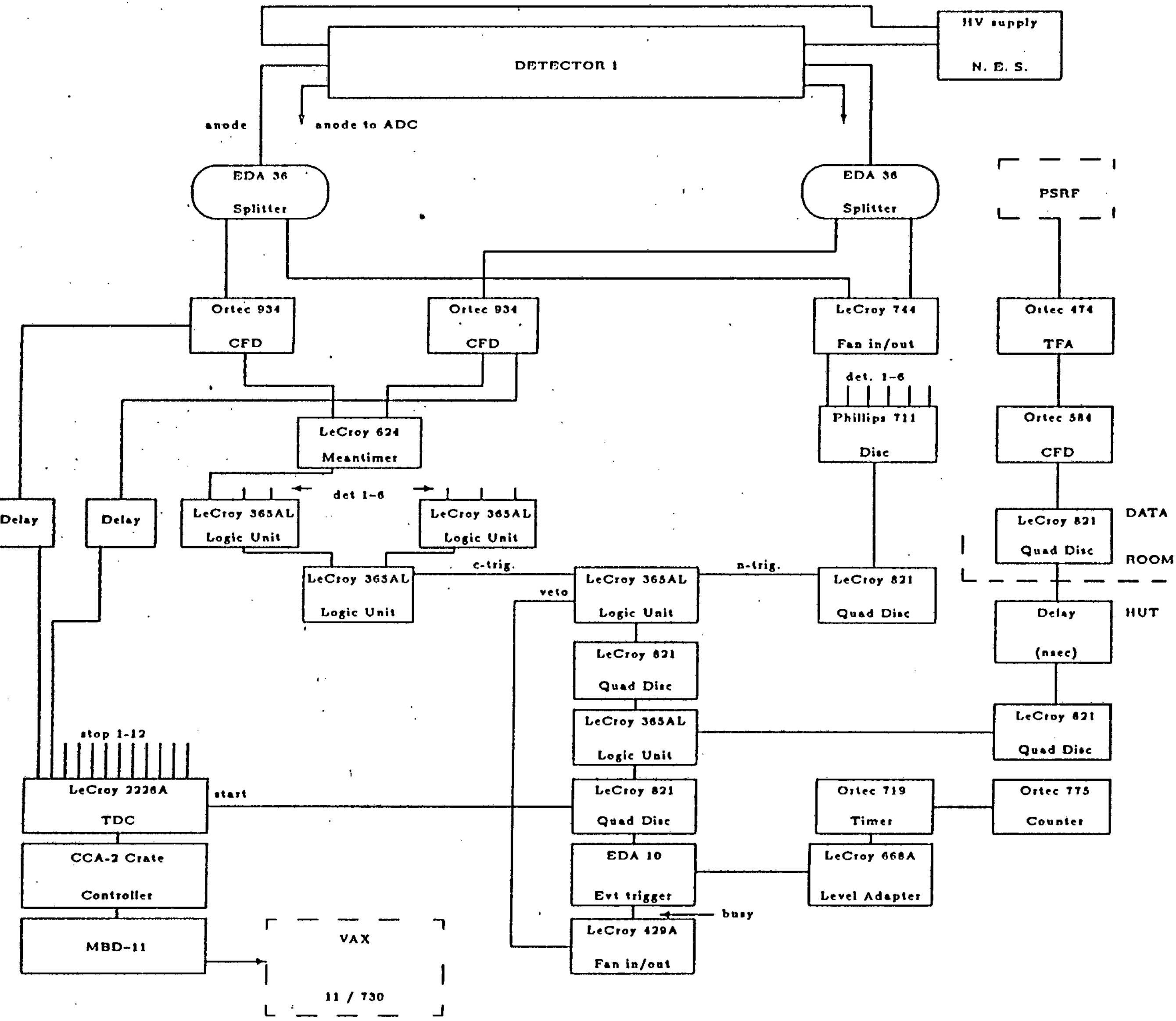

Figure 3.5: Electronics for neutron times.

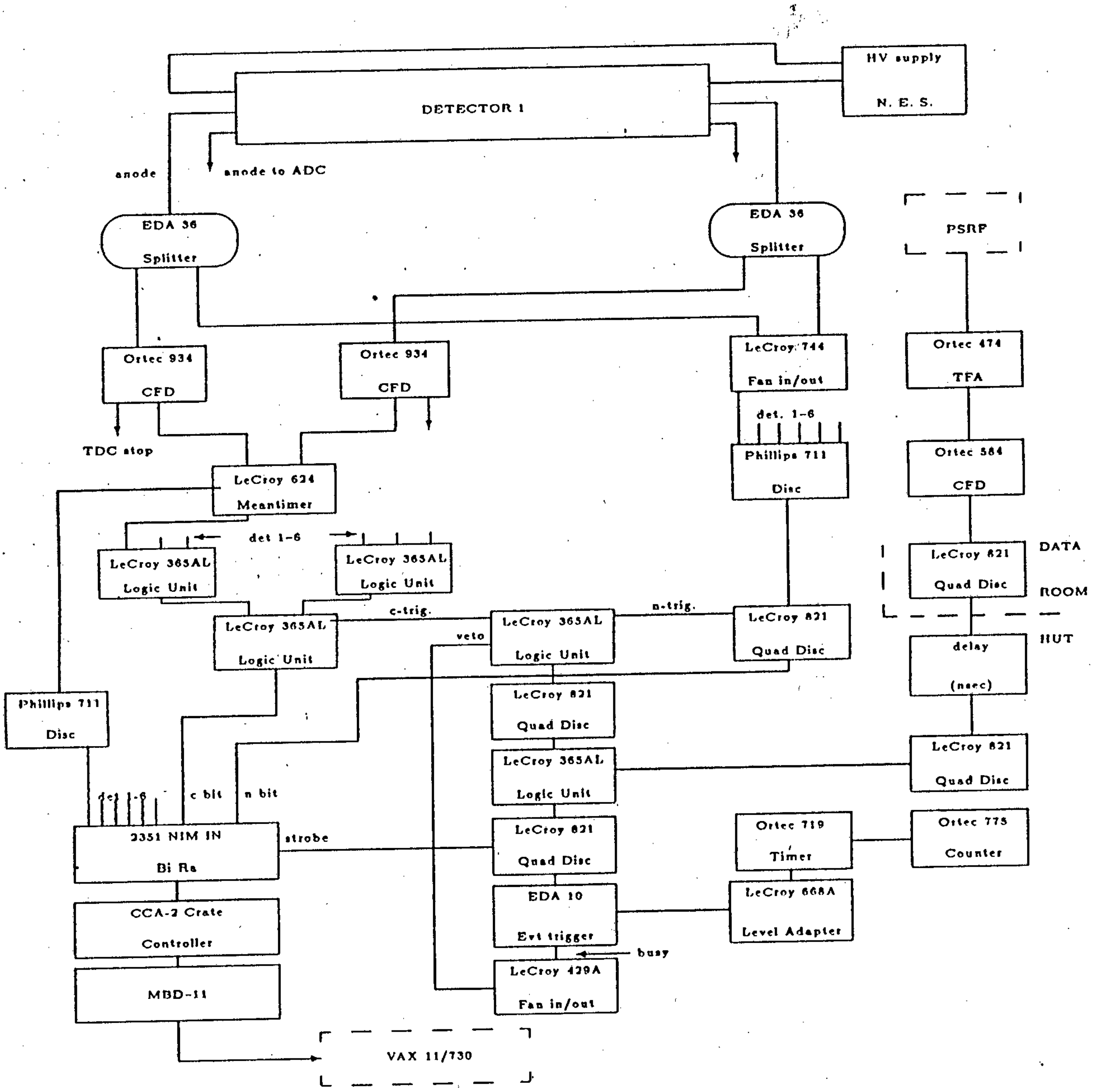

Figure 3.6: The electronics for counter pattern register.

tube.

3.3.4 The Current Integrator

The Faraday Cup detects the number of charged particles in the incident beam. This is converted into current in the Brookhaven Instrument Corporation model 1000C current integrator(BIC 1000C). (See electronic circuit shown in figure 3.8). The EDA14-4 serves as the digital current display. The sine-wave signal from the BIC 1000C is discriminated in the Ortec 436 100MHz Discriminator to provide logic pulse. Its output is fed in the LeCroy 365AL Logic unit, since this module can take a veto. This is vetoed by the busy from the event trigger module described in Sec. 3.3.1, which determines the rate at which the LeCroy 2551 scaler reads the LeCroy 365AL Logic unit output(current).

The BNC tail pulse generator forms single pulses at a rate of 100Hz which are discriminated in the LeCroy 821 Quad Disc. The pulses from of the LeCroy 821 Quad Disc are counted by the Ortec 875 counter and also by the LeCroy 2551 scaler. The second output is vetoed in the LeCroy 365AL Logic unit to give the number of pulses that went through when the event trigger(VAX 11/730) was alive. This is read by the LeCroy 2551 scaler and also the Ortec 875 Counter.

These two scalers record are used to estimate the fraction of particles that went through the target during the computer dead time. These scaler records are read by the VAX 11/730 computer

3.3.5 The Beam Timing

The beam-burst widths which give a measure of the beam resolution were measured with a fast-plastic scintillator telescope which detects protons elastically scattered from the target. The electronic circuit is shown in figure 3.9. These protons deposited some of their energy in the ΔE detector before they stop in the E detector. The Ortec 556 high voltage supplies of the ΔE and E photomultiplier tubes were set at -2.7 kV and -1.2 kV respectively. The pulse from the E photomultiplier tube was split by the 4901.01A SUHNER 50Ω splitter to the fast 300MHz Oscilloscope. The

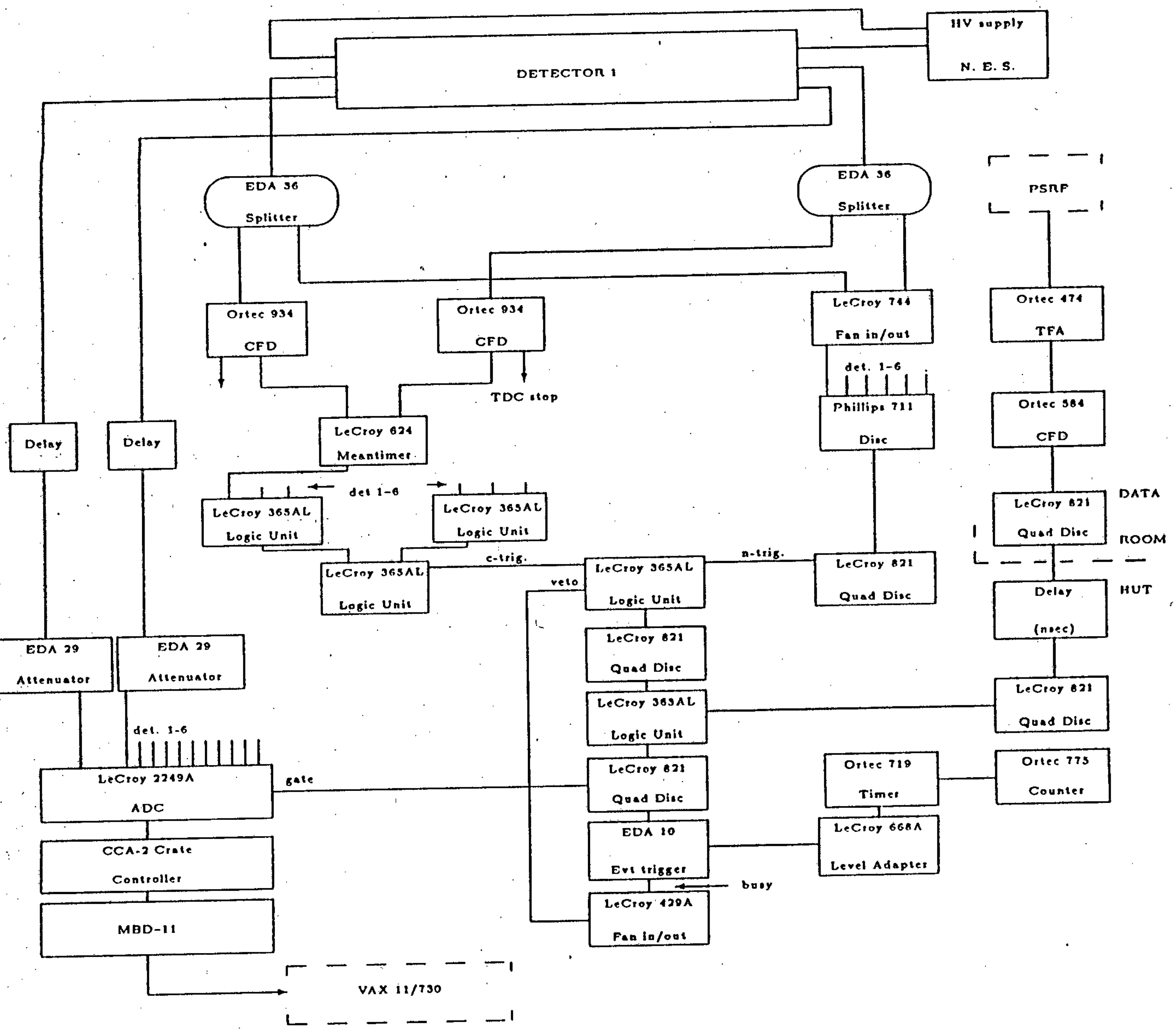

Figure 3.7: Electronics for amplitudes

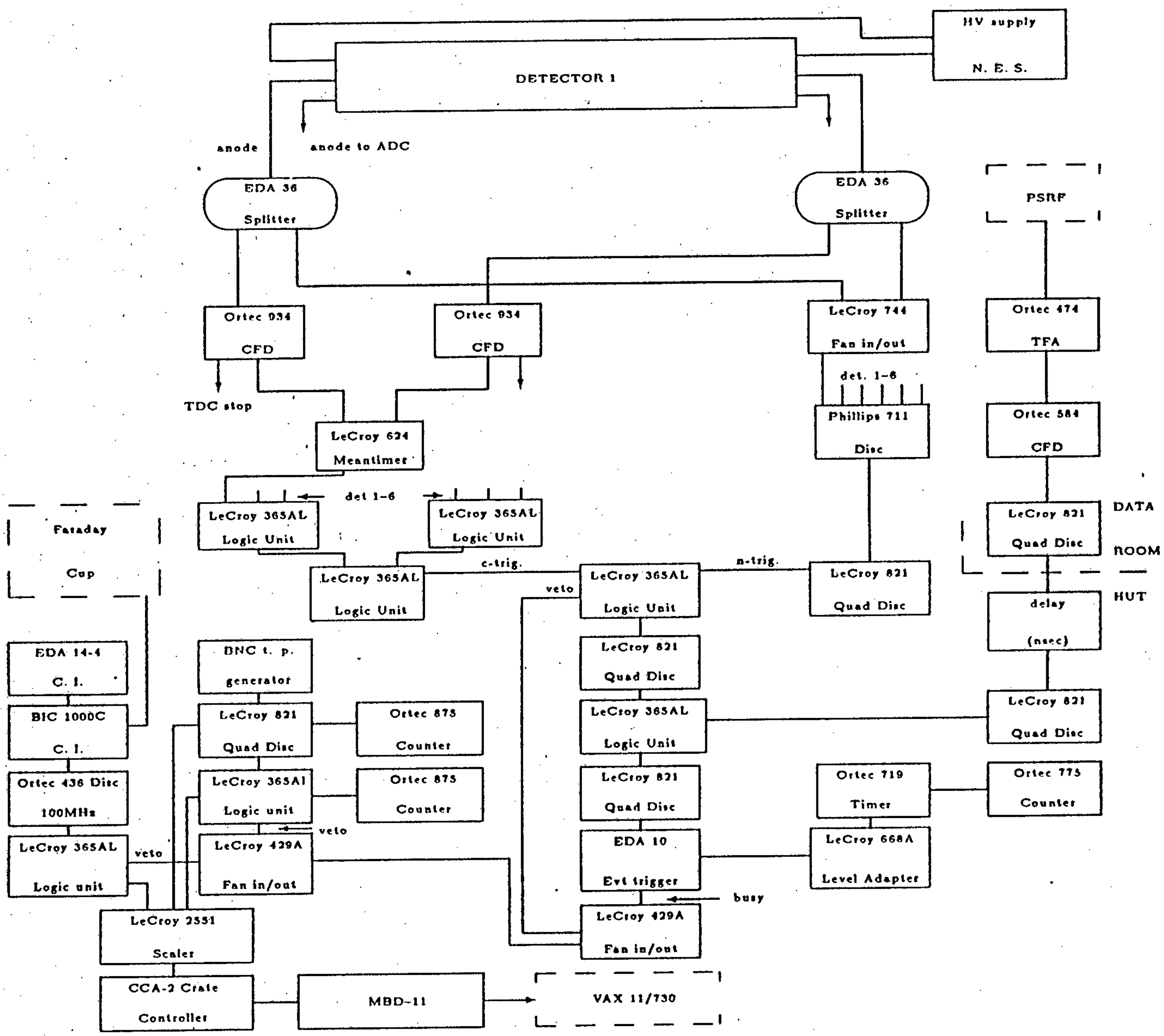

Figure 3.8: Electronics for computer dead time determination.

other pulse was fed into the Ortec 584 CFD whose lower threshold was set to select only the highest energy protons i.e the elastically scattered ones, which forms the brightest band on the oscilloscope. The output was discriminated in the LeCroy 821 Quad Disc. Triggering the oscilloscope on this E pulse, the position of the ΔE on the oscilloscope was noted.

The pulse from the ΔE photomultiplier tube was split by the 4901.01A SUHNER splitter to the fast 300 MHz Oscilloscope and the other pulse went to the Ortec 583 Constant Fraction Discriminator(CFD). Triggering the oscilloscope on the ΔE pulse, the window of the Ortec 583 CFD was set such that the selected ΔE band falls on the position noted above. The output was discriminated by the LeCroy 821 Quad Disc. The width of this pulse was set and delayed to fit in the discriminated E pulse. The ΔE and E pulses were set in coincidence in the LeCroy 365AL Logic unit. The coincidence ensures selection of the elastically scattered protons that went through the telescope. The output was discriminated in the LeCroy 821 Quad Disc, delayed by a 260 ns cable, after which it was fanned out in the LeCroy 821 Quad Disc. The output provided the start for the Ortec 567 Time-to-Amplitude Converter(TAC).

The discriminated PSRF(in Sec.3.3.1) provides stops for the Ortec 567 TAC. The times of the stops relative to the starts are converted to analogs in the Ortec 567 TAC. The analogue signals were digitized in the Canberra 8077 fast Analog-to-Digital Converter(ADC). The ADC was read by the VAX 11/730 computer. This provides the beam measurement of time width resolution. The time resolution ΔE and E was measured to be 250ps.

3.4 Data Acquisition

Data was acquired during three independent run periods, 16 March to 1 April 1990, 16 November to 26 November 1990 and 23 March to 21 April 1991. The experiment was performed at five different nominal beam energies, 66 MeV, 90 MeV, 120 MeV, 160 MeV and 200 MeV. Beam angles varied from 0°, 2°, to 4° and 10° during the first run period.

The beam bunch periods were set at 270 ns, 246 ns, 282 ns, 266 ns and 300 ns

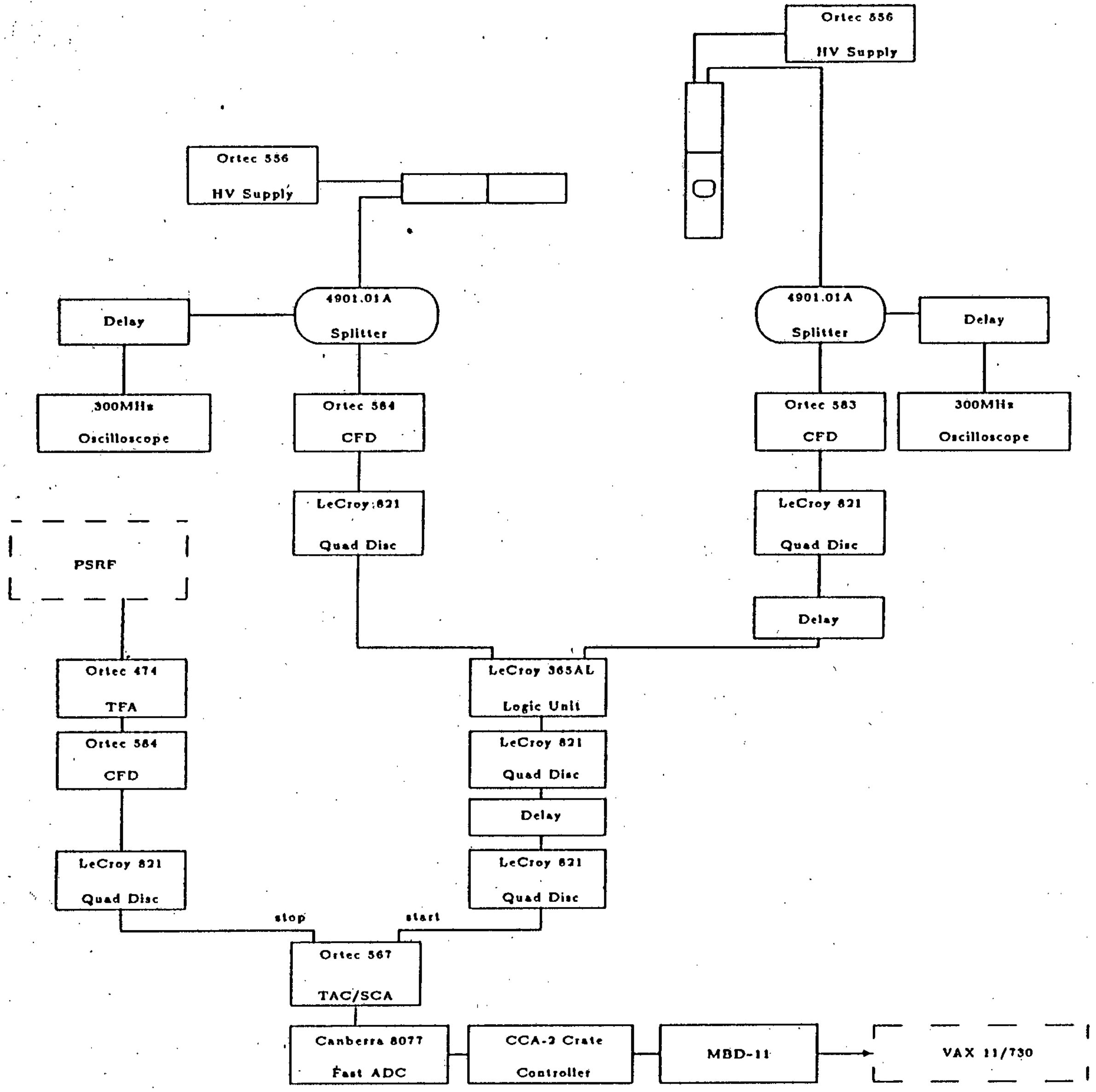

Figure 3.9: Electronics for beam resolution

for beam energies 200 MeV, 160 MeV, 120 MeV, 90 MeV and 66 MeV respectively. These were obtained by selecting one out of seven beam pulses, one out of six beam pulses, one out of six beam pulses, one out of five beam pulses and one out of five beam pulses respectively.

The beam current was approximately 200nA, 500nA, 500nA, 250nA and 1000nA, for 200 MeV, 160 MeV, 120 MeV, 90 MeV and 66 MeV respectively. The beam resolution varied between 500 ps and 850 ps.

Data was acquired using the XSYS software on the NAC VAX 11/730. The VAX is interfaced to the CAMAC crates through a Bi–Ra Microprogrammable Branch Driver(MBD–11).

The software is divided into the Data Acquisition Program(DAP) and the Event Analysis Language(EVAL). The DAP file contains the list of instructions that are loaded into the MBD–11. This controls the CAMAC crates and reads event data from the interface in the crates. EVAL program controls the incrementing of the histograms. See ref [Pil 90] for more details. Data were written to tape (density 6250bpi) for offline analysis on the University of Cape Town VAX (UCTVAX).

Chapter 4

Results and Discussion

4.1 Identification of states

The neutron energy spectrum from the ^{51}V(p,n)^{51}Cr reaction at 0° and energy 120 MeV is shown in figure 4.1.

Table 4.1 gives a list of peaks in the spectrum with corresponding excitation energies in ^{51}Cr.

The ground state of the ^{51}V nucleus has $J^\pi = \frac{7}{2}^-$ and T = $\frac{5}{2}$ ($T_z = -\frac{5}{2}$). The Gamow–Teller transition excites states in ^{51}Cr with $J^\pi = \frac{5}{2}^-, \frac{7}{2}^-, \frac{9}{2}^-$ and T = $\frac{3}{2}, \frac{5}{2}, \frac{7}{2}$ ($T_z = \frac{3}{2}$) [Rap 84]. The transition at E_x = 0.00 MeV is from the $\frac{7}{2}^-$ gs of ^{51}V to the $\frac{7}{2}^-$ ground state of ^{51}Cr. The Isobaric Analog of ^{51}V(g.s) in ^{51}Cr occurs at E_x = 6.61 MeV. The broad giant Gamow–Teller resonance occurs between excitation energies 8.00 and 19.00 MeV above the ^{51}Cr ground state.

The neutron energy spectra from ^{51}V(p,n) at 0° and energies 90, 120, 160 and 200 MeV are shown in figure 4.2.

Excitation Energy (MeV)	Peak
0.00	Ground state
6.61	Isobaric Analog State
8.00 -19.00	giant Gamow-Teller resonance

Table 4.1: Peaks of interest in the ^{51}V(p,n)^{51}Cr spectrum with their corresponding excitation energies.

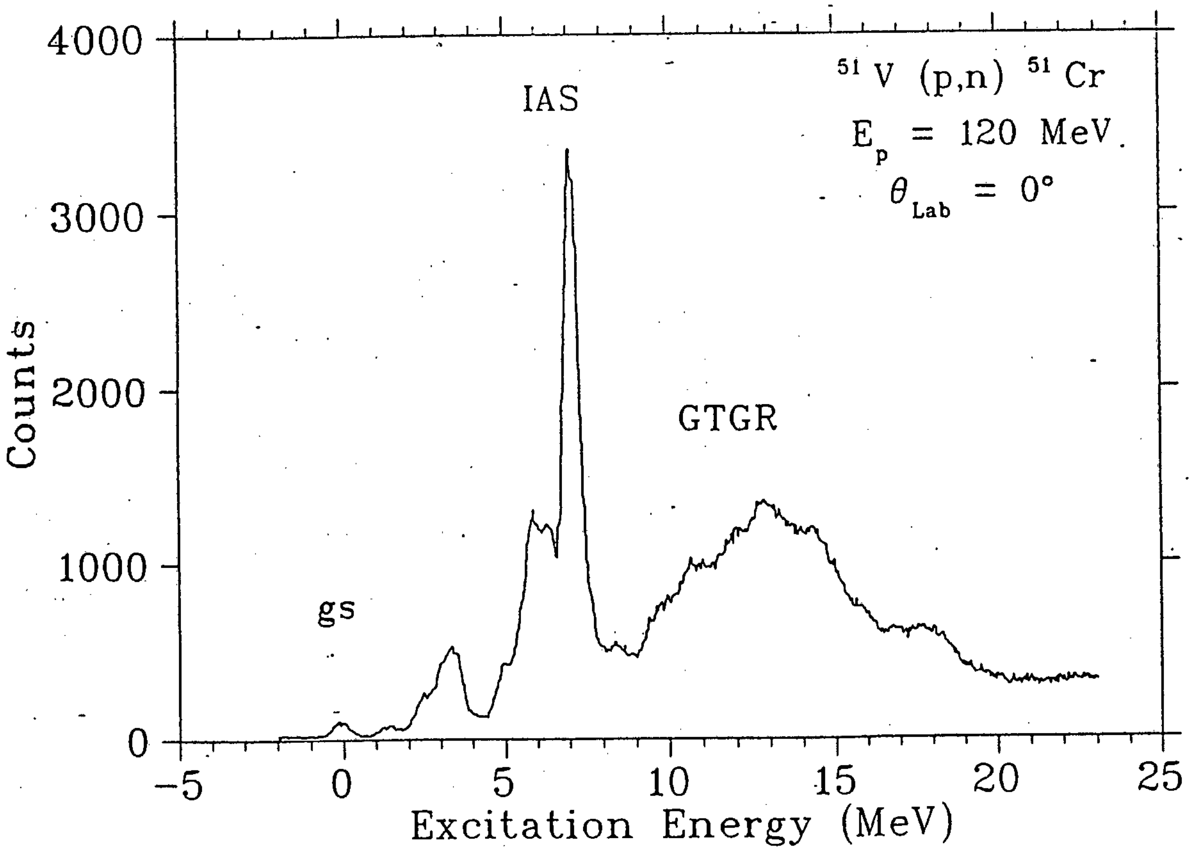

Figure 4.1: The neutron energy spectrum from ^{51}V at 0° and beam energy 120 MeV.

Additional evidence in support of the identification of the peaks as GT transitions is their increased strengths relative to the Isobaric Analogue State (IAS) transition at 200 MeV compared to 90 MeV. This increase is consistent with an increase in $(\frac{V_{\sigma\tau}}{V_\tau})^2$ as suggested in [Go2 80].

In figure 4.3 the neutron energy spectra at beam energy 120 MeV and beam angles 0° to 4° is shown as a function of excitation energy. The neutron energy spectra at beam energy 160 MeV and beam angles 0° to 2° is shown in figure 4.4 as a function of excitation energy. Figure 4.5 shows the neutron energy spectra at beam energy 200 MeV and beam angles 0° to 4°.

The $\theta = 0°$ spectra are dominated by the L = 0 GT resonances. As θ_{LAB} increases L>0 resonances are expected to emerge [Gaa 81]. In order to obtain the "background" contribution in the 0° spectrum of other than the Fermi or GT processes, an empirical approach can be used [Goo 82]. A spectrum taken at an angle near 0° can be scaled so that known ΔL=0 transitions have yields equal to those in the 0° spectrum. The 0° spectrum is then subtracted from the normalized near 0° spectrum. The resulting spectrum is assumed to represent the non $\Delta L = 0$ "background" shape. However, this is beyond the scope of the present work.

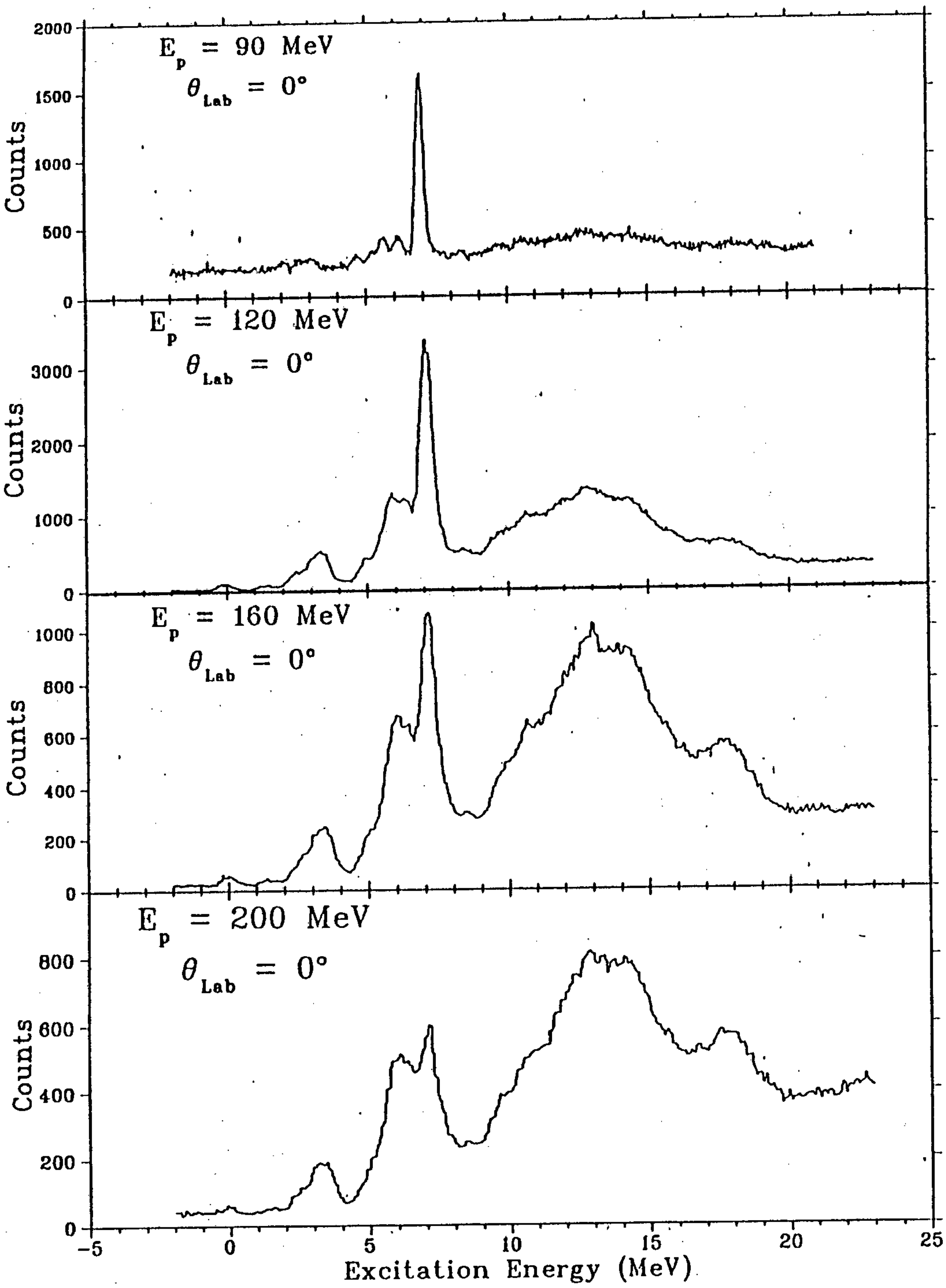

Figure 4.2: The neutron energy spectra at beam angle 0° at four different beam energies.

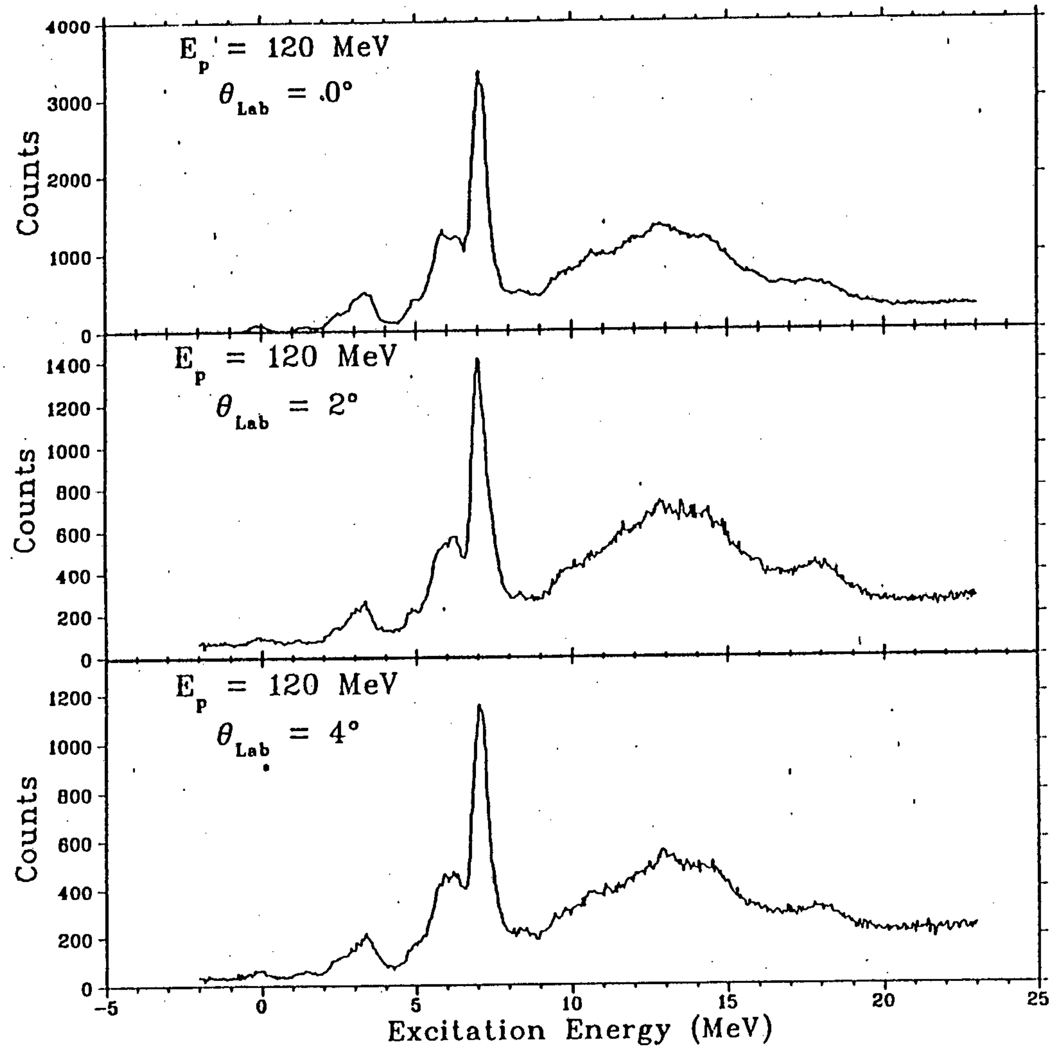

Figure 4.3: The neutron energy spectra at beam energy 120 MeV and beam angles 0° to 4°.

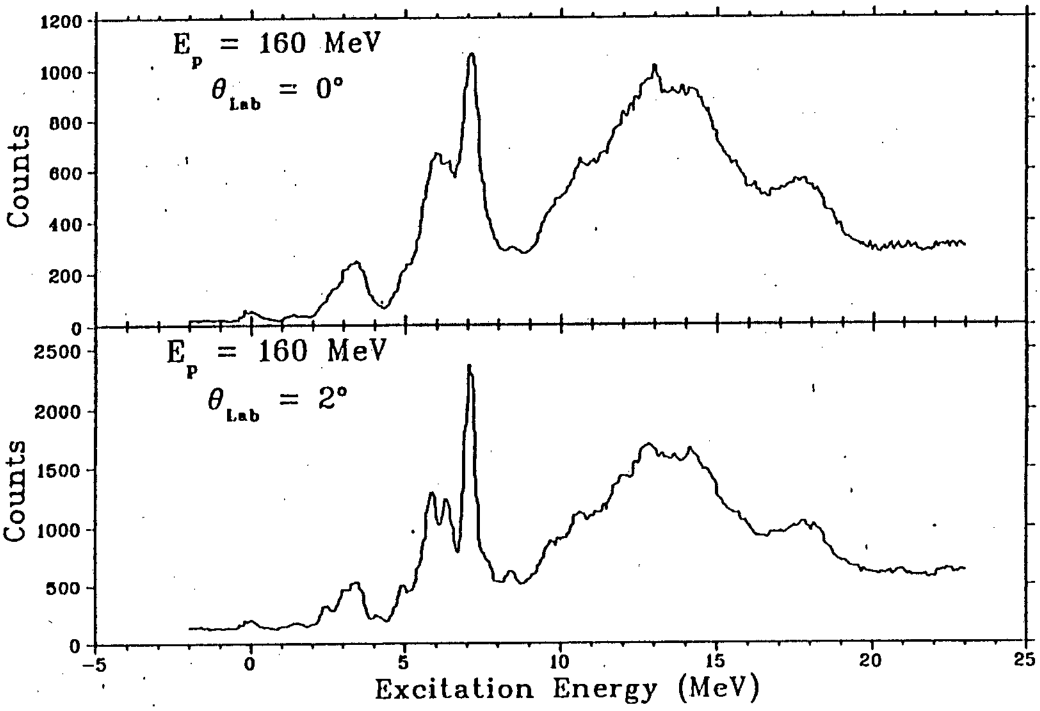

Figure 4.4: The neutron energy spectra at beam energy 160 MeV and beam angles 0° to 2°.

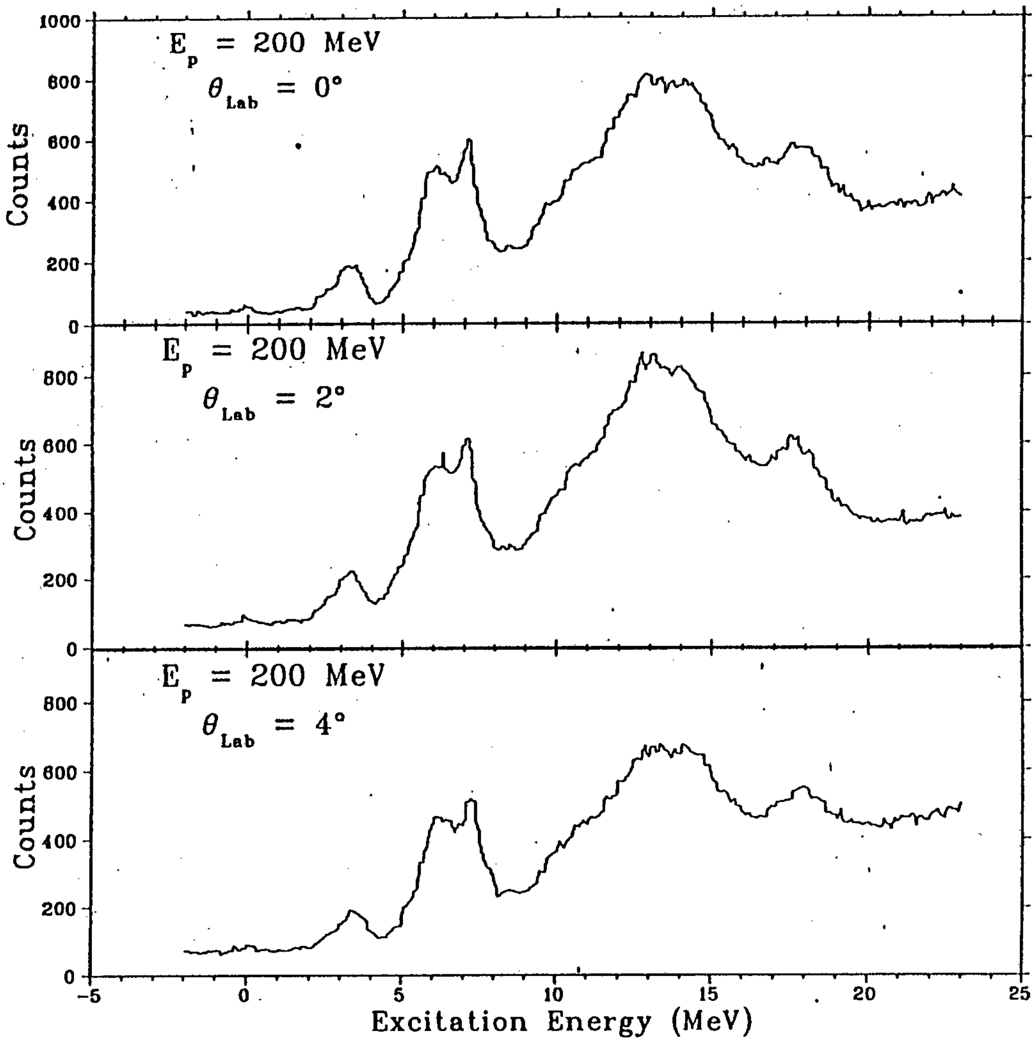

Figure 4.5: The neutron energy spectra at beam energy 200 MeV and beam angles 0° to 4°.

4.2 The yield of each state.

The yields were found by fitting individual gaussian lineshapes to each peak of interest using a gaussian fitting program; the non-linear least squares minimization program MINUIT [Jam 75] from the CERN library. The background which is due to low energy neutron and cosmic rays was estimated by fitting a quadratic background.

Figure 4.6 shows the fitted 90 MeV spectra. At this beam energy the resolution is not good enough to see the ground state. The yield on the IAS was extracted by fitting three gaussian on the IAS and the two neighboring Gamow–Teller peaks. The broad giant Gamow–Teller peak was modelled by fitting one gaussian.

The peaks on the 120 MeV spectra were modelled by fitting one gaussian to the ground state, four gaussians to the IAS and the three neighboring Gamow-Teller peaks, and three gaussians to the giant Gamow–Teller resonance. The representative fits are shown in figure 4.7. The fit to the ground state is shown in the magnified window.

The ground state on the 160 MeV spectra was fitted with one gaussian. Four gaussians were fitted to the IAS and the three neighboring Gamow–Teller peaks. The giant Gamow–Teller peak is fitted with the three gaussians. The representative fits are shown in figure 4.8. The fit to the ground state is shown in the magnified window.

The representative 200 MeV spectra are shown in figure 4.9. Contributing to the smallness of the ground state peak at 200 MeV is the reduction in the excitation probability at this energy. The tiny ground state peak was fitted with one gaussian. The IAS and its neighboring peaks were fitted with four gaussians. The giant Gamow–Teller peak was fitted with three gaussians. The fit to the ground state is shown in the magnified window. More fitted spectra are shown in appendices A – D.

When fitting the gaussians to the 90, 120, 160 MeV spectra no constraints were made on the positions and widths of the peaks. The IAS and its two neighbouring states are close to each other at 200 MeV proton energy. At this energy the width of

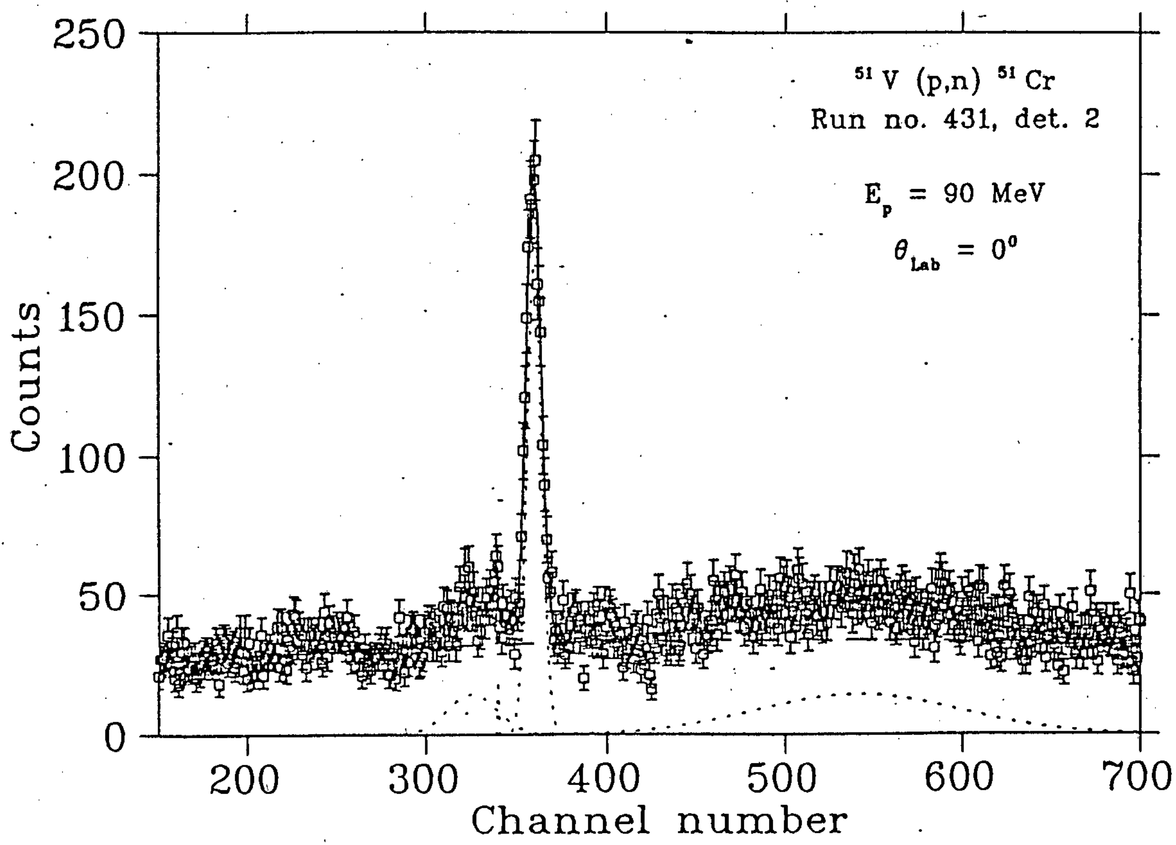

Figure 4.6: The fitted spectrum of run 431 detector 2 at proton energy 90MeV and beam angle 0°.

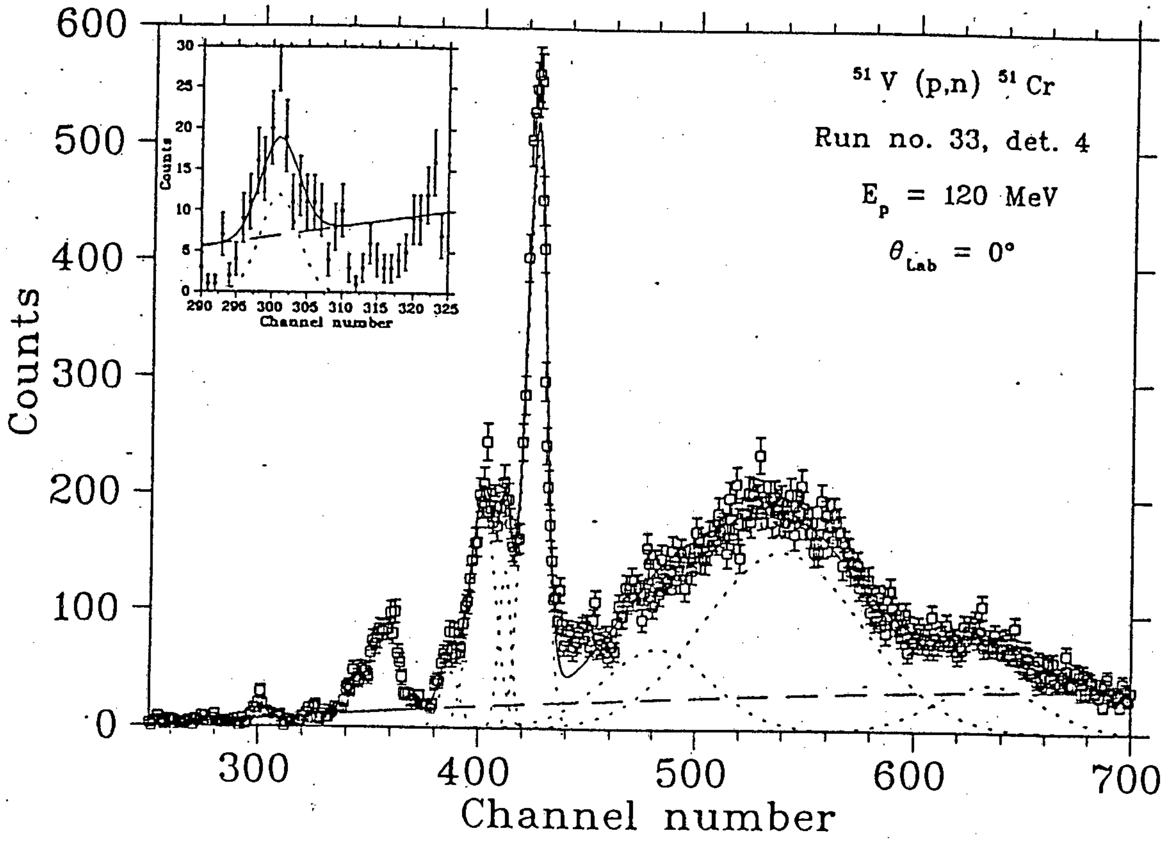

Figure 4.7: The fitted spectrum of run 33 detector 4 at proton energy 120 MeV and beam angle 0°.

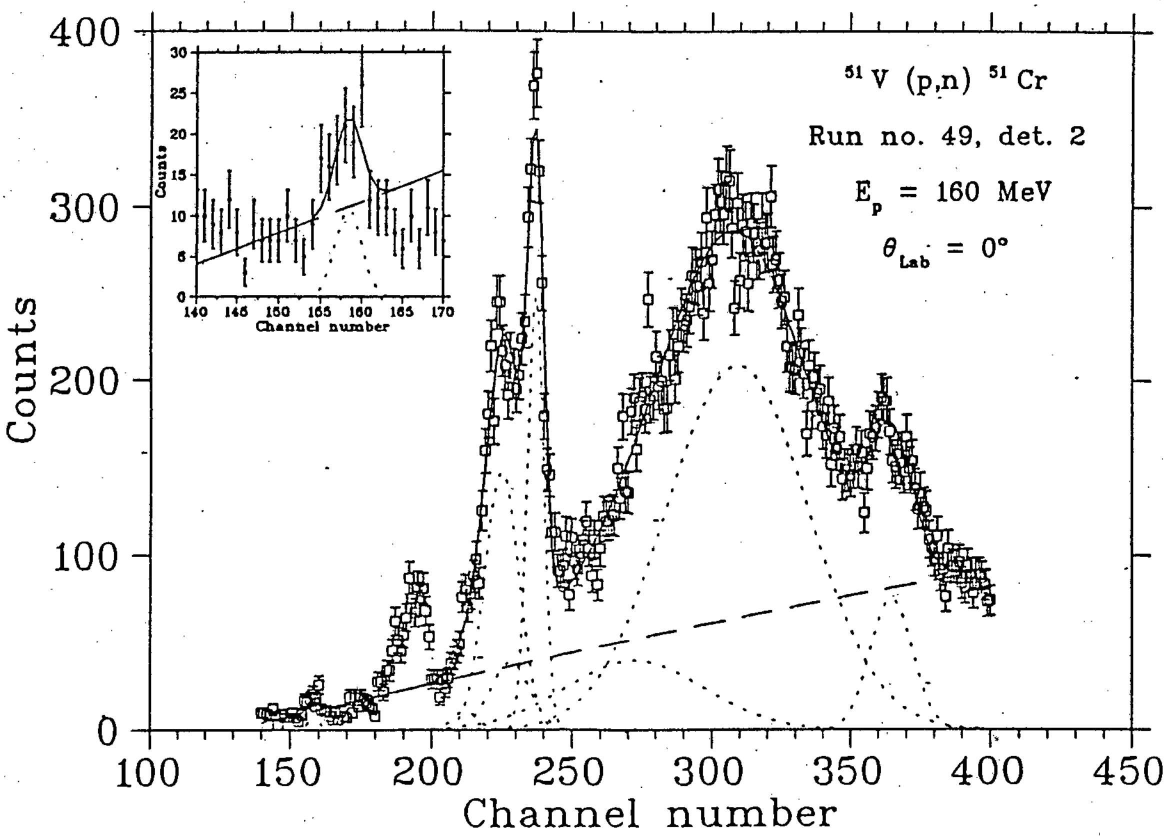

Figure 4.8: The fitted spectrum of run 49 detector 2 at proton energy 160 MeV and beam angle 0°.

the IAS was fixed to be the same as the average of the widths of the IAS at 120 MeV and 160 MeV. The IAS width is consistent with our energy resolution, as expected.

Figure 4.2 shows the best neutron energy spectra at each beam energy. Appendix D.1 to D.6 show some spectra at 200 MeV from different run numbers, where we could hardly see (or fit on) ground state. The error bars were calculated directly from the non-linear least squares minimization program. These error bars could have been reduced by collecting more data at each energy. The ground state of the 120 and 160 MeV in the appendix B to C reflect the same pattern.

The representative fit on the spectra at beam angles 2° to 4° are shown in figures 4.10 to 4.14.The yield of each peak of interest was obtained by integrating the area under the gaussian.

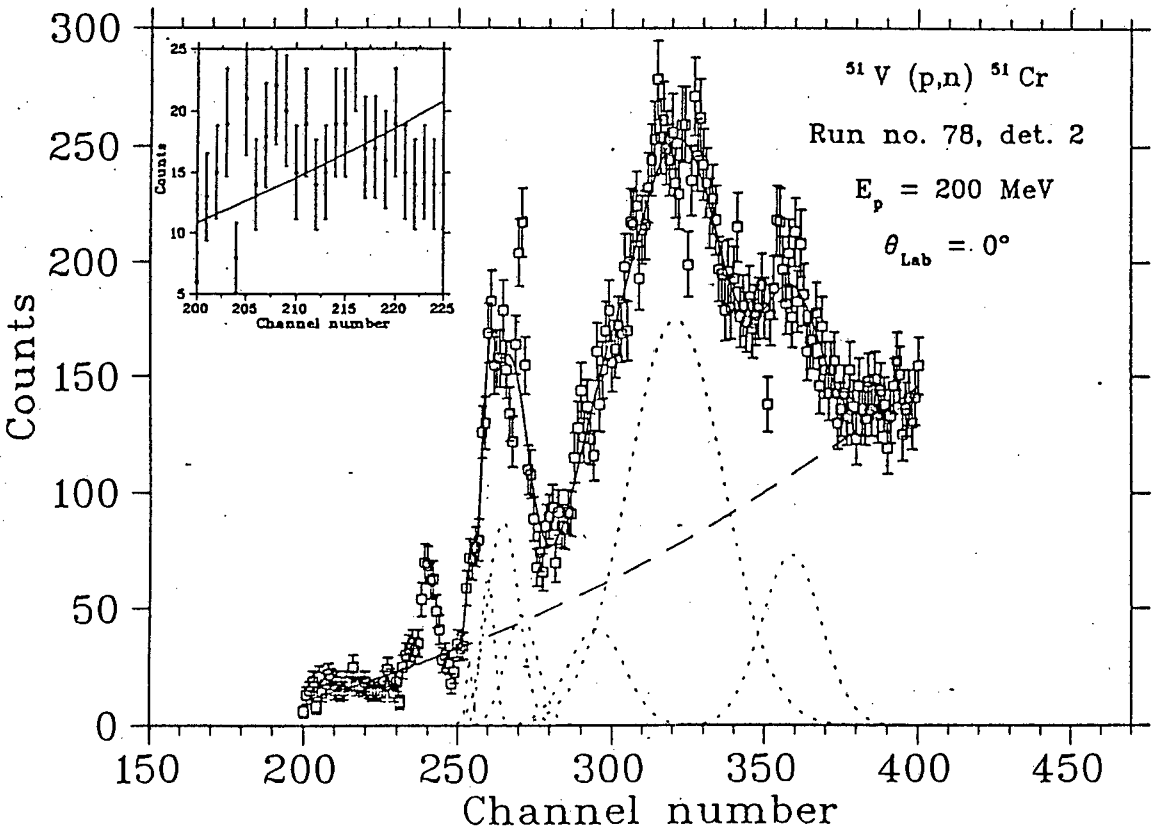

Figure 4.9: The fitted spectrum of run 78 detector 2 at proton energy 200 MeV and beam angle 0°.

4.3 Cross sections.

Once the yield of each peak is known the cross sections were calculated using eqn 4.1

$$\sigma = \frac{Y}{N\Delta\Omega t\,[LT\,\epsilon(E)]} \tag{4.1}$$

where:

- Y is the number of neutrons detected,
- N is the number of protons incident on the ^{51}V target,
- $\Delta\Omega$ is the solid angle subtended by the detectors,
- t is the target thickness [nuclei/cm^2],
- L is the fractional livetime of the data acquisition system,
- T is the neutron transmission factor from target to detector,
- $\epsilon(E)$ is the efficiency for detecting a neutron of energy E incident on the front face of the detector.

The value of the term in brackets was as calculated by [New 91].

The ground state cross section is plotted as a function of beam energy in figure 4.15. It remains constant with beam energy, and ranges between 0.04 mb/sr and 0.08 mb/sr. The cross-section at 160 MeV is in good agreement with the value of 0.09 mb/sr determined by Rapaport et al. [Rap 84] [Tad 87].

The Isobaric Analog State cross section is plotted as a function of beam energy in figure 4.16. It decreases from 6.0 mb/sr to 3.0 mb/sr. The cross section at 160 MeV is in good agreement with the estimated value of 3.1 mb/sr from Rapaport et al. [Rap 84].

The giant Gamow-Teller resonance cross section is plotted as a function of beam energy in figure 4.17. It increases rapidly with beam energy ranging between 7.0 mb/sr and 40.0 mb/sr.

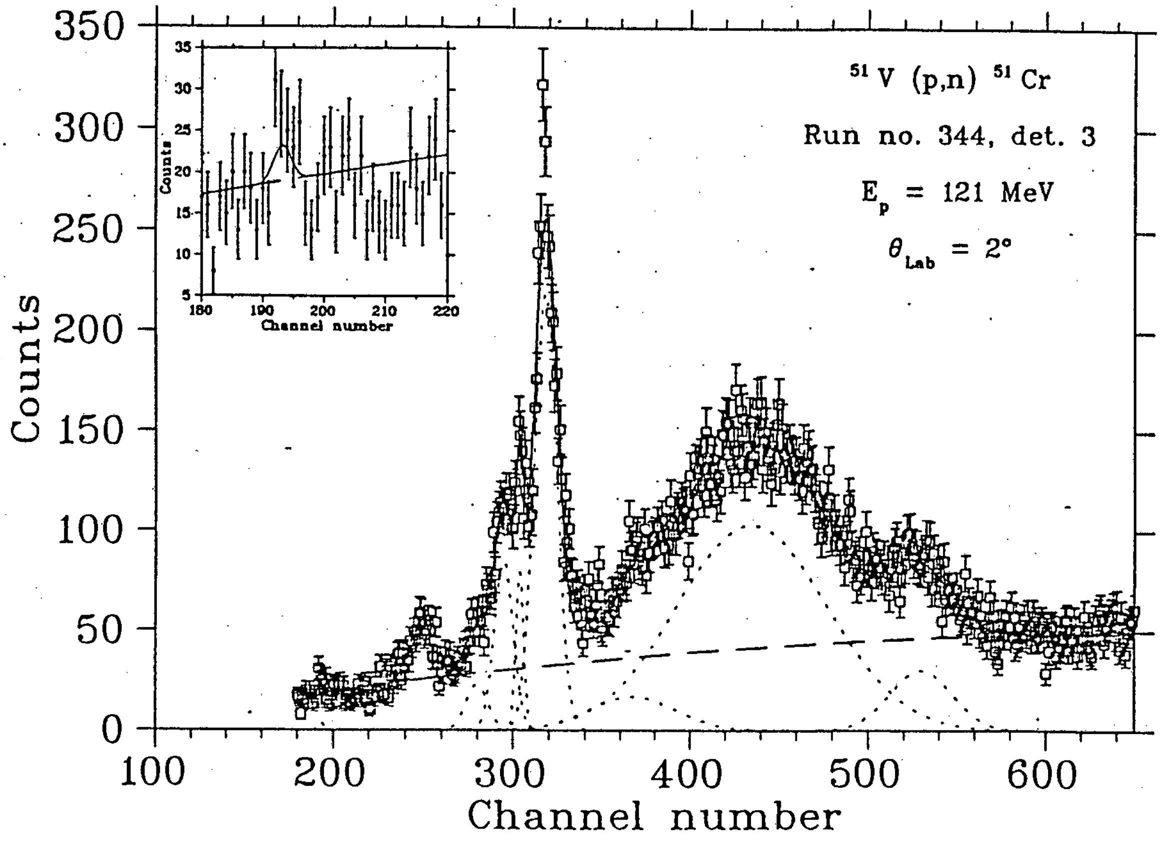

Figure 4.10: The fitted spectrum of run 344 detector 3 at proton energy 120 MeV and beam angle 2°.

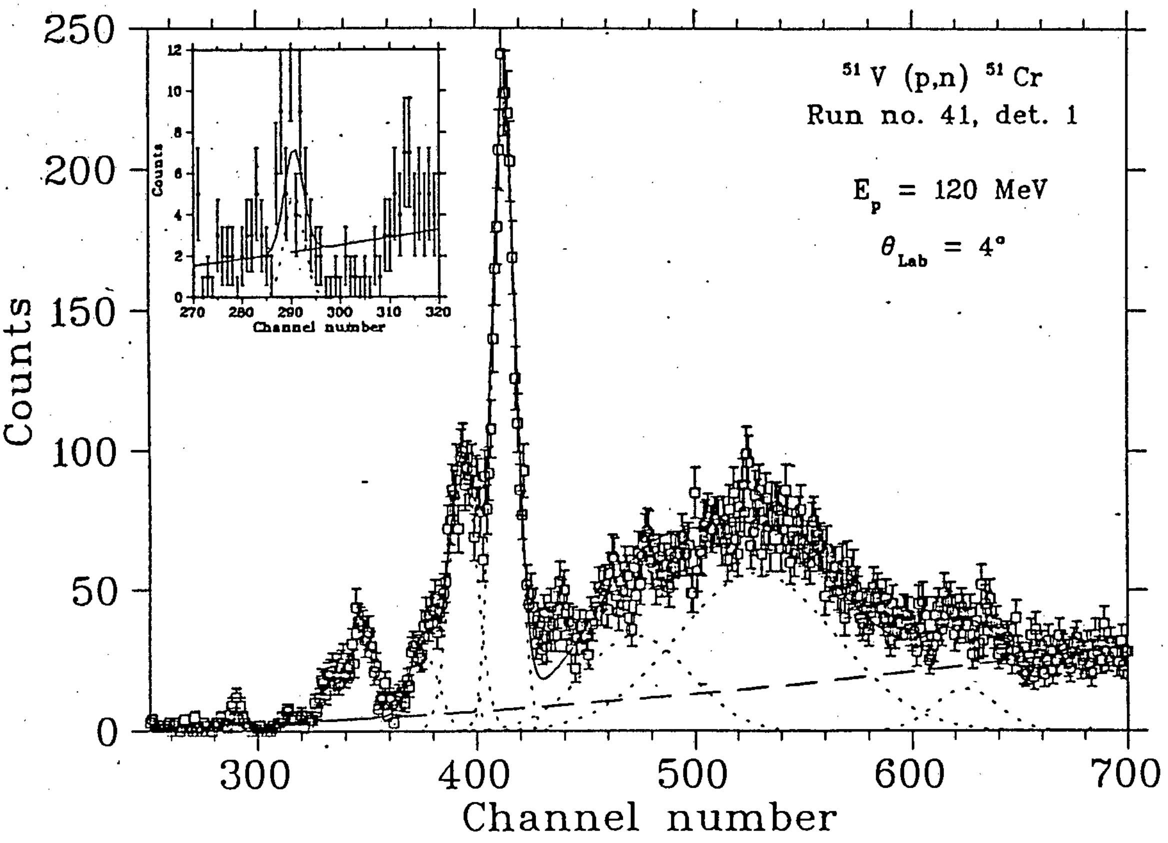

Figure 4.11: The fitted spectrum of run 41 detector 1 at proton energy 120 MeV and beam angle 4°.

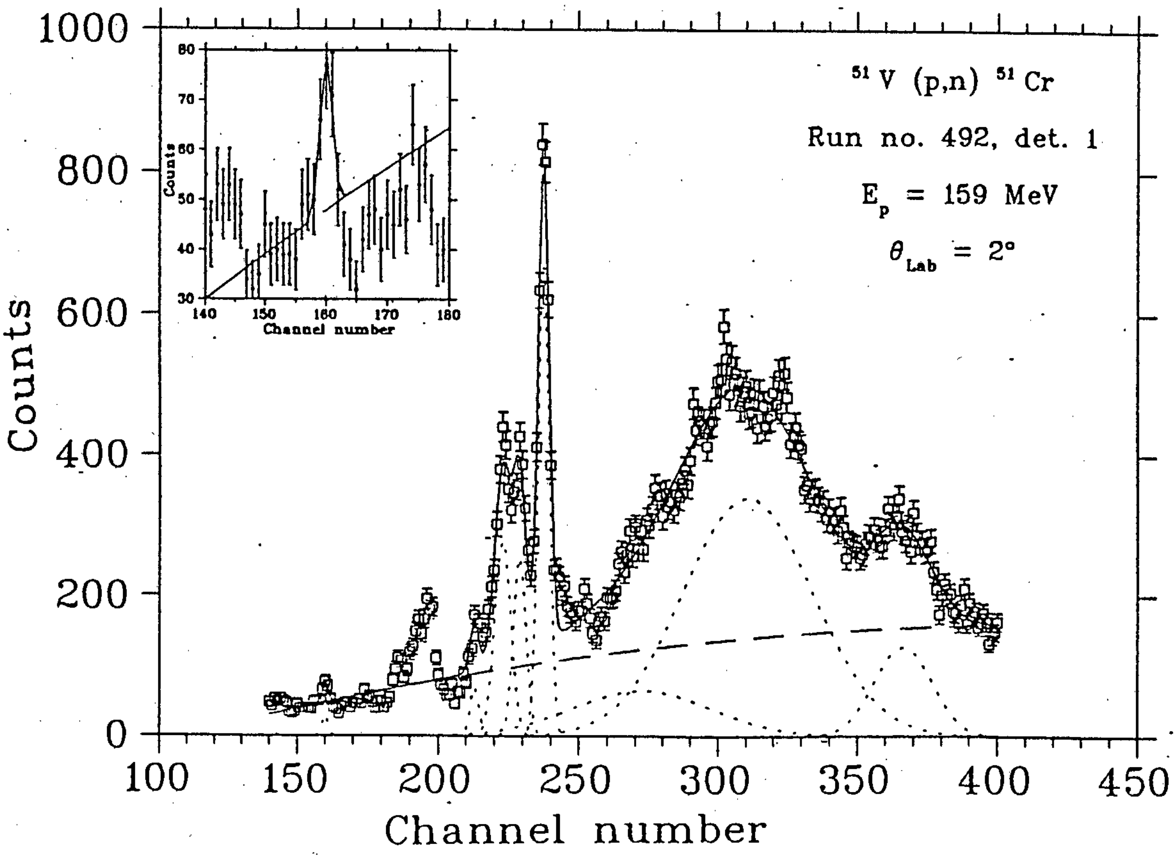

Figure 4.12: The fitted spectrum of run 492 detector 1 at proton energy 160 MeV and beam angle 2°.

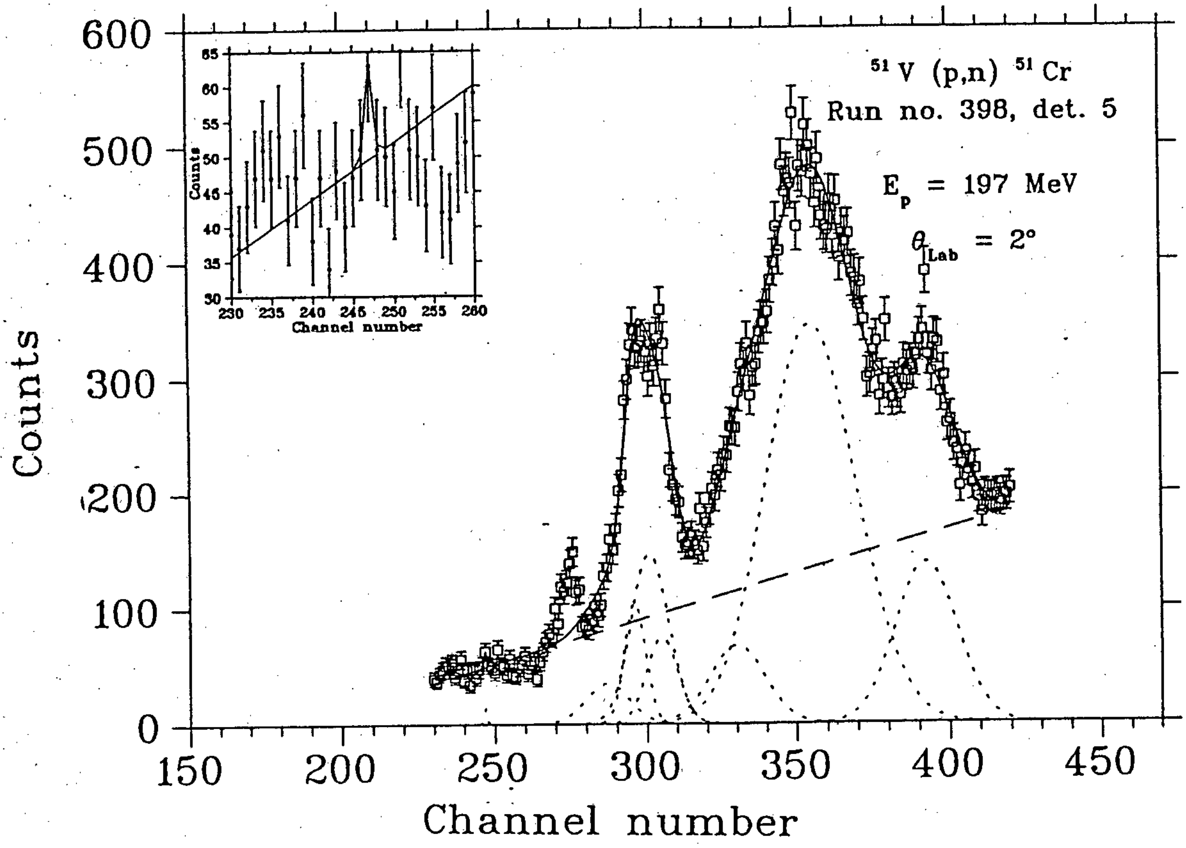

Figure 4.13: The fitted spectrum of run 398 detector 5 at proton energy 200 MeV and beam angle 2°.

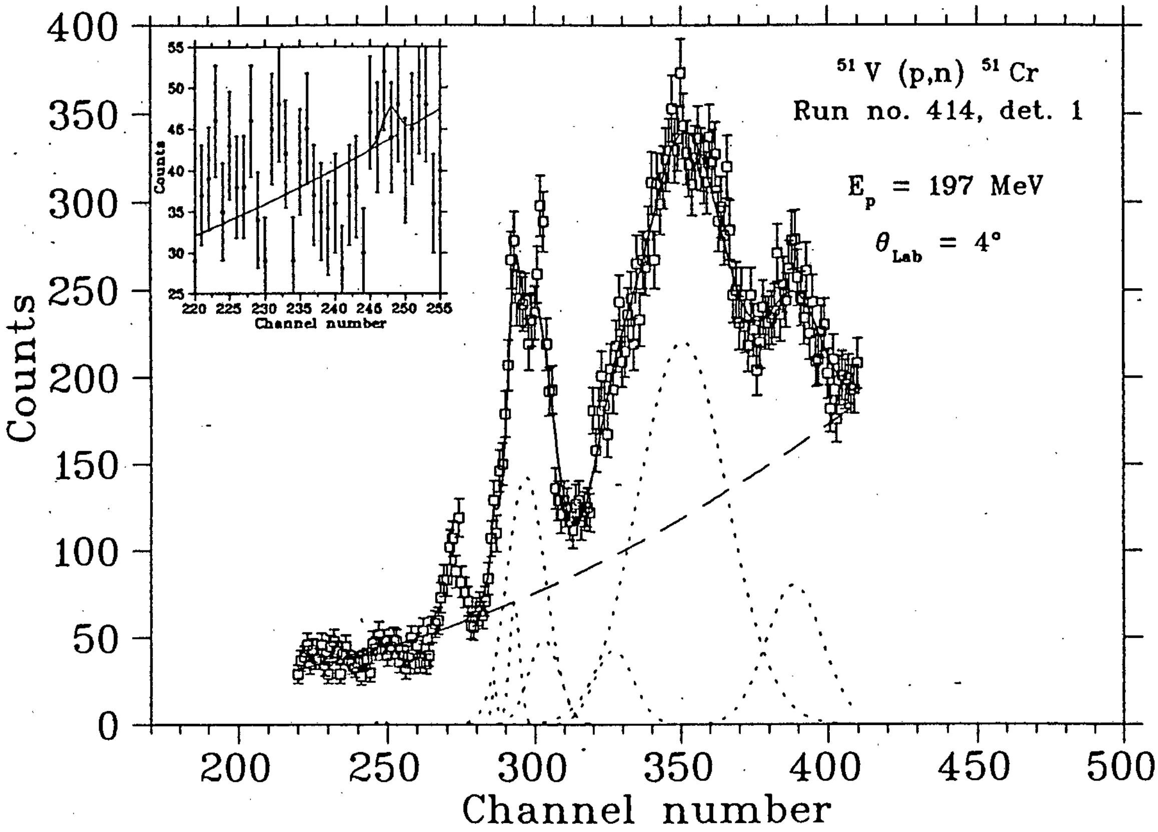

Figure 4.14: The fitted spectrum of run 414 detector 1 at proton energy 200 MeV and beam angle 4°.

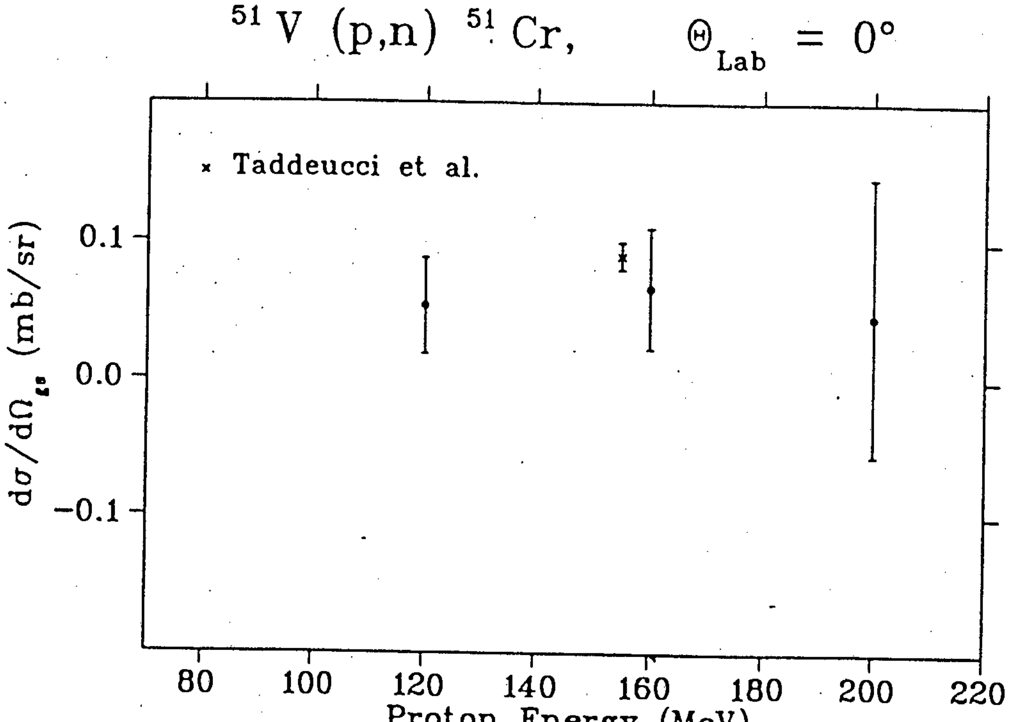

Figure 4.15: The cross section of the transitions to the ^{51}Cr ground state at three different beam energies compared with the measurements of Taddeucci et al. at 160 MeV. reference [Tad 87].

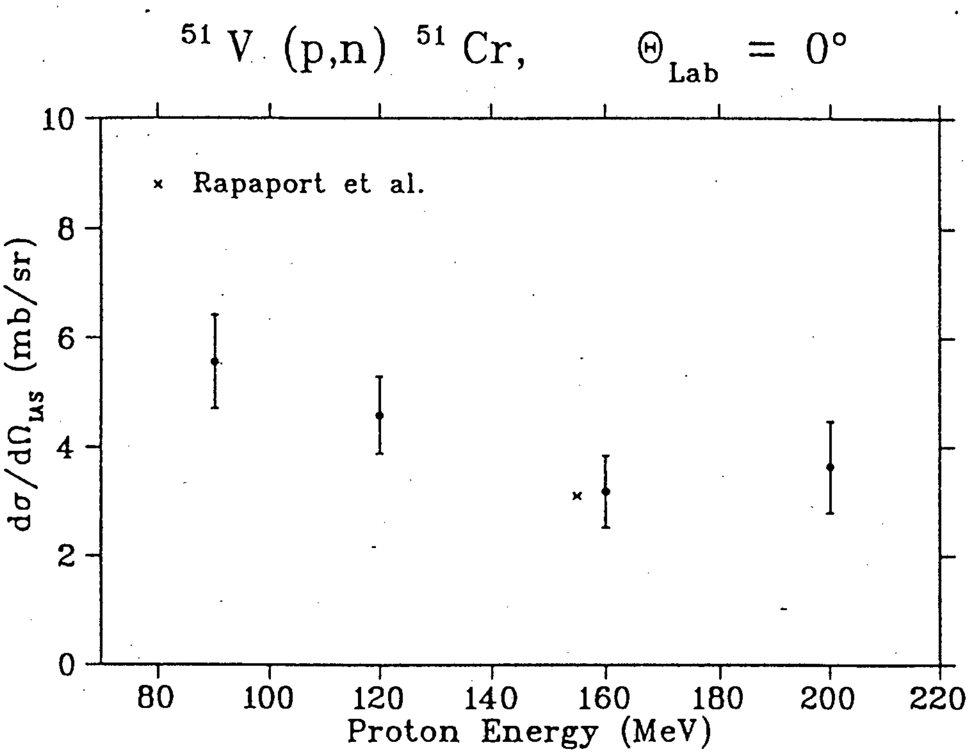

Figure 4.16: The cross sections of the Isobaric analog state at three different beam energies compared to the estimated value by Rapaport et al. measurement at 160 MeV. reference [Rap 84].

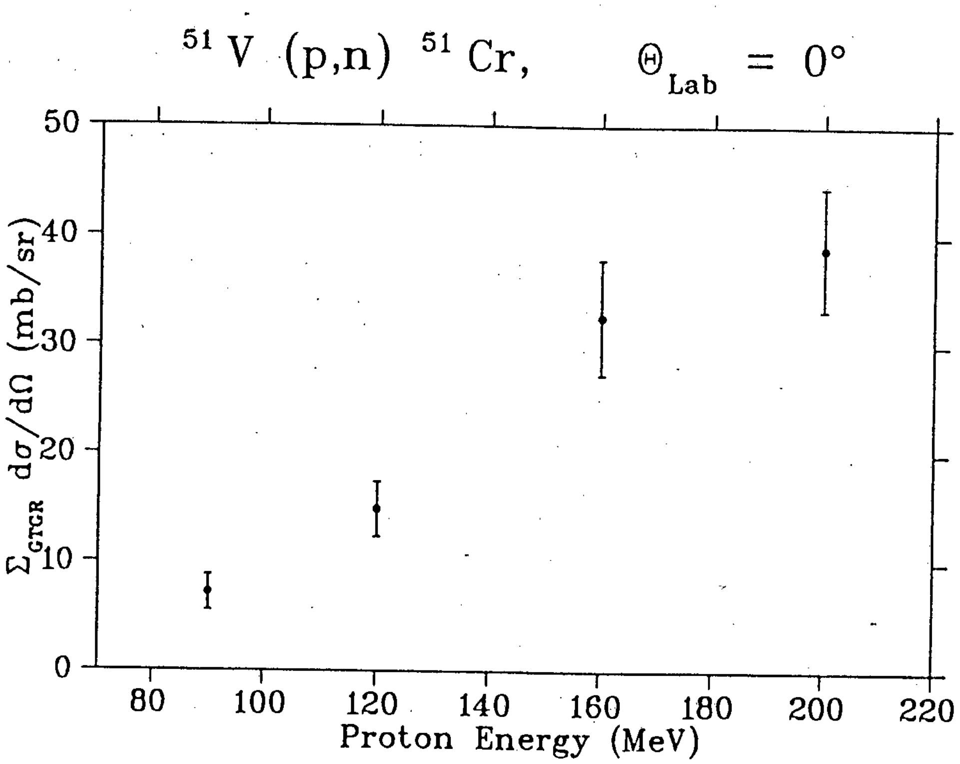

Figure 4.17: The cross sections of the giant Gamow-Teller resonance at three different beam energies.

4.4 The Gamow–Teller strength.

The strength of the ground state in beta decay was calculated using the eqn 2.1.

$$(G_V)^2 B(F) + (G_A)^2 B(GT) = \frac{K}{ft}$$

The value of the Fermi strength was obtained from 2.8

$$B(F) = N - Z = 5$$

The (p,n) reaction was calibrated to beta decay using the ground state. The (p,n) reaction and beta decay are related to each other by eqn 2.3.

$$B(GT)_{p,n} = \frac{(2J_i + 1)_{p,n}}{(2J_i + 1)_{beta}} B(GT)_{beta}$$

The strength of the giant Gamow–Teller resonance was calculated using the proportionality relation 2.4.

$$B(GT)_2 = \frac{\sigma_2}{\sigma_1} \frac{k_1}{k_2} \frac{N^1_{\sigma\tau}}{N^2_{\sigma\tau}} B(GT)_1$$

B(GT)$_1$ is the strength of the ground state in (p,n) reaction. The ratio $\frac{\sigma_2}{\sigma_1}$ of the cross sections is independent of the solid angle and the target thickness. The ratio $\frac{k_1}{k_2}$ depends on the neutron energies only. The ratio $\frac{N^1_{\sigma\tau}}{N^2_{\sigma\tau}}$ is approximately equal to unity [Tad 87].

The strength is plotted as a function of beam energy in figure 4.18. The shell model calculation predicted the total Gamow–Teller strength of 20.14. Rapaport et al. could only probe the total Gamow–Teller strength of 12.6, reference [Rap 84] at beam energy 160 MeV. In figure 4.19 the strength in the giant Gamow–Teller resonance is compared with total strength predicted by shell model calculation and Rapaport et al. measurement.In the present experiment at 160 MeV, the Gamow–Teller strength in the giant Gamow–Teller resonance is 11.24. More strength is probed at higher energy.

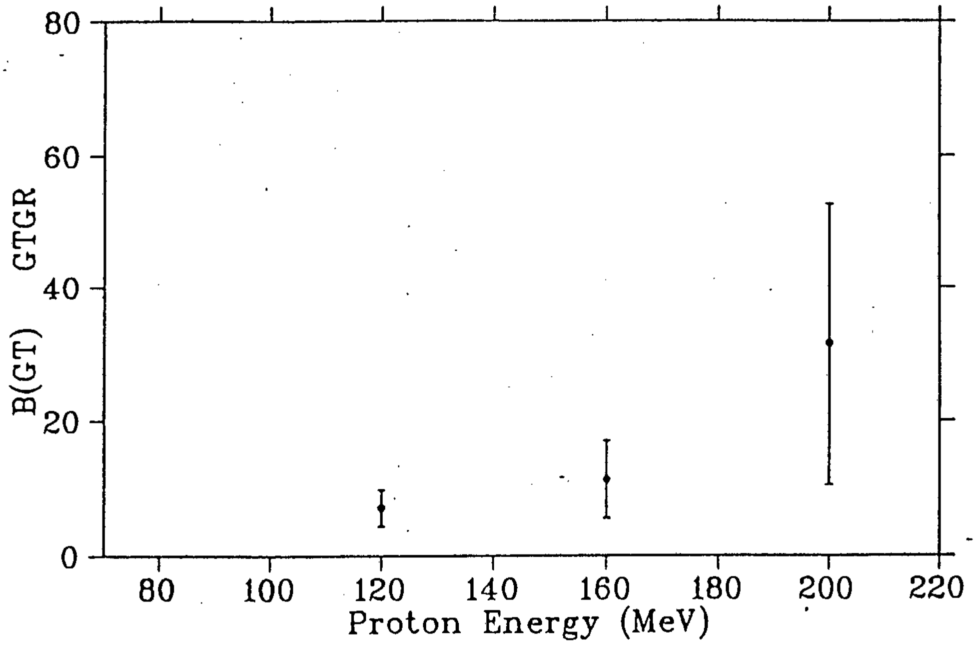

Figure 4.18: The Gamow-Teller strength as a function of beam energy.

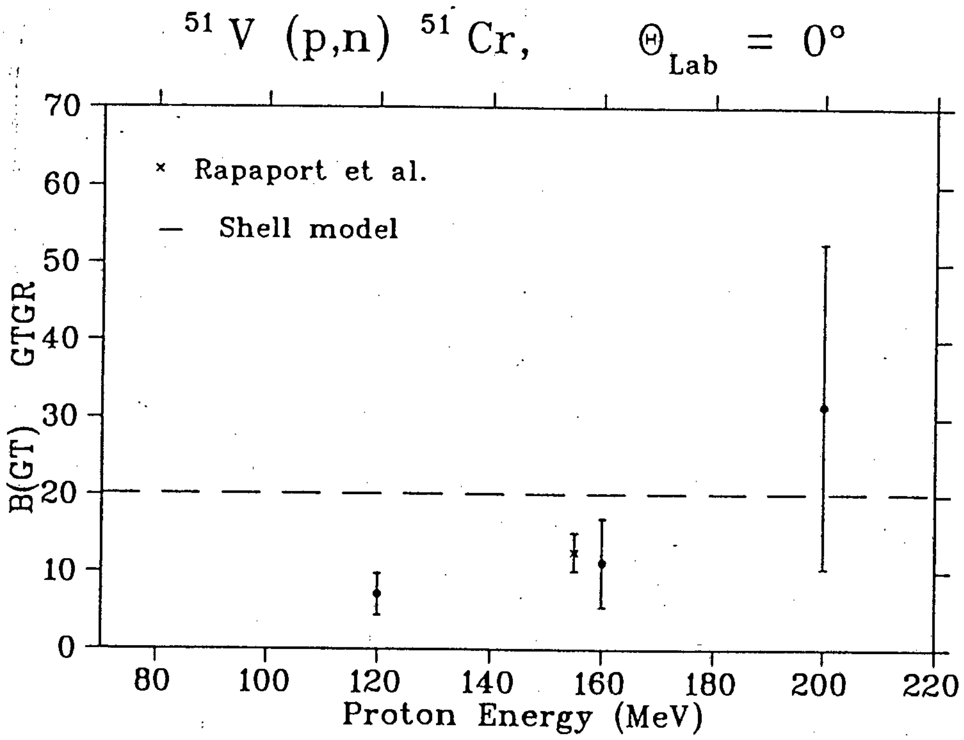

Figure 4.19: The Gamow-Teller strength as a function of beam energy compared to the Rapaport et al. measurement at 160 MeV, and also to the shell model calculation. reference [Rap 84].

4.5 The fraction of Gamow–Teller strength in IAS

For even A nuclei the ground state has spin parity $J^P = 0^+$ and the transition to the IAS only has a contribution from the Fermi operator. However in odd A nuclei such as ^{51}V where the ground state is $\frac{7}{2}^-$ the Gamow–Teller operator also contributes to the transition to the IAS. The fraction of Gamow–Teller strength in the IAS transition is estimated using eqn 2.7:

$$f_{GT} = \left[1 + \frac{B(F)}{B(GT)R(E_p)^2}\right]^{-1}$$

The R(E_p) values for 120 and 160 MeV were obtained from [Goo 90]. The value for 200 MeV was estimated using eqn 2.5

$$R(E_p) = \frac{E_p}{E_\circ}$$

where $E_\circ = 45$ MeV.

The Gamow–Teller strength in the Isobaric Analog State B(GT) was estimated using the equation

$$B(GT) = B(GT)_{gs}\left(\frac{\sigma_{IAS}}{\sigma_{gs}}\right) - \frac{B(F)}{R(E_p)^2}$$

where:

- $B(GT)_{gs}$ is the Gamow-Teller strength in the ground state,
- σ_{IAS} is the cross section of the Isobaric Analog State,
- σ_{gs} is the cross section of the ground state,
- B(F) is the Fermi transition strength,
- and $R(E_p)$ is defined in equation 2.5.

The fraction of Fermi strength in IAS is estimated using eqn 2.6.

$$f_F = 1 - f_{GT}$$

The cross section of the the Fermi in the IAS is estimated by

$$\sigma_F = \sigma_{IAS} \times f_F$$

where

- σ_{IAS} is the measured cross section.

The ratio of the Fermi cross section to the Fermi strength–Unit Fermi cross section, $\widehat{\sigma}_F$ is calculated using

$$\widehat{\sigma}_F = \frac{\sigma_F}{B(F)}$$

The Gamow–Teller and Fermi fractions for three different beam energies are tabulated in table 4.2.

Proton Energy (MeV)	BGT(IAS)	FGT(IAS)	FFermi	UnFeCro
120	1.26 ± 0.48	0.03 ± 0.01	0.96 ± 0.37	0.89 ± 0.37
160	0.98 ± 1.69	0.005 ± 0.007	0.98 ± 0.50	0.63 ± 0.35
200	2.57 ± 1.69	0.04 ± 0.03	0.96 ± 0.69	0.69 ± 0.49

Table 4.2: The fraction of the Fermi and Gamow-Teller transition in the isobaric analog transition.

- BGT(IAS) - Gamow-Teller strength in the Isobaric Analog State (B(GT)).
- FGT(IAS) - Fraction of Gamow–Teller transition in the Isobaric Analog State (f_{GT}).
- FFermi - Fraction of Fermi transition in the Isobaric Analog State (f_F).
- UnFeCro - Unit Fermi cross section $\widehat{\sigma}_F$ is the ratio of the Fermi cross section to the Fermi strength.

Chapter 5

Conclusion

The ^{51}V(p,n)^{51}Cr reaction has been used to study the cross sections of the ground state, Isobaric Analog State and giant Gamow-Teller resonance at four different beam energies, viz. 90, 120, 160 and 200 MeV. The cross section of the ground state at 160 MeV is in good agreement with 0.09 ± 0.01mb/sr determined by Rapaport et al. [Rap 84] [Tad 87]. The cross section of the Isobaric Analog State at 160 MeV is in good agreement with the value of 3.1 mb/sr estimated by Rapaport et al. [Rap 84]. The cross section of the giant Gamow-Teller resonance increases rapidly from 7.0 mb/sr at 90 MeV to 40.0 mb/sr at 200 MeV.

The Gamow-Teller strength in the IAS (BGT(IAS)) ranges from 1.26 ± 0.48 at 120 MeV to 2.57 ± 1.69 at 200 MeV. The fraction of the Gamow-Teller strength contribution in the IAS ranges between 0.005 ± 0.008 at 160 MeV and 0.04 ± 0.03 at 200 MeV. The fraction of the Fermi strength contribution is close to one as expected; it ranges between 0.96 ± 0.37 at 120 MeV and 0.98 ± 0.50 at 160 MeV.The unit Fermi cross section was estimated and ranges between 0.63 ± 0.35 at 160 MeV and 0.89 ± 0.37 at 120 MeV.

Shell model calculation, as discussed by Rapaport et al. [Rap 84], estimated the total Gamow-Teller strength of 20.14. The empirical total Gamow-Teller strength of 12.6 ± 2.5 was obtained at 160 MeV [Rap 84]. The giant Gamow-Teller strength of 11.2 ± 5.8 obtained in the present work, is 56% of the total estimated Gamow-Teller strength and it ranges from 7.1 ± 2.7 at 120 MeV to 31.5 ± 21.1 at 200 MeV.

From the 3(N-Z) sum rule one expects $B(GT_-) = 15$ if all the $B(GT_+)$ strength

	$\sum B(GT_-)_{Empirical}$	$S_{\beta^-_{theoretical}}$	$Q_f = \frac{\sum B(GT_-)}{S_{\beta^-}}$	Ref.	E_p (MeV)
${}^{51}_{23}$V(p,n)^{51}Cr	12.6 ± 2.5	20.14	0.63 ± 0.13	[Rap 84]	160
${}^{51}_{23}$V(p,n)^{51}Cr	11.2 ± 5.80	20.14	0.56 ± 0.29	[this work]	160
${}^{54}_{26}$Fe(p,n)^{54}Co	7.8 ± 1.9	16.3	0.48 ± 0.12	[Rap 83]	160
${}^{54}_{24}$Cr(p,n)^{54}Mn	7.7 ± 1.9	20.5	0.38 ± 0.09	[Wan 88]	120
${}^{57}_{26}$Fe(p,n)^{57}Co	10.2 ± 2.6	-	-	[Wan 88]	120
${}^{58}_{28}$Ni(p,n)^{58}Cu	7.4 ± 1.8	19.2	0.39 ± 0.09	[Rap 83]	160

Table 5.1: The Gamow-Teller strength for some medium mass nuclei.

were Pauli blocked. In the present work, at 120 MeV the B(GT_-) strength is less than that predicted by the sum rule by 7.9 and at 160 MeV is less than the sum rule prediction by 4.8. At 200 MeV the strength was overestimated at 31.5 ± 21.1 due to the ground state cross section which could not be accurately determined.

The quenching factors $Q_f = 0.353$, 0.556 and 1.564 were observed at 120, 160, and 200 MeV proton energies respectively. This Q_f increases with proton energy. The Q_f values of some medium mass nuclei are shown in table 5.1.

If the full GT strength could be integrated out of the background the Q_f value is expected to be unity. This work shows that the Q_f value is even less than the value estimated by Rapaport et al. (see table 5.1). The spectra were analyzed by assuming quadratic background. This fit leads to errors in the giant GT resonance and the ground state yields. For the ground state transition, the background resulting from the global fit underestimate the ground-state yield, as reflected in figure 4.15, but this value of the cross section is in agreement with Taddeucci et al. measurements.[Tad 87].

Comparison with other medium mass nuclei indicates large variation of Q_f values. The additional GT strength may possibly reside in many small transitions above 20 MeV excitation energy and in the two states neighbouring the Isobaric Analog State. The large variation of the Q_f values deserves further study.

Appendix A

Fitted 90 MeV spectra

A.1 Run 431 detector 1.

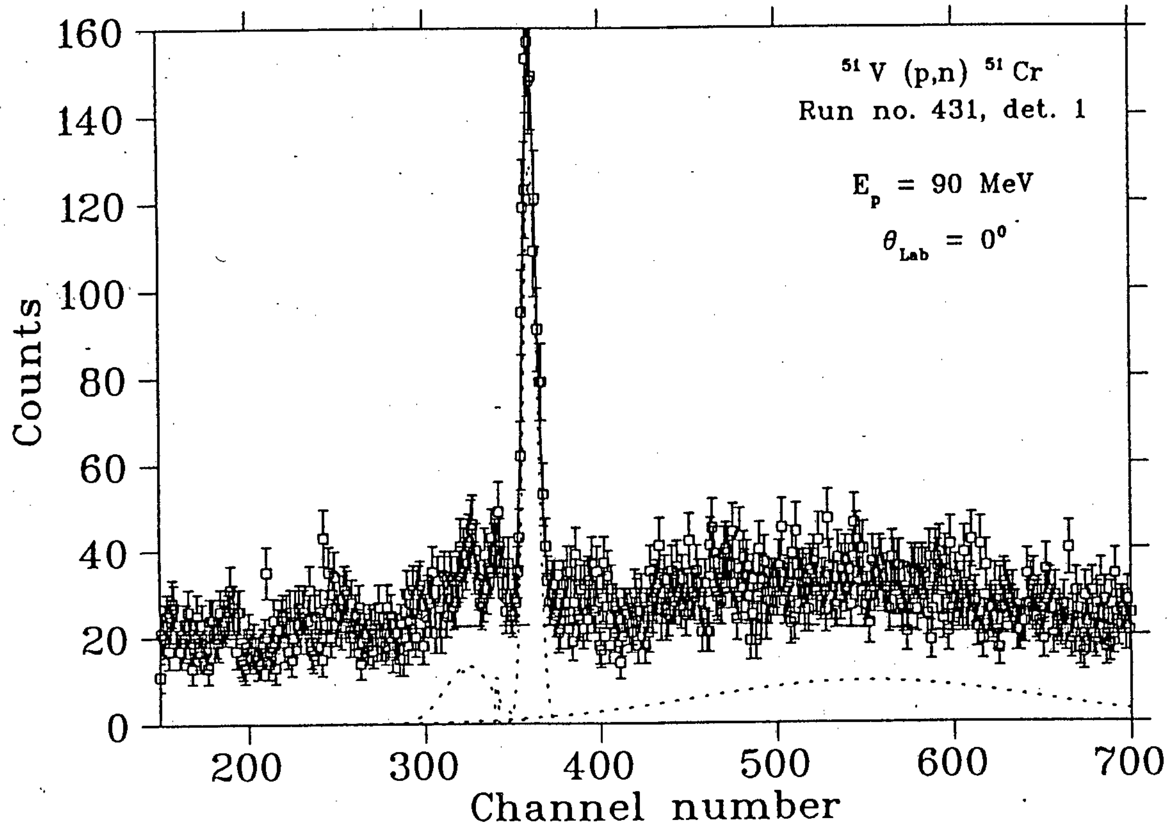

A.2 Run 438 detector 3.

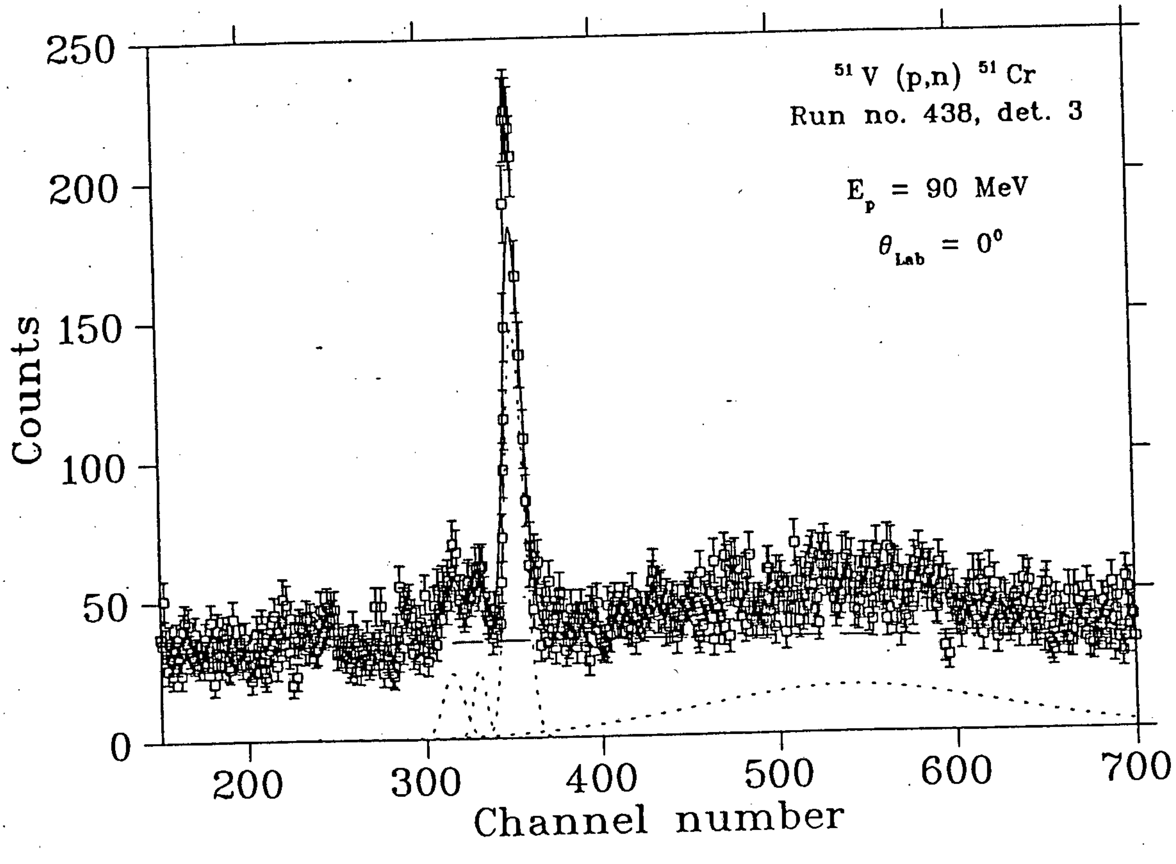

A.3 Run 438 detector 5.

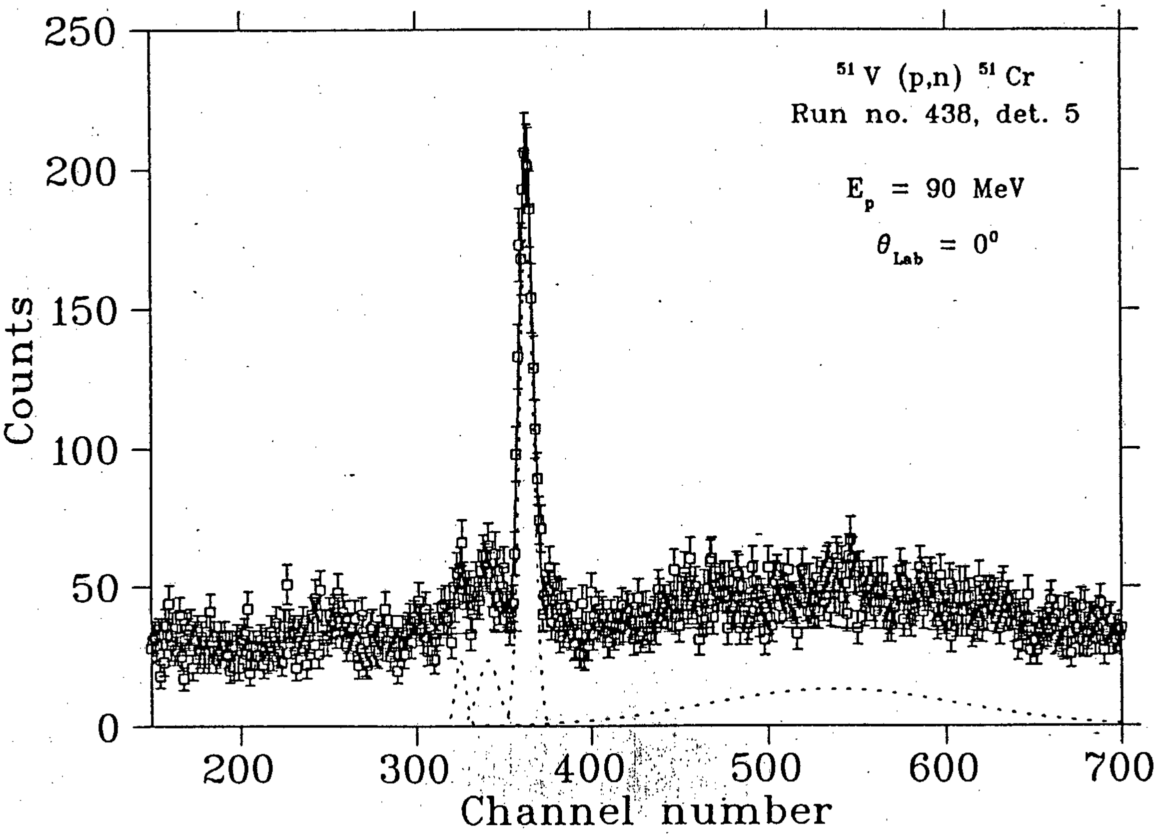

A.4 Run 445 detector 5.

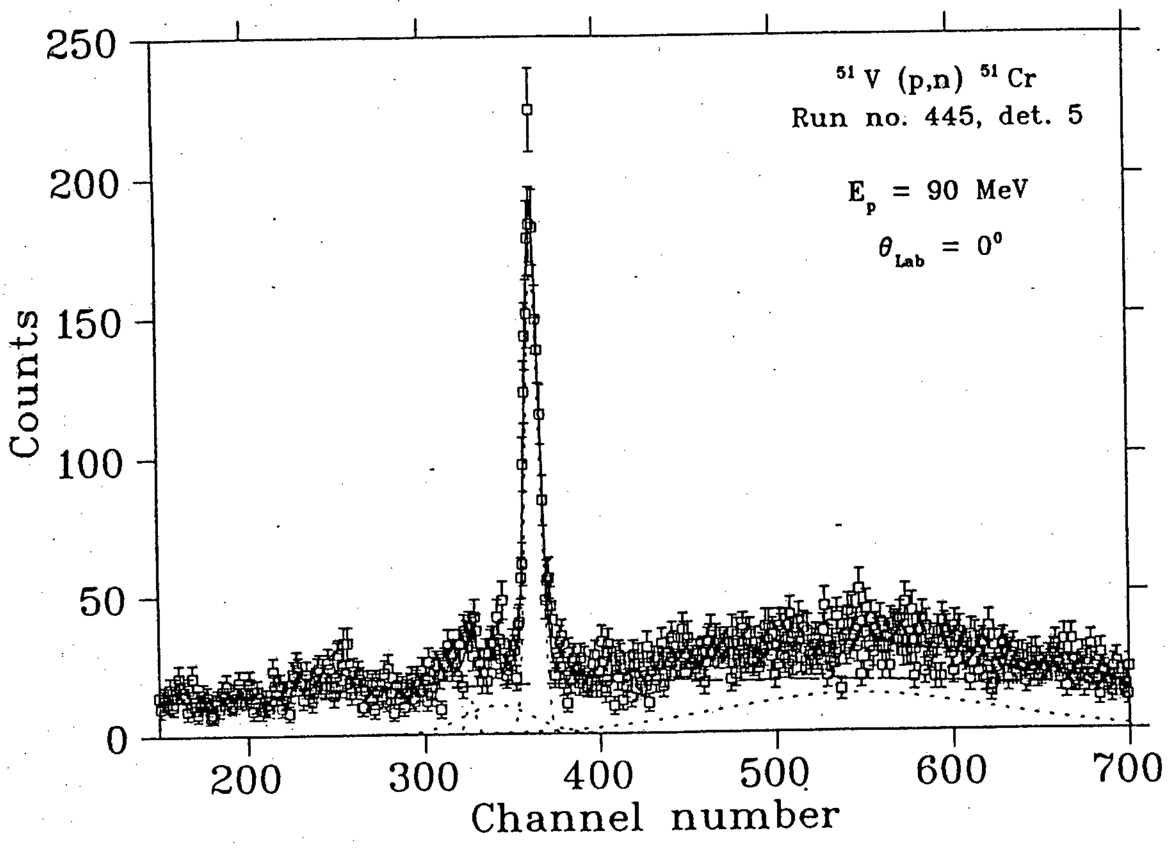

A.5 Run 445 detector 6.

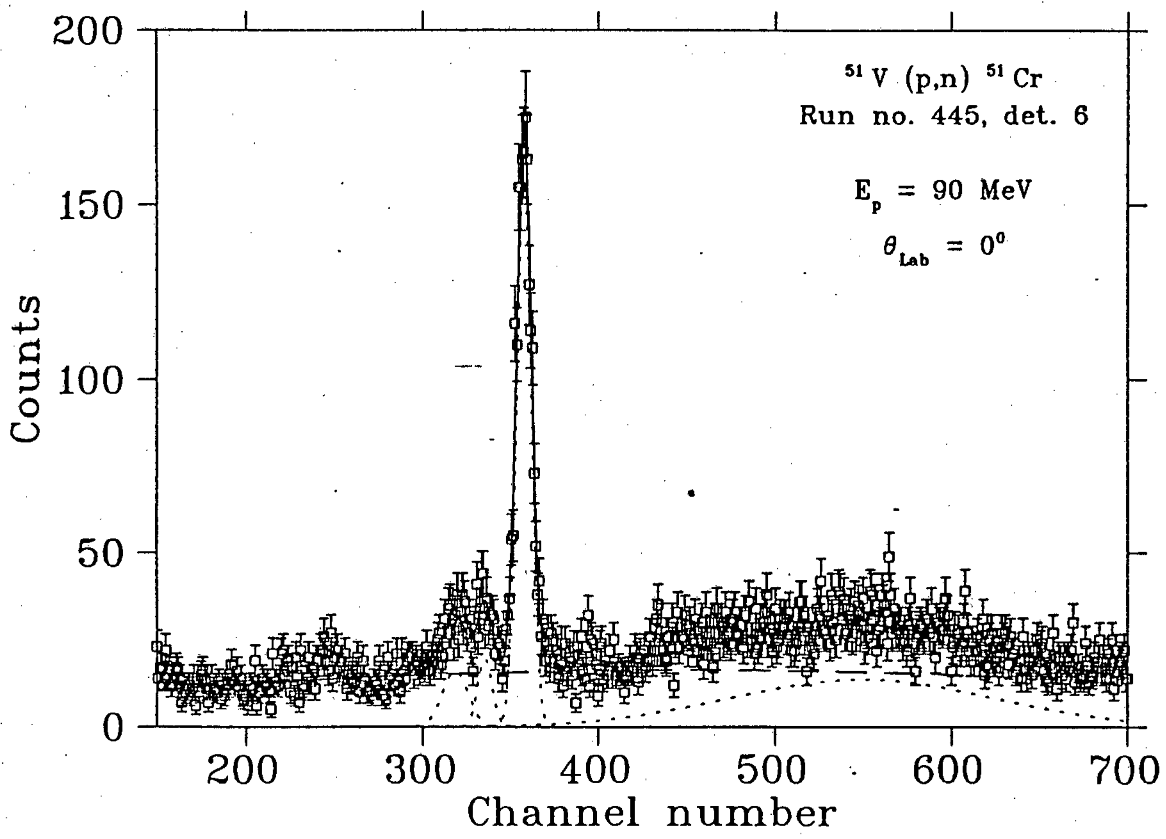

A.6 Run 446 detector 1.

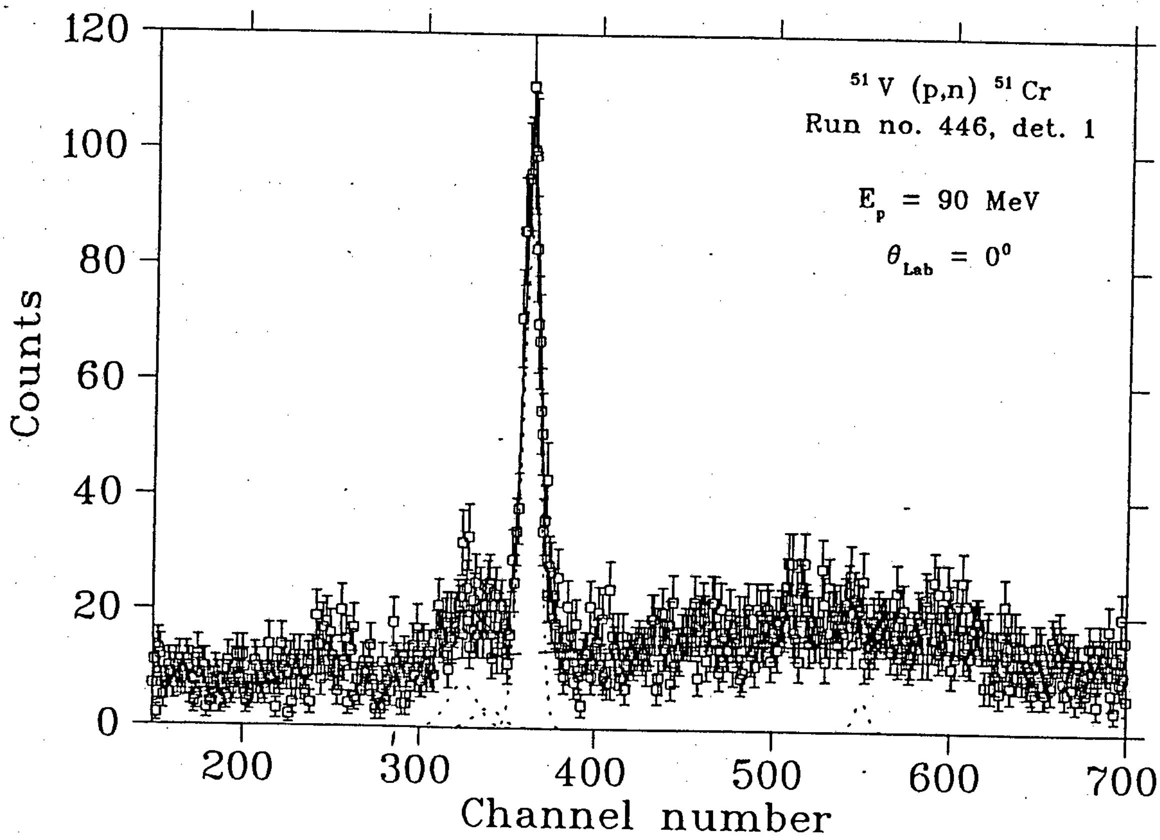

Appendix B

Fitted 120 MeV spectra

B.1 Run 33 detector 1.

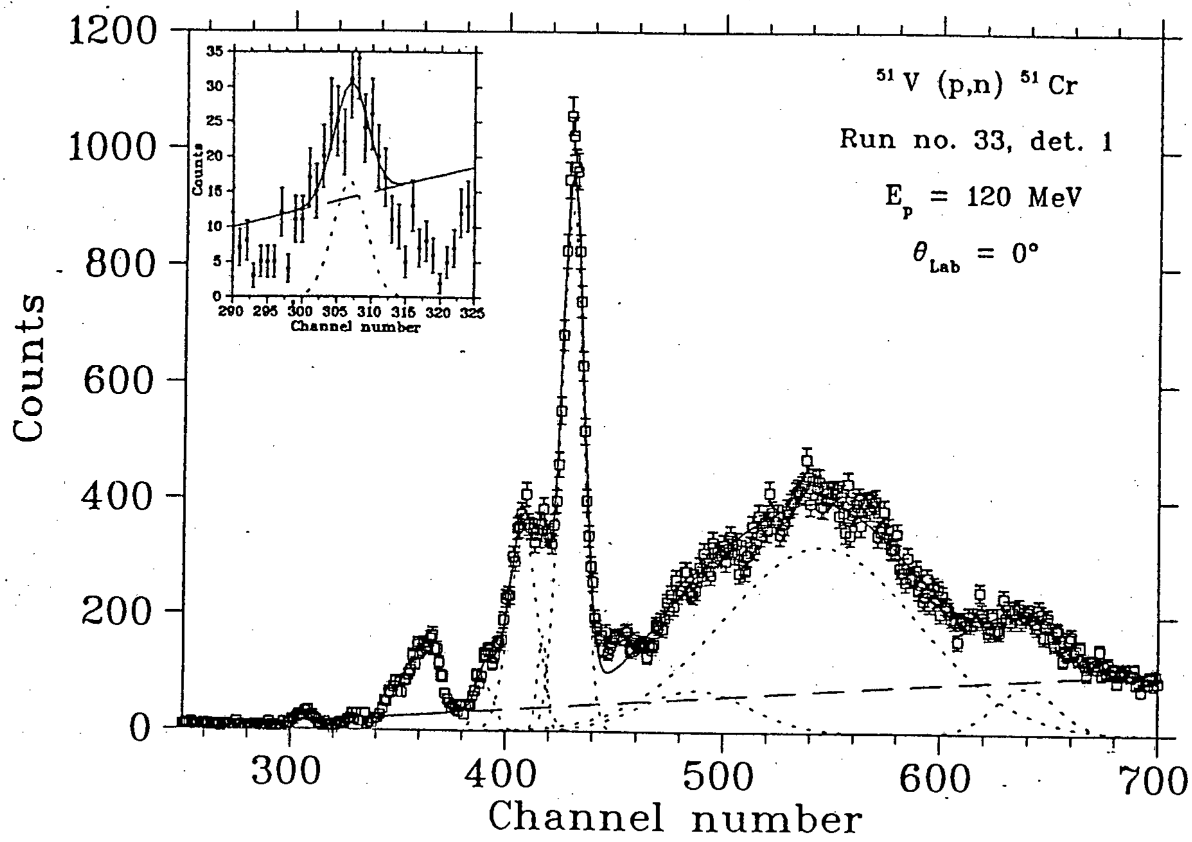

B.2 Run 37 detector 5.

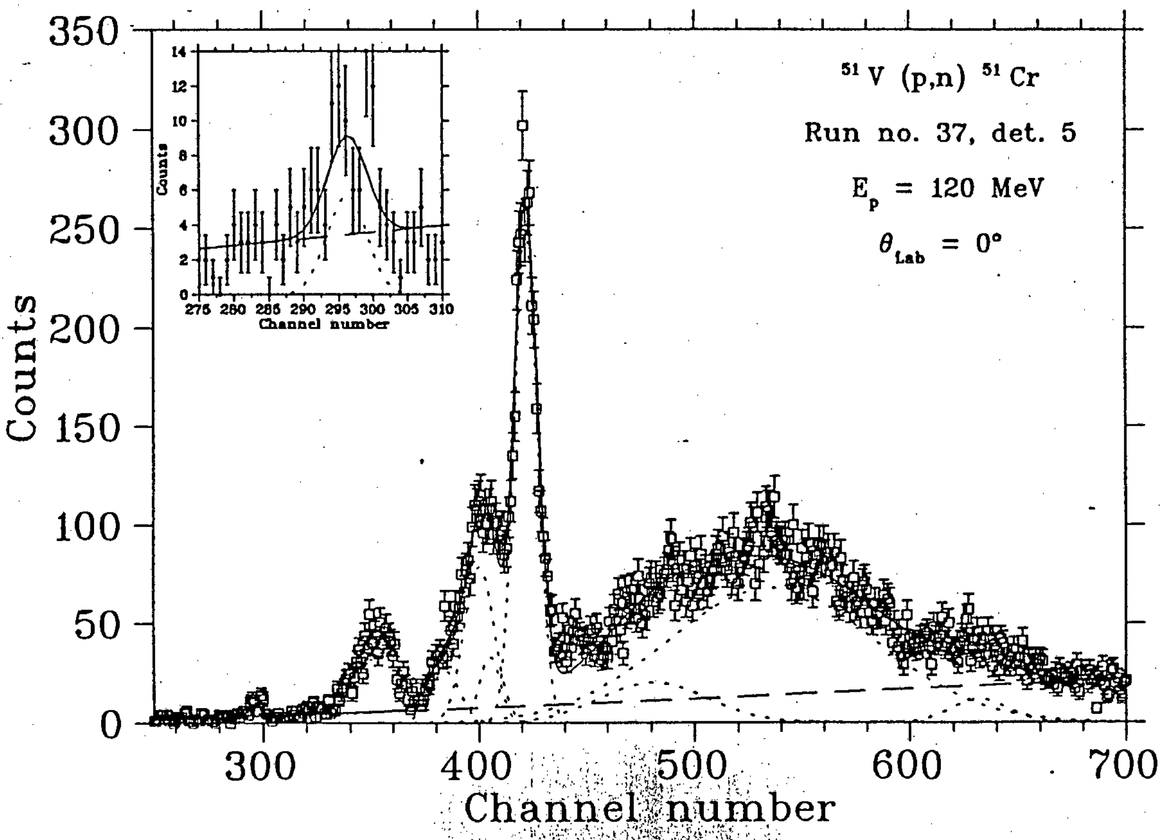

B.3 Run 38 detector 3.

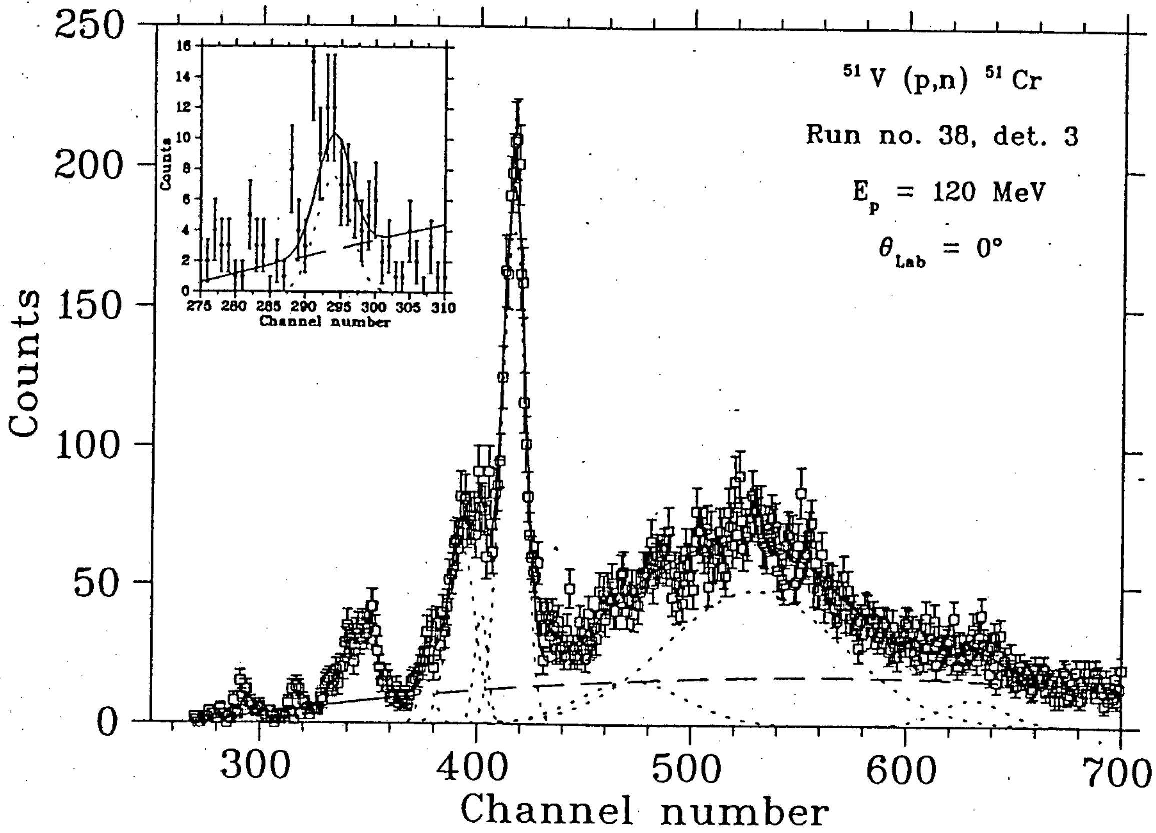

B.4 Run 325 detector 2.

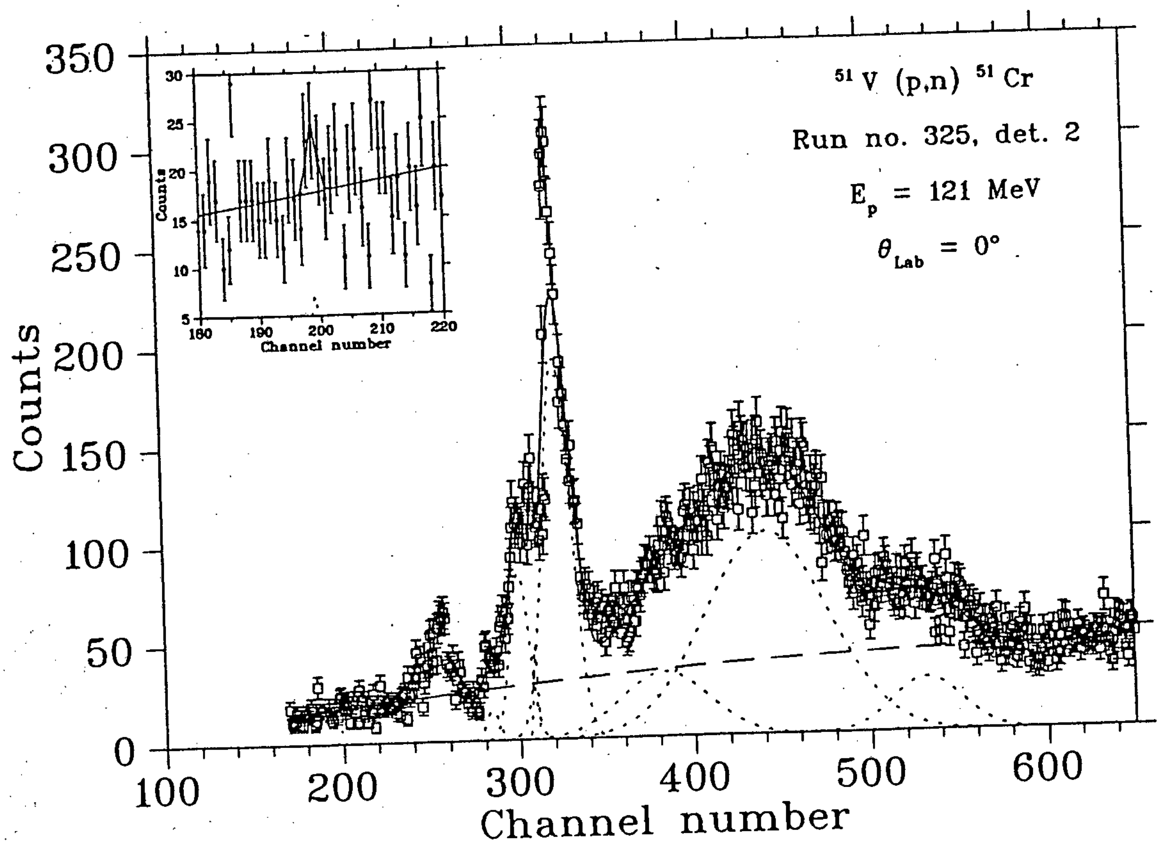

B.5 Run 325 detector 4.

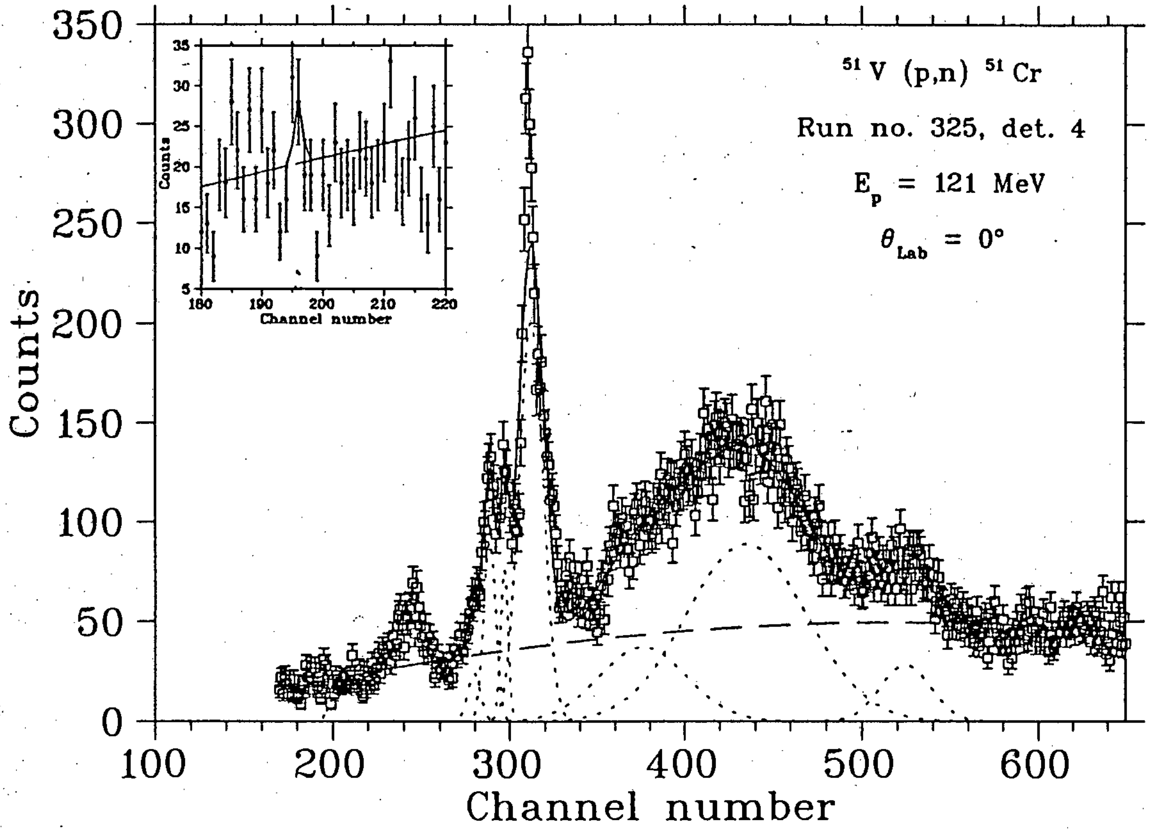

B.6 Run 332 detector 3.

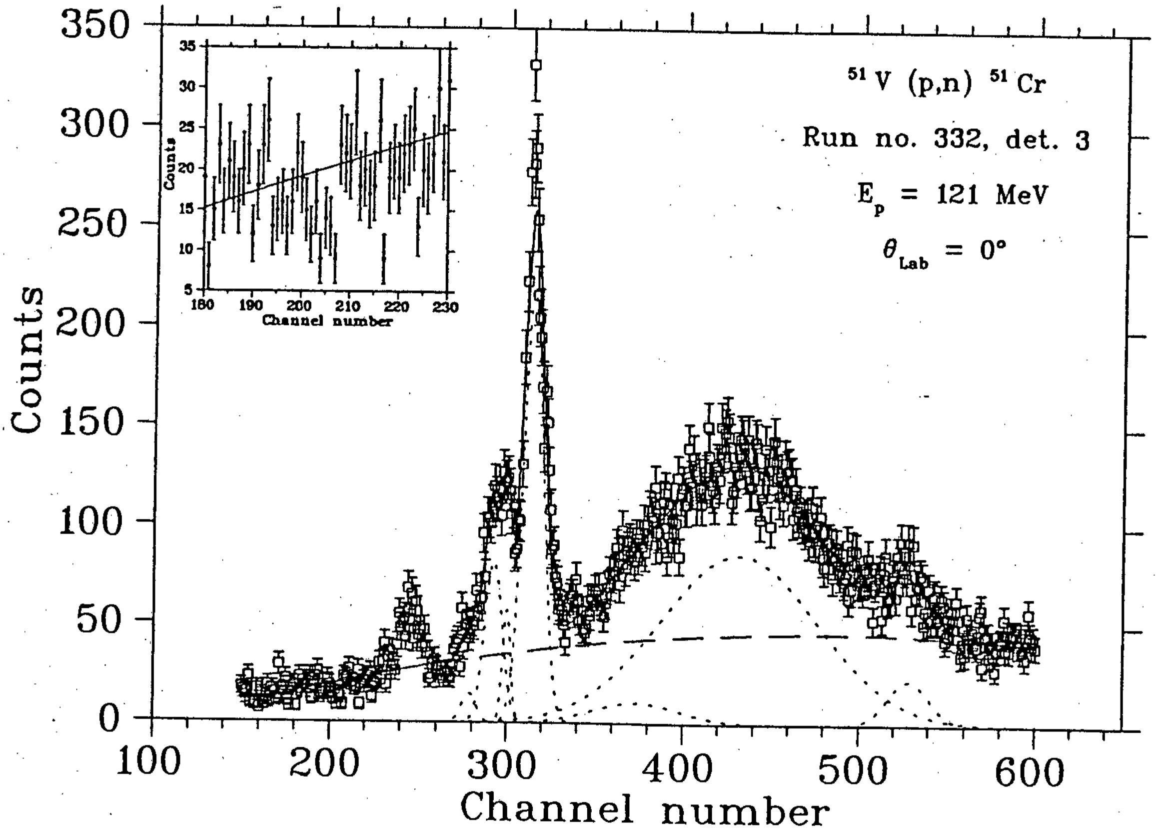

Appendix C

Fitted 160 MeV spectra

C.1 Run 49 detector 1.

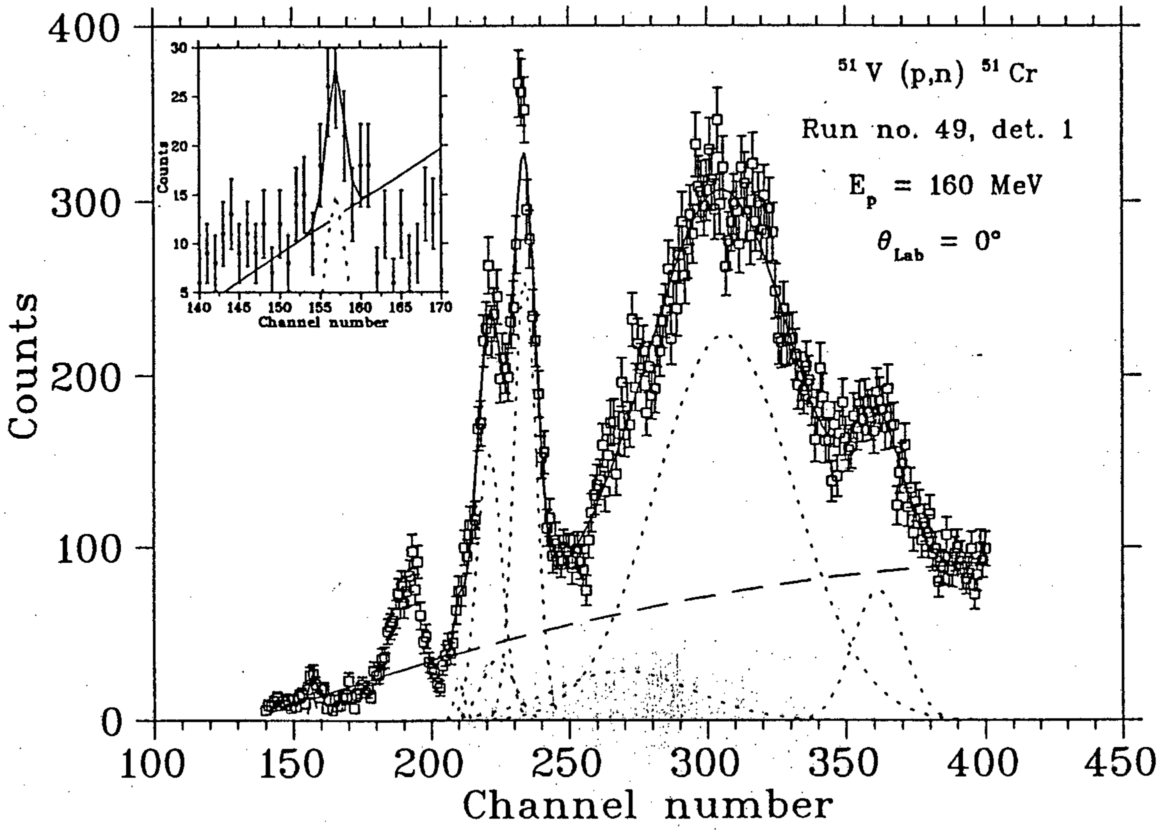

C.2 Run 49 detector 6.

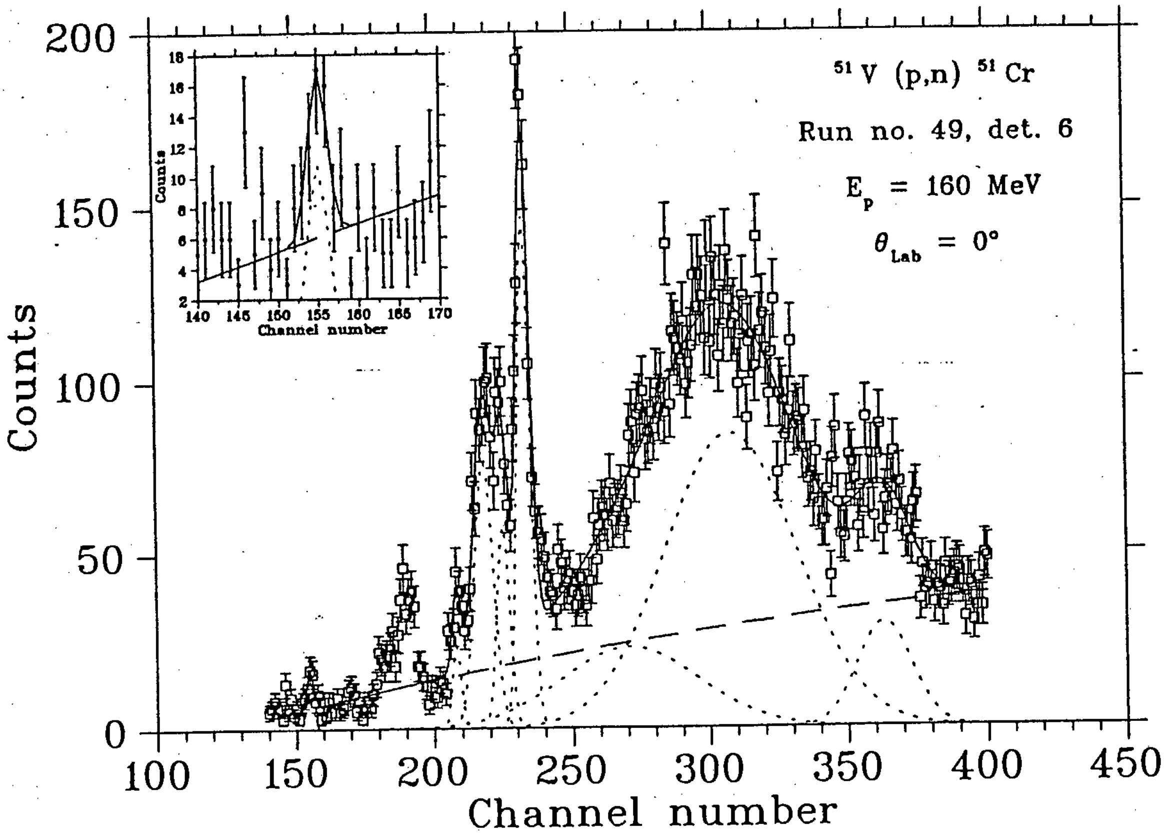

C.3 Run 62 detector 1.

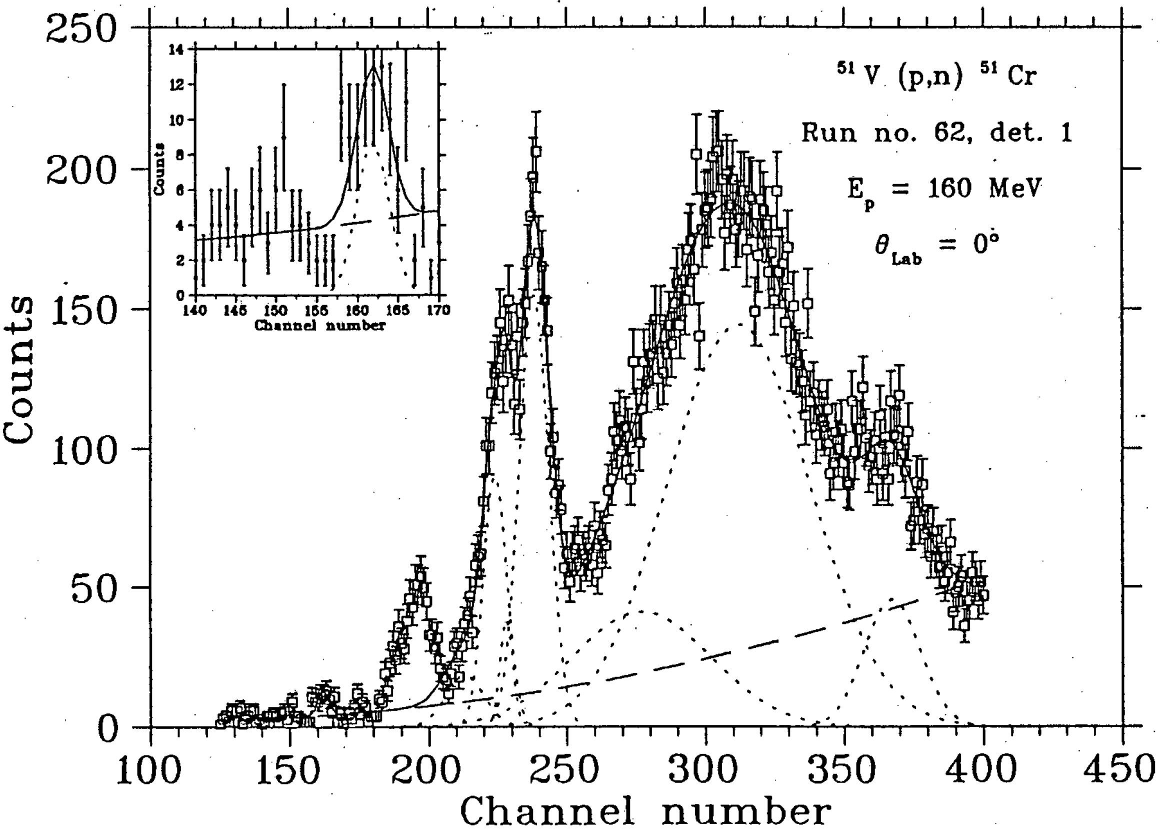

C.4 Run 62 detector 5.

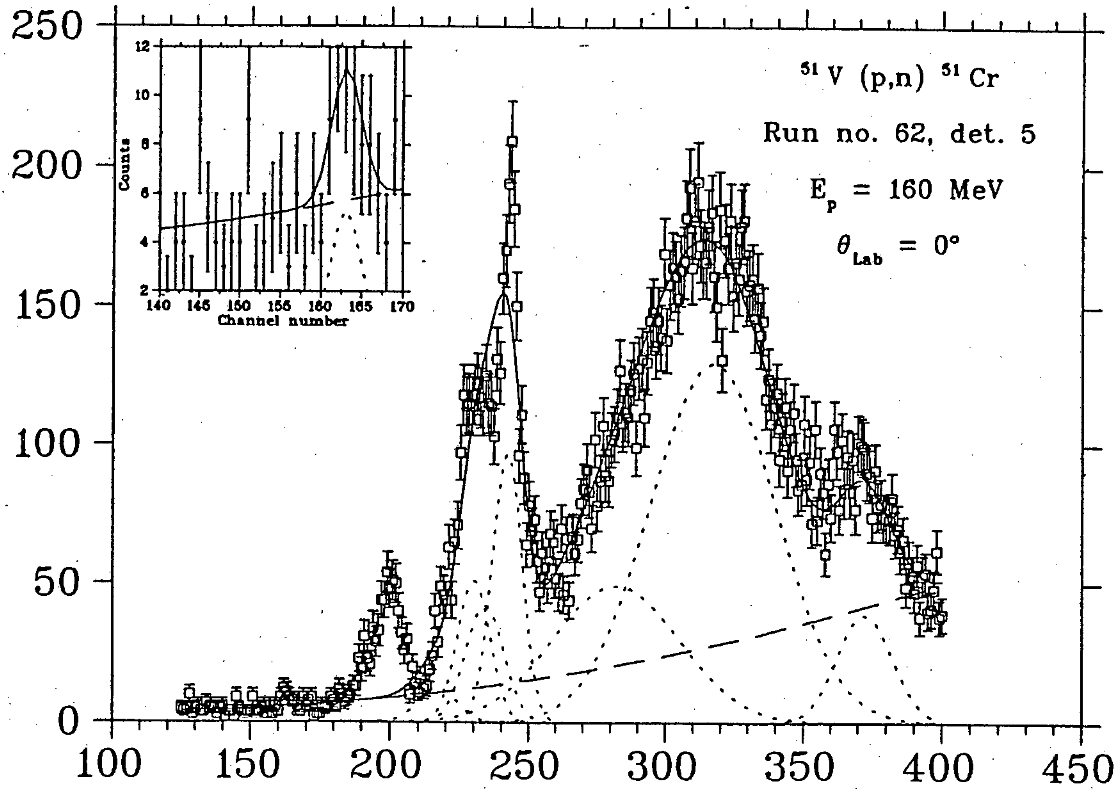

C.5 Run 470 detector 3.

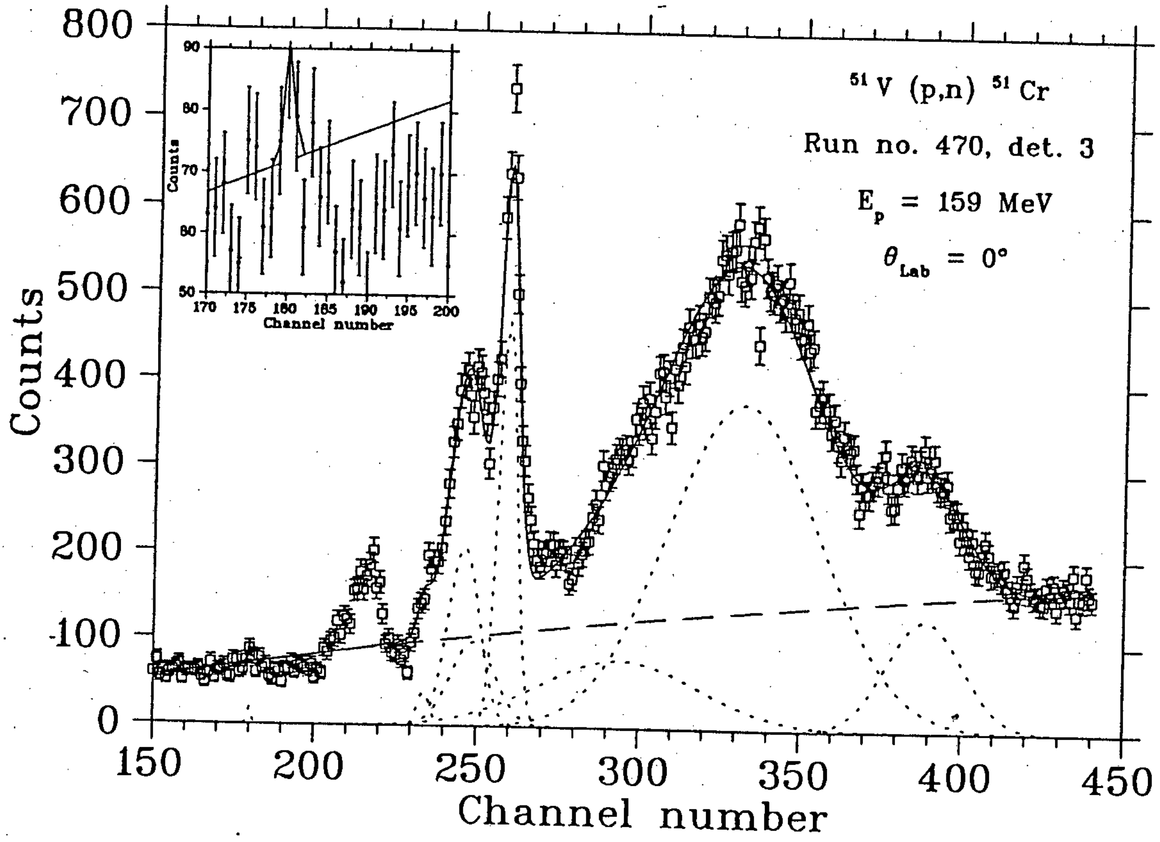

C.6 Run 480 detector 5.

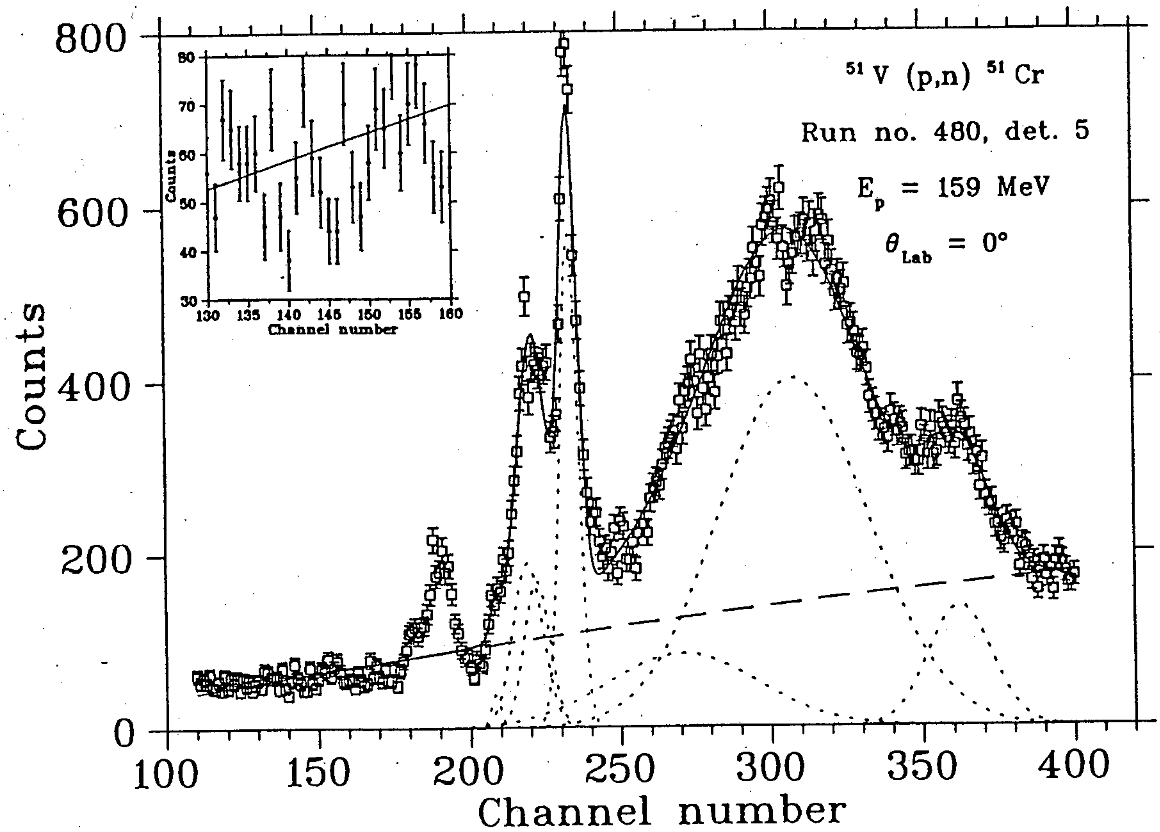

Appendix D

Fitted 200 MeV spectra

D.1 Run 78 detector 5.

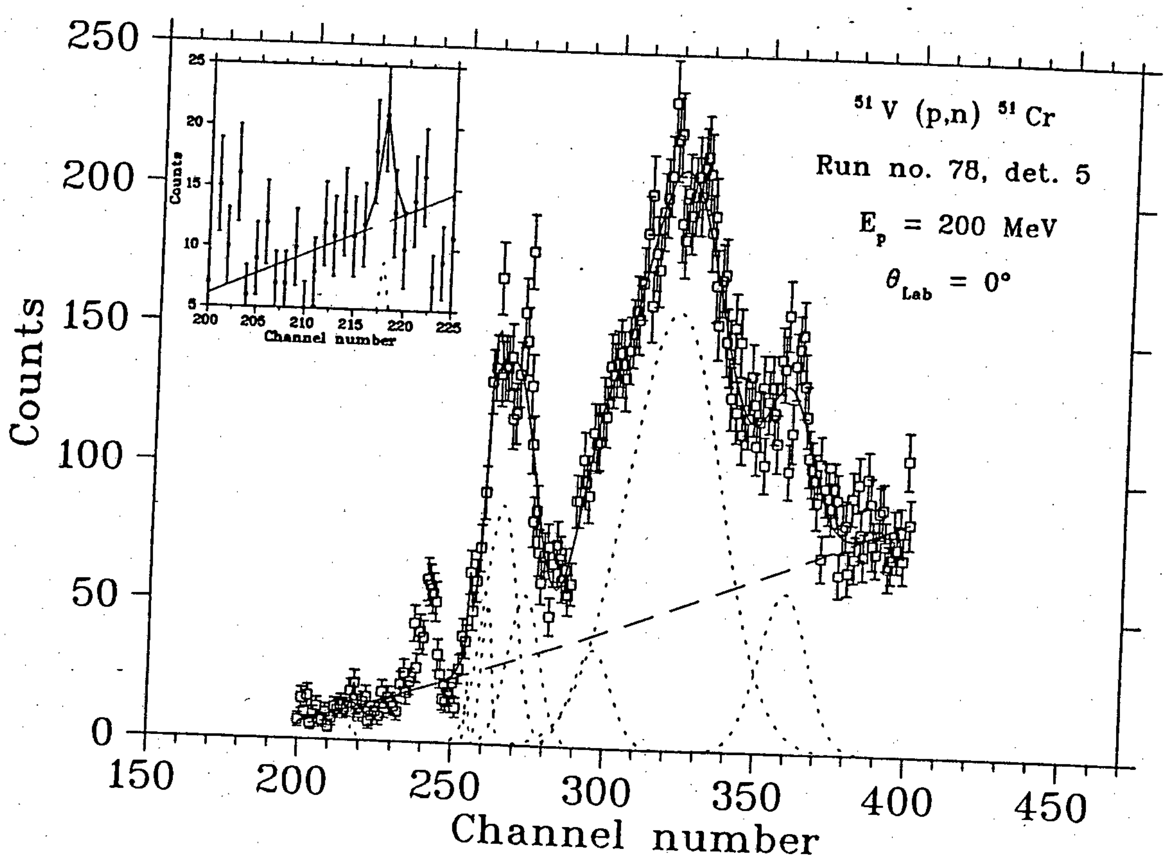

D.2 Run 80 detector 1.

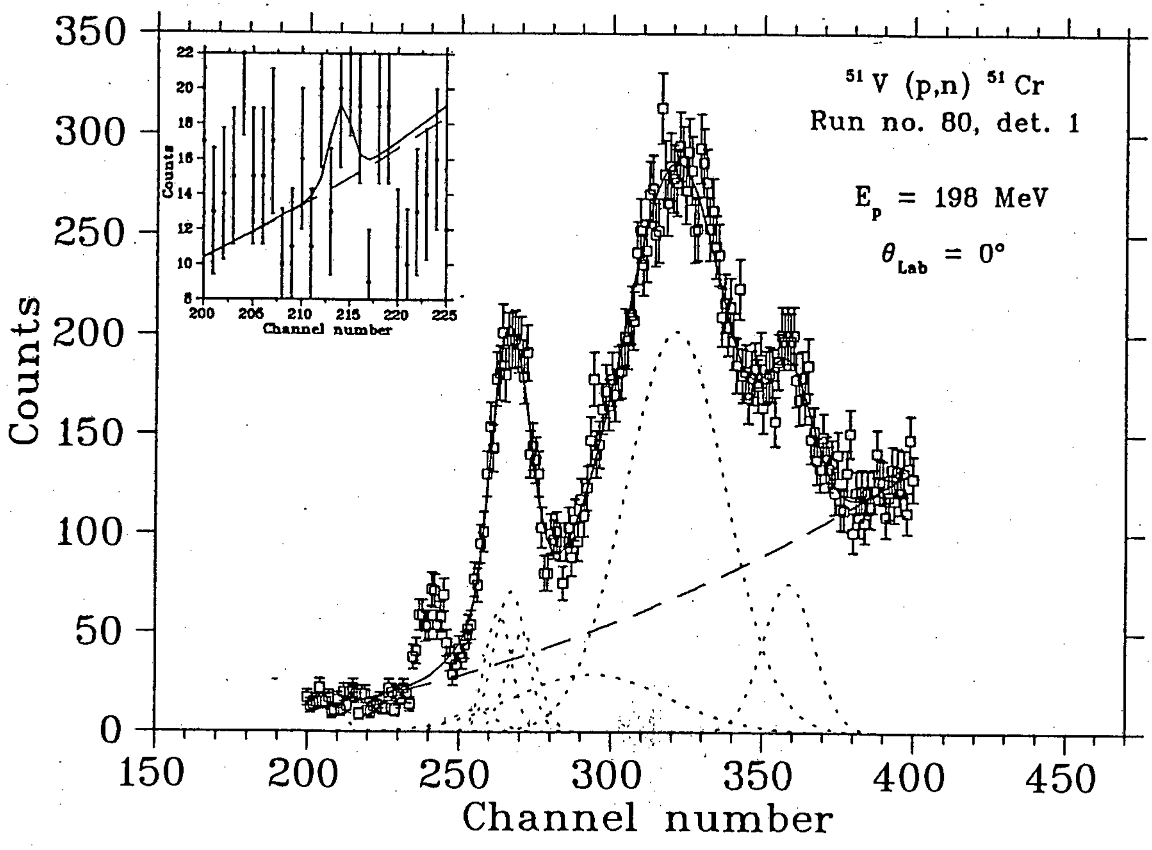

D.3 Run 80 detector 5.

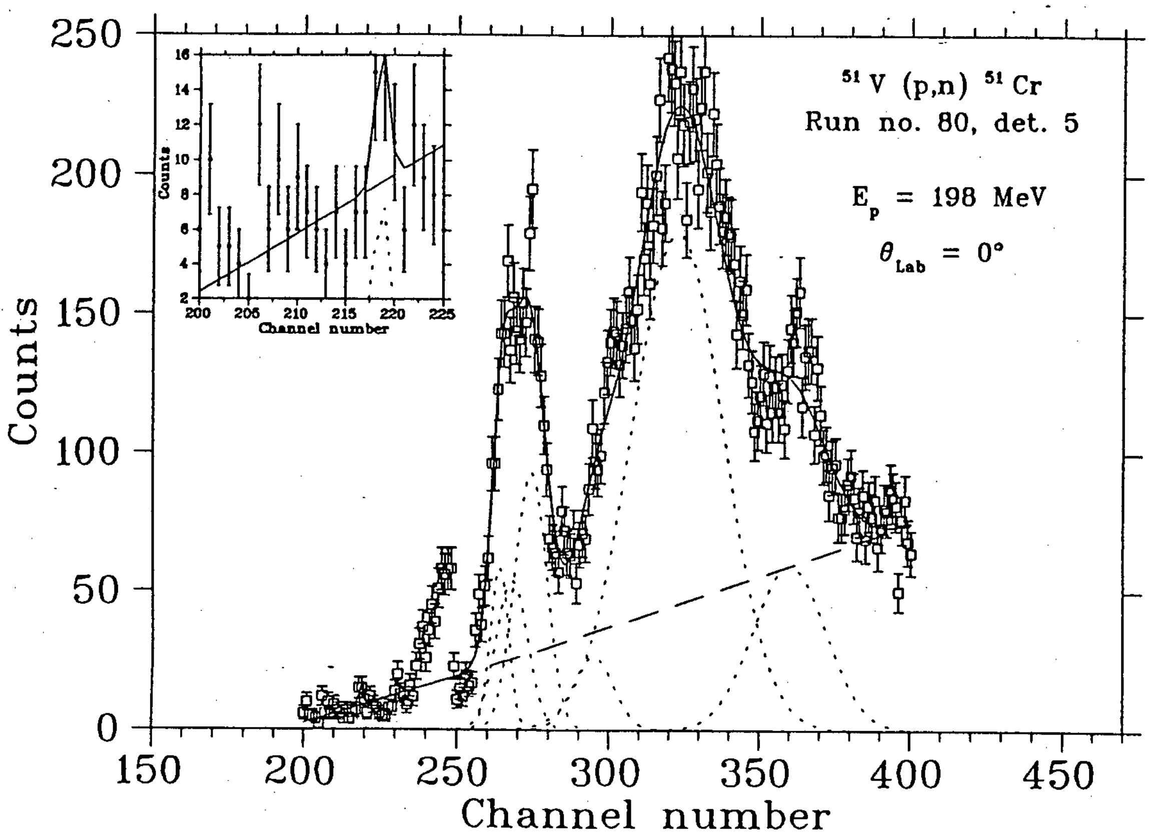

D.4 Run 286 detector 5.

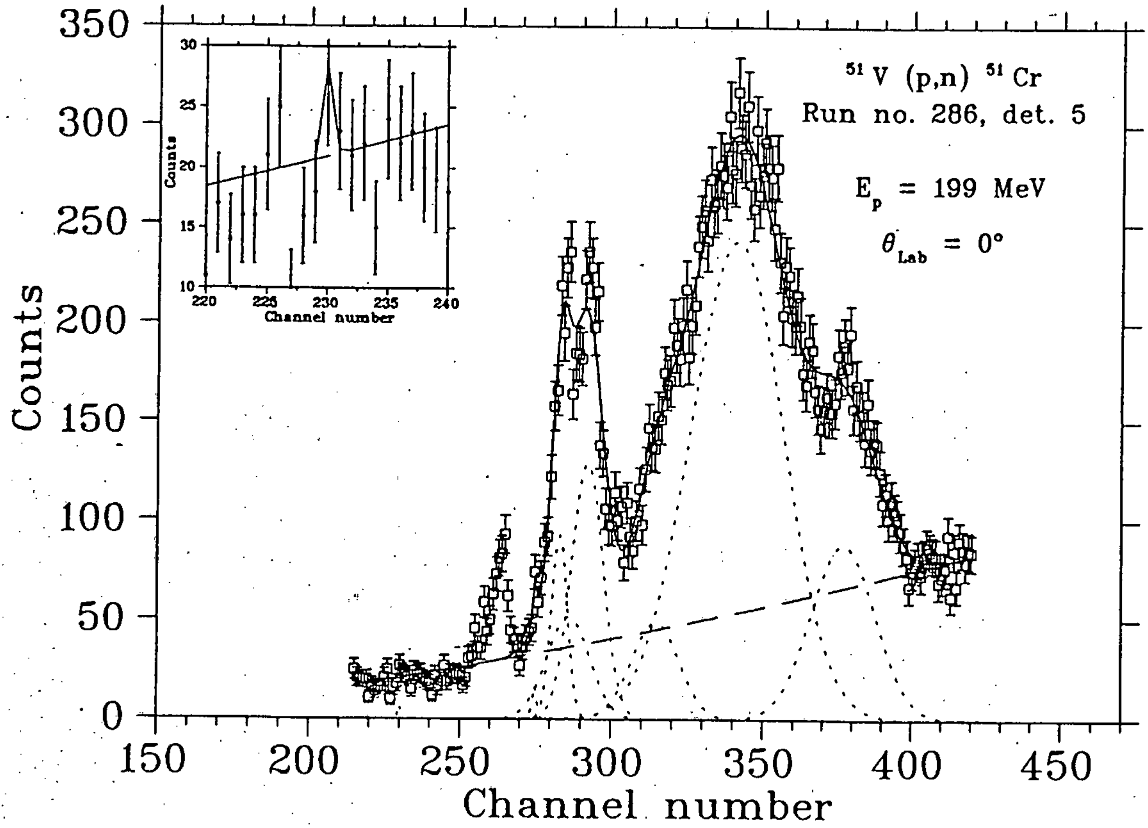

D.5 Run 287 detector 1.

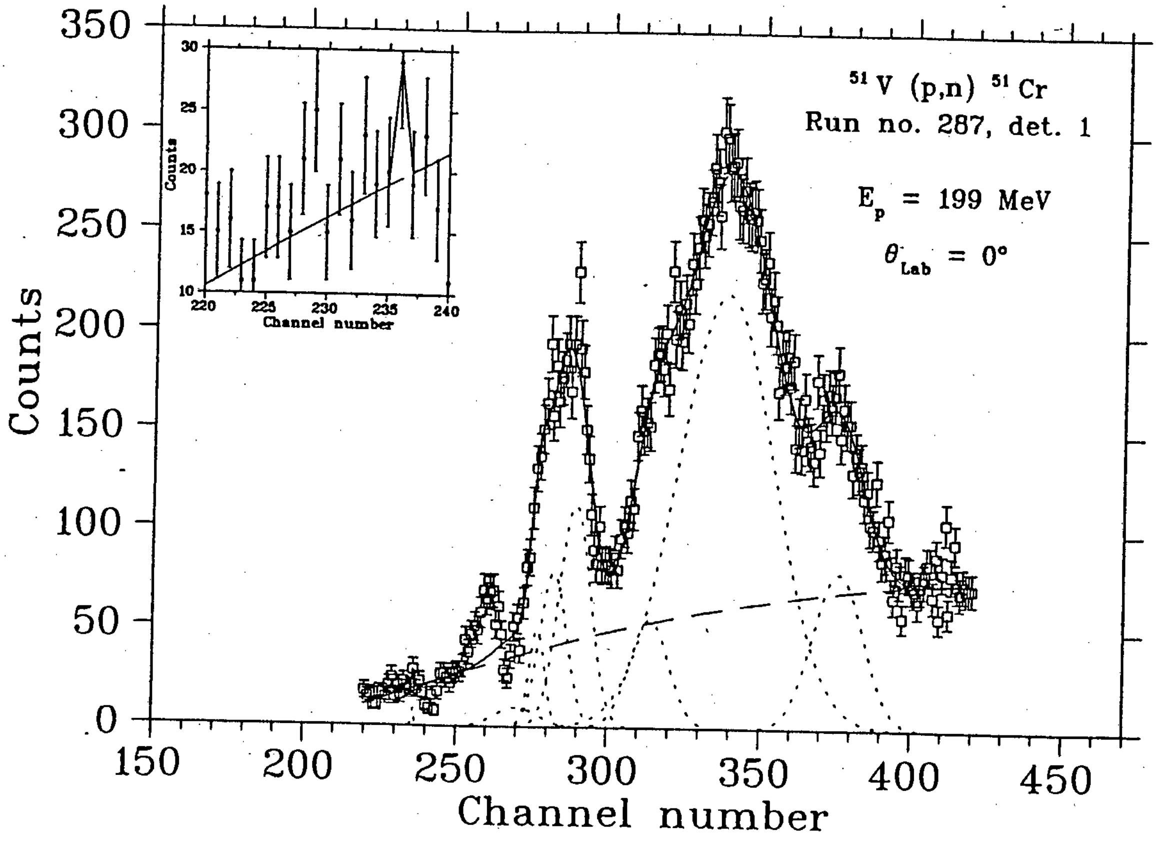

D.6 Run 287 detector 6.

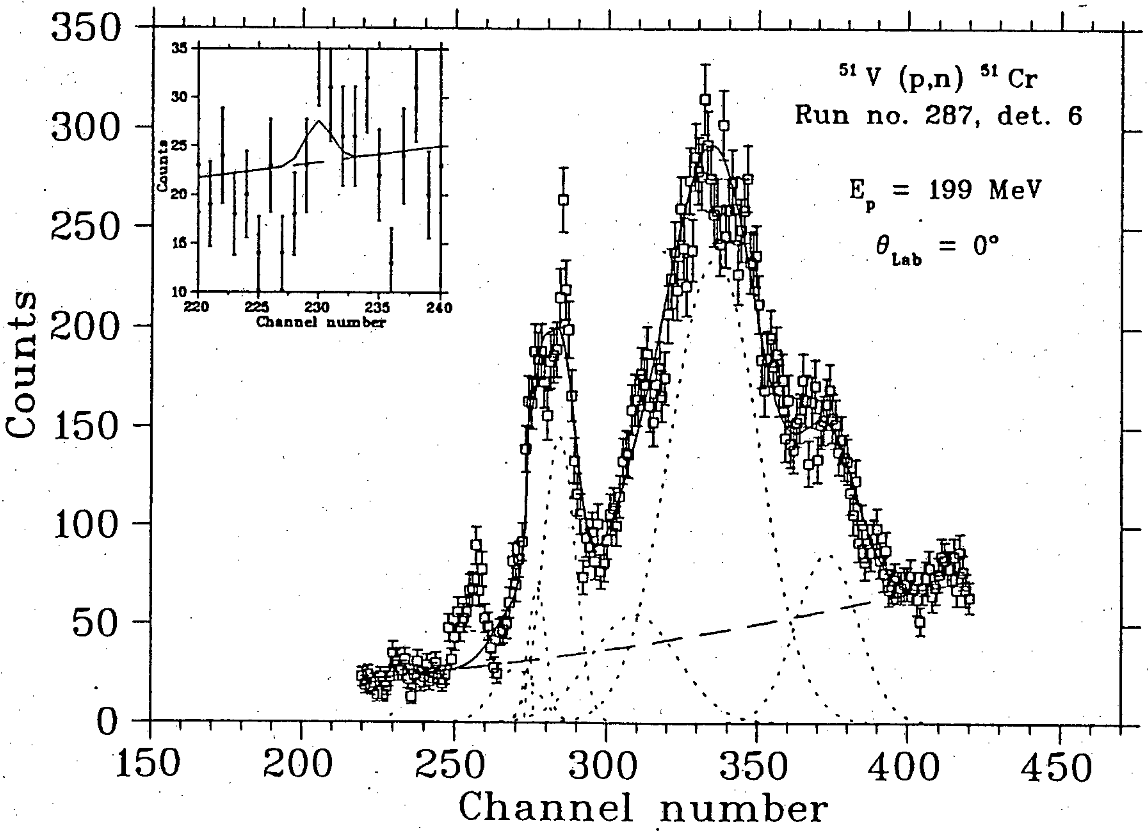

Bibliography

[And 62] J.D. Anderson, C. Wong, and J. W. McClure, Phys. Rev. **126**, 2170 (1962).

[Aub 78] R. L. Auble, Nucl. Data Sheets **23**, 163 (1978).

[Ber 87] G. F. Bertsh and H. Esbensen, Rep. Prog. Phys. **50**, 607 (1987).

[Fra 75] Hans Frauenfelder, Ernest M. Henley, Nuclear and Particle Physics (W. A. Benjamin, Inc. 1975) pp 327.

[Gaa 81] C. Gaarde, J. Rapaport, T. N. Taddeucci, C. D. Goodman, C. C. Forster, D. E. Bainum, C. A. Goulding, M. B. Greenfield, D. Horen and E. Sugarbaker Nucl. Phys. **A369** (1981).

[Ger 22] W. Gerlach and O. Stern, Z. Physik **8**, 110 (1922).

[Gle 83] N. K. Glendenning, Direct Nuclear Reactions (Academic Press, London, 1983) pp 175 - 189.

[Go1 80] C. D. Goodman, C. A. Goulding, M. B. Greenfield, J. Rapaport, D. E. Bainum, C. C. Forster, W. G. Love and F. Petrovich, Phys. Rev. Lett. **44**, 1755 (1980).

[Go2 80] C. D. Goodman, The (p,n) reaction and Nucleon-Nucleon Force, edited by C. D. Goodman, S. M. Austin, S. D. Bloom, J. Rapaport and G. R. Satchler (Plenum, New York, 1980 pp 170).

[Goo 83] C. D. Goodman, Prog. in Part. and Nucl. Phys. 475 (1983).

[Goo 82] C. D. Goodman and S.D Bloom, contribution to the 1982 Telluride Conference.

[Goo 83] C. D. Goodman, Prog. in Part. and Nucl. Phys. 475 (1983).

[Goo 89] C. D. Goodman, Y. Wang, W. Huang, G. C. Kiang, C. A. Gaarde, J. Rapaport, E. R. Sugarbaker, D. Marchlenski and J. Wagner, IUCF Sci. and Tech. Report p48 1989.

[Goo 90] C. D. Goodman, Y. Wang, W. Huang, G. C. Kiang, R. C. Byrd, L. J. Rybarcyk, T. N. Taddeucci, J. Rapaport, D. Marchlenski and E. R. Sugarbaker, IUCF Sci. and Tech. Report p49 1990.

[Hua 91] W. Huang, Ph.D. thesis I.U.C.F. 1991.

[Hod 71] P. E. Hodgson, Nuclear reactions and nuclear structure (Clarendon Press, Oxford 1971) p 575.

[Jam 75] F. James and M. Roos, Computer Physics Communications 10 (1975) p343-367.

[Kab 90] R Kabutz, Honours Project, University of Cape Town (1990).

[Ker 59] A. K. Kerman, H. McManus, and R. M. Thaler, Ann. Phys. (N.Y.) **8**, 551 (1959).

[Lov 80] W. G. Love, in The (p,n) Reaction and the Nucleon-Nucleon Force, edited by C. D. Goodman, S. M. Austin, S. D. Bloom, J. Rapaport, G. R. Satchler (Plenum, New York, 1980), p. 23.

[Lov 81] W. G. Love and M. A. Franey, Phys. Rev. **C24**, 1073 (1981).

[Lov 85] W. G. Love and M. A. Franey, Phys. Rev. **C31**, 488 (1985).

[Nac 90] NAC Annual Report NAC AR 90-01 p29.

[New 91] R. T. Newman, forthcoming M.Sc. thesis University of Cape Town (1991).

[Pau 24] W. Pauli, Naturwiss. 12, 741 (1924).

[Pau 27] W. Pauli, Z. Physik 43, 601 (1927).

[Pet 79] F. Petrovich, W. G. Love, in the Proceedings of the LAMPF Workshop on Pion Single Charge Exchange, Los Alamos, New Mexico, 1979 (unpublished), Document No. LA-7892C, Addendum.

[Pel 80] F. Petrovich, in The (p,n) Reaction and the Nucleon-Nucleon Force, edited by C. D. Goodman, S. M. Austin, S. D. Bloom, J. Rapaport, G. R. Satchler (Plenum, New York, 1980), p. 115.

[Pe2 80] F. Petrovich, W. G. Love, and R. J. McCarthy, Phys. Rev. **C21**, 1718 (1980)

[Pil 90] J. V. Pilcher, Ph.D. thesis, University of Cape Town (1989) unpublished.

[Rap 83] J. Rapaport, T. N. Taddeucci, T. P. Welch, C. Gaarde, J. Larsen, D. J. Horen, E. Sugarbaker, P. Koncz, C. C. Foster, C. D. Goodman C. A. Goulding and T. Masterson, Nucl. Phys. **A410** 371 (1983).

[Rap 84] J. Rapaport, R. Alarcon, B. A. Brown, C. Gaarde, J. Larsen, C. D. Goodman, C. C. Forster, D. Horen, T. Masterson, E Sugarbaker and T. N. Taddeucci Nucl. Phys. **A427** 332 (1984).

[Sat 64] G. R. Satchler, Nucl. Phys. 55, 1 (1964).

[Sat 83] G. R. Satchler, Direct Nuclear Reactions (Clarendon Press, New York, 1983).

[Som 16] A. Sommerfeld, Phys. Z. 17, 491 (1916); P. Debye, Phys. Z. 17, 507 (1916)

[Tad 87] T. N. Taddeucci, C. A. Goulding, T. A. Carey, R. C. Byrd, C. D. Goodman, C. D. Gaarde, I. Larsen, D. Horen, J. Rapaport and E. Sugarbaker, Nucl. Phys. **A469** 125 (1987).

[Wan 88] D. Wang, J. Rapaport, D. J. Horen, B. A. Brown, C. Gaarde, C. D. Goodman, E. Sugarbaker and T. N. Taddeucci, Nucl. Phys. **A480** 285 (1988).

[Wan 90] Y. Wang, C. D. Goodman, W. Huang, G. C. Kiang, R. C. Bryd, L. J. Rybarcyk, T. N. Taddeucci, J. Rapaport, D. Marchlenski and E. R. Sugarbaker, Bull. Am. Phys. **35** 1666 (1990).

[Won 90] Samuel S. M. Wong Introductory Nuclear Physics (Prentice–Hall International Editions) 1990 pp 216 – 230.